AN ABSTRACT OF THE DISSERTATION OF

Eduardo Francisco Guerrero for the degree of Doctor of Philosophy in Geology presented on May 31, 2016.

Title: Quaternary Landscape Evolution and the Surface Expression of Plume-Lithosphere Interactions in the Greater Yellowstone Area.

Abstract approved:

_____

Andrew J. Meigs

Numerous investigations demonstrate that mantle convective processes such as upwelling affect the surface topography of the overriding plate. The surface expression of mantle flow has been coined 'transient topography'. Transient topography in the North American plate is thought to result from a mantle thermal anomaly beneath the Yellowstone volcanic center, the so-called Yellowstone hotspot. This work explores the sensitivity of the surface of Western North America by testing the hypothesis that advection of a transient topographic wave through the North American plate drove the post-Pliocene landscape evolution of the greater Yellowstone region. This study presents results from three approaches to assessing the expression of dynamic topography in continental lithosphere. First, analysis of digital elevation data reveals an asymmetric topographic swell that has an amplitude of 400-1200 m and a wavelength of ~600 km which was disentangled from overlapping signals preserved in the topography that result from other processes that shape the Earth's surface. The transient topography swell data is then used to parameterize a model of advection of dynamic topography to estimate deformation rates and patterns that may be expected in the Yellowstone area. Second, analysis of stream channel morphology extracted from digital elevation data is used to identify crustal deformation, changes in streambed lithology, and erosional patterns throughout the Yellowstone area. Forcing of landscapes by dynamic topography in

continental landscapes is below the detection limit of channel steepness indices (k_{sn}). The final chapter in this study presents an updated geochronology of erosion of the Bighorn Basin of Wyoming and Montana. The geochronology is the result of geomorphic mapping and paleodrainage interpretations of fluvial terraces preserved throughout the Bighorn basin that record the post-Pliocene erosional story in the basin. A new interpretation of the Basin's erosion story is presented, and conclude that the change from a south to north drainage to a west to east drainage pattern and lateral migration of the Bighorn river away from Yellowstone coincides with the model of advection of dynamic topography.

Quaternary Landscape Evolution and the Surface Expression of Plume-Lithosphere Interactions in the Greater Yellowstone Area

by
Eduardo Francisco Guerrero

A DISSERTATION

submitted to

Oregon State University

in partial fulfillment of
the requirements for the
degree of

Doctor of Philosophy

Presented May 31, 2016
Commencement June 2017

Doctor of Philosophy dissertation of Eduardo Francisco Guerrero presented on May 31, 2016

APPROVED:

Major Professor, representing Geology

Dean of the College of Earth, Ocean, and Atmospheric Sciences

Dean of the Graduate School

I understand that my dissertation will become part of the permanent collection of Oregon State University libraries. My signature below authorizes release of my dissertation to any reader upon request.

Eduardo Francisco Guerrero, Author

ACKNOWLEDGEMENTS

First, thanks to my advisor, Andrew Meigs, because he took a chance on being willing to work with me despite the fact that my background was to be more of an educator. Over the past 6 years we have pursued an exciting project, and he helped to mold me into a researcher and helped to prepare me for a career aimed at pursuing interesting questions. He always treated me with kindness and respect, and always as a collaborator. He knew how to push me to fulfill my potential, even when I couldn't see it myself. I appreciate that he always encouraged me to have a work-life balance, and he demonstrated that one can lead a successful professional career and still have a life. I am not only a better scholar thanks to Andrew, but I am a better person thanks to his mentorship and guidance.

Thanks to Shan DeSilva, Bob Duncan, and Dawn Wright for allowing me to join the Increasing Diversity in Earth Sciences (IDES) program in 2011. I was afforded an extraordinary opportunity to collaborate with a tremendous group of undergraduate students, who's drive and passion for the Earth sciences which was incredibly inspiring. Thank you to Lynette DeSilva for being a valuable collaborator in my IDES experience.

Thanks to my committee for their input and feedback on my project. Shan De Silva, Peter Clark, Rob Harris, and Lorenzo Cianelli who served as the Graduate College Representative.

My PhD was supported by grants from: Tobacco Root Geological Society, Wyoming Geological Association, Geological Society of America, American Association of Petroleum Geologists, PRIME Lab Seed Grant, and the OSU General Research Fund. I also need to acknowledge George and Danielle Sharp, who've endowed the Sharp fellowship, which also contributed to funding my PhD.

Thanks to Ken Bork, David Greene, Tod Frolking, and Dave Hawkins who each introduced me to the different facets of Geology at Denison University and through example inspired me to pursue a career in education and research, and set me off on the path that has led me to this point. To Colin Amos for suggesting I talk to Andrew as a potential PhD advisor back in 2006.

Thanks to Andrew's students, we started out with the Center for Topographic Expression (RIP) and are now a part of the Structure Tectonics and Geomorphology Group. I wouldn't have been able to figure out my first year at OSU without the friendship of Chris Madugo, Yann Gavillot. Nick Legg, Trevor Waldien, and Ellen Lamont. Thanks to Eric Kirby for providing valuable feedback, good conversation, and career and research ideas. To the current members of the STAG group, for your friendship: Gabe Creason, Na Hyung Choi, Fritz Freudenburger, and Wes Van Dassow.

One of the most enriching experiences I had at OSU was the weekly Geomorphology Roundtable. I cannot list all the students and faculty who participated, but I do want to acknowledge Sarah Lewis (without who the GRT would not happen). Thanks to Gordon Grant, Stephen Lancaster, Jay Noller, Jack Zunka, and Laura Hempel.

My experience at OSU would not have been the same without my friendship with Josh Cuzzone. I foresee us driving around the 2050 AGU on rascal scooters, don't know if we'll be able to ride bikes in Tamarancho at that point... but I'm sure we'll try. Iria Gimenez and Alberto Blanco, who are my chosen family. To my friends from Corvallis Cyclery Racing, who share my love for riding bicycles in the dirt. To Aaron Barth, Nilo Bill, and Andrea Balbas for their friendship and for being good colleagues.

I wouldn't have made it without the love and support of my family. My wife, partner, and best friend, Amoreena, whose constant patience, kindness, and thoughtful support allowed me to finish. I can't wait to continue our adventure! To my mother, Carolyn, my sister, Christina, my brother in law, Angel, and my niece Feliciana. I need to mention our pups, Molly and Guinness, who were the best de-stressors in the world when I needed them to be. To Barbara Bessey, Alea Joy, Dominique McKoy, and Peter King for welcoming me to the family. Amoreena and I are lucky to have you in our lives!

I dedicate this work to the memory of my father, Vicente Alfredo Guerrero Flores (1949-2008).

TABLE OF CONTENTS

TABLE OF CONTENTS (CONTINUED)

TABLE OF CONTENTS (CONTINUED)

LIST OF FIGURES

LIST OF FIGURES (CONTINUED)

Surface Expression of Plume-Lithosphere Interactions in the Greater Yellowstone Area

INTRODUCTION

The advent of the plate tectonic paradigm shift relied on the early observation that oceanic islands increased in age away from mid-ocean ridges towards continents (Wilson, 1965). The absolute motions of lithospheric plates across the Earth's surface were further constrained by the realization that volcanic island chains and seamounts increased in age away from the active volcanic island (Morgan, 1971). Morgan (1971) proposed a model that explained the existence of these volcanic chains: upwelling hotter material that originates in the lower mantle formed plumes that result in hotspots in the overriding lithosphere. Hotspots remain relatively fixed and their position is indicated by active volcanism, however the horizontal motion of the overriding plate leads to the formation of newer volcanic centers and thus hotspot tracks evolve over time. Morgan noted that "*the gravity pattern and regionally high topography around each hotspot suggest that more than just surface volcanism is involved at each hotspot"*. The homogenous nature of oceanic crust permitted the identification of broad topographic swells that are spatially coincident with volcanic hotspots, and can exceed ~1 km in height at their apex. The topographic swell extends a slight distance in front of the youngest volcano, but is elongated decreases in height along the hotspot track with increasing distance from the hotspot uplift source (Crough, 1983). The topographic swells associated with a hotspot as 'transient topography' because these swells are a temporary response to deformation and is advected through the lithosphere as a plate moves relative to the hotspot.

This dissertation presents an approach to quantify transient topography on the surface of continental lithosphere using the greater Yellowstone landscape and topography as a natural laboratory. Topography in the Yellowstone region reflects the heterogeneous nature of continental lithosphere. Key geologic events include Sevier and Laramide crustal shortening, Eocene magmatism, Basin and Range extension and normal faulting, caldera-forming supervolcano eruptions, glacial erosion, and fluvial erosion. The principal challenge in quantifying transient topography is isolating it from the other the compounded signals associated with these different landscape forcing mechanisms.

Chapter 1 deals with deconvolving the topography in continental lithosphere using elevation data to isolate and identify the long-wavelength topography, which is interpreted to be the hotspot-related transient topography. Deconvolving topography of the greater Yellowstone area relies on analysis of digital elevation models, where wavelengths of the various geologic forcing mechanisms are identified and progressively removed through filtering. Once known topographic signals associated with specific geologic events have been filtered out, the remaining topography represents the long wavelength topography of the lithosphere's surface. The long wavelength topography is compared to seismic velocity and gravity data to assess the correlation between topography and the structure of the earth's interior. Having identified the transient topography signal, it is possible to make predictions for magnitudes and rates of deformation of North American lithosphere as it passes of the hotspot at 29 mm yr^{-1}.

The second chapter uses stream channel morphology to identify spatial patterns of deformation in the greater Yellowstone area in order to test the hypothesis that transient topography is actively deforming landscapes. Channel steepness patterns in the greater Yellowstone area indicate that steepness is controlled by lithologic contacts, differential motion

along crustal faults, or glacial erosion. This suggests that the style of deformation associated with transient topography is either below the detection limit of channel steepness analysis, the rates of deformation are low enough that rivers are able to efficiently erode any transient topography-related deformation signal, or the response time of the rivers is short relative to the advection rate.

Chapter 3 explores the drainage evolution and erosional history of the Bighorn Basin of Montana and Wyoming preserved as series of fluvial terraces to consider if drainage evolution and incision patterns record advection of transient topography. The Bighorn Basin is an ideal natural laboratory in which to study the surface expression of transient topography because the basin's western margin is within 100 km of the Yellowstone Volcanic Field, the most recent evidence of active tectonism is the eruptive period of Absaroka Volcanic centers during the Eocene. Therefore, advection of transient topography should be considered one of the contributing processes to the basin's erosion and drainage evolution. The oldest preserved terraces in the basin are thought to be late Pliocene in age. A new geochronology is presented that updates Reheis et al.'s (1991) basin-wide terrace geochronology to include results of cosmogenic radionuclide dating of landforms within the the greater Bighorn drainage system. Paleoflow measurements are used to interpret the stream capture and drainage evolution since the Plio-Pleistocene transition. A new model for erosion of the Bighorn Basin interprets the drainage evolution as resulting from transient topography advecting into the basin as the lithosphere is translated over the hotspot towards the southwest.

SOURCES CITED

Crough, S.T., 1983, Hotspot swells: Annual Review of Earth and Planetary Sciences.

Morgan, W.J., 1971, Convection Plumes in the Lower Mantle: Nature, v. 230, no. 5, p. 42–43.

Wilson, J.T., 1965, Evidence from Ocean Islands Suggesting Movement in the Earth: Philosophical Transactions of the Royal Society A: Mathematical, Physical and Engineering Sciences, v. 258, no. 1088, p. 145–167.

CHAPTER 1

Deconvolving controls of topography in Continental Lithosphere

Eduardo Guerrero and Andrew Meigs

Manuscript to be submitted to *Lithosphere*

INTRODUCTION

Whereas the topography at the Earth's surface is controlled mainly by differences in crustal and lithospheric density structure and is known as isostatic topography, mantle flow can force long-wavelength and low amplitude deformation and is transient in nature due to plate motion at the surface (Flament et al., 2013). Numerous investigations document the coincidence of broad topographic swells and hotspots in oceanic crust and attribute the deflection of the surface as a response to the interaction of mantle plumes with the lithosphere (Morgan, 1971; Crough, 1983; Hager et al., 1985; Olson and Nam, 1986). Identifying this transient topography in continental crust is complicated by the inherited topography that results from crustal thickening and thinning that results from the interaction of lithospheric plate motion (Braun, 2010; Molnar et al., 2015). In this study, we propose an approach to deconvolve topography that progressively strips away inherited topography and explores the long-wavelength structure of the lithosphere in the vicinity of the Yellowstone hotspot.

The earliest development of the transient topography concept focused on homogeneous oceanic lithosphere (Crough, 1983). Recent work points to transient topography driving phenomena ranging from drainage reorganization of continent-scale rivers, patterns to uplift and subsidence in mountain belts, and to marine inundation of continents (Wegmann et al., 2007; Carminati et al., 2009; Karlstrom et al., 2012; Saleeby et al., 2012; Shephard et al., 2012; Braun et al., 2013; Nereson et al., 2013; Heller and Liu, 2016). Whereas processes associated with lateral motions of lithospheric plates leads to high amplitude (< 4 km) and variable (10 - 100's km) wavelength topography in the continents (Molnar, 1988), low amplitudes (~1 km) and long wavelengths (100 to 1000's km) characterize transient topography (Lowry et al., 2000; Braun, 2010; Becker et al., 2013; Flament et al., 2013; Heller and Liu, 2016). Identification of the surface

expression of transient topography related to hotspots beneath continental lithosphere is complicated by inherited topography that results from solid Earth and surface processes (Braun 2010).

The focus of this study is to determine if there is a correlation between long wavelength surface topography and the geophysical data that has been used to describe the hotspot. We assess the implications for surface uplift and deformation signal in North American crust as it passes over the hotspot in the Greater Yellowstone area (Figure 1.1, 1.2, and 1.3). Deconvolving the preserved signals in topography highlights those characteristics of continental crust topography not explained by crustal processes, and may be attributable to other controlling mechanisms. We identify macrogeomorphic features (>1km) associated with crustal processes and the known geologic record in order to characterize the surface expression of plume-lithosphere interactions in the Yellowstone region.

A lithospheric-scale cross section reveals the relationship between the Yellowstone plume and North American lithosphere (Figure 1.4). A P-wave velocity anomaly is interpreted as mantle that is hotter than the surrounding material, and it is associated with the Yellowstone plume (Schmandt and Humphreys, 2010). The low velocity zone extends beneath the Snake River plain from Yellowstone (denoted by star in figure 1.4), and is interpreted as plume head being sheared as North America passes to the southwest (Humphreys et al., 2000; Pierce and Morgan, 2009; Puskas and Smith, 2009; Schmandt et al., 2012). Evidence that suggests that a transient topographic deflection related to the Yellowstone hotspot includes: (1) The highest geoid values in North America correlate with the position of the Yellowstone Volcanic Field (Figure 1.5) (Humphreys et al. 2000; Pierce & Morgan 2009). (2) Low velocity mantle that extends under the Snake River Plain with a width of 200 km (Schmandt et al. 2012). (3) Analyses of seismic

tomography and gravity datasets that point to topography supported by vigorous mantle flow (Lowry et al. 2000; Becker et al. 2013), and (4) a parabolic region of high topography, high relief, and concentrated seismicity surrounding the caldera (Figure 1.2) (Anders et al., 1989; Pierce and Morgan, 2009; Smith et al., 2009)

Deconvolving the transient topography signal is complicated by the fact that the lithosphere changes in thickness from West to East (Figure 1.4) (Lowry et al. 2000; Smith et al. 2009). Thus, in spite of the fact that a mantle plume underlies the North American plate beneath the Yellowstone region (Saunders et al., 1992; Lowry et al., 2000; Pierce and Morgan, 2009; Puskas and Smith, 2009; Schmandt and Humphreys, 2010; Becker et al., 2013), the scale and impact on the landscape evolution of transient topography is not well resolved (Riihimaki et al., 2007; Pierce and Morgan, 2009; Karlstrom et al., 2012). We present an approach to deconvolve the controls of topography in a continental setting as a first order link between surface topography and sub-lithospheric processes.

Timing and Processes in Regional Geologic Provinces

Detection of the transient topography signal on the surface requires accounting and understanding the series of geologic processes that make up present topography. The greater Yellowstone area's landscape and geologic character is the result of of 2.8 Ga of evolution where there is a spatial and temporal variability, and these signals preserved in the topography must be deconvolved in order to assess the influence of present-day dynamic topography on the region's landscape.

Whether the Yellowstone hotspot volcanism formed due to mantle plume processes is debated. One camp argues that crustal processes localize magmatism at Yellowstone (Christiansen et al., 2002). Seismic velocity data cited by Christiansen et al. suggest that a thermal anomaly

beneath the Yellowstone caldera resides near the base of the North American plate and extends no deeper than 200 km. Alternatively, observations and analyses of seismic velocity, thermal data are describe a complex thermal structure beneath Yellowstone that is interpreted as a plume because of a distinct thermal anomaly that exists to depths of 660 - 700 km (Humphreys et al., 2000; Smith et al., 2009; Schmandt et al., 2012; Becker et al., 2013). Additionally, P-wave velocity perturbation (V_p) data interpreted from seismic tomography datasets (Schmandt et al., 2012) at 100 km depth beneath the Yellowstone region indicates that the slowest travel times for these waves is correlated with the position of the Yellowstone Volcanic field, making the transition from Yellowstone to the surrounding areas the largest V_p gradient in Western North America. Regardless of the depth of origin, the track of the hotspot preserved by age-progressive calderas indicates that the hotspot has remained relatively fixed as North America since 12.7 Ma (Figure 1.1) (Christiansen, 2001), and any transient topography signal must have been advected through the crust accompanying the plate motion.

The present location of the hotspot is identified on the surface by the Yellowstone Volcanic Field, which developed in crust characterized by Late Mesozoic - Early Cenozoic Crustal shortening, Middle-Late Cenozoic extension, volcanism and Pleistocene glaciation (Figures 1.2 and 1.3). Prior to the Laramide Orogeny, the Yellowstone region existed as a broad Late Cretaceous foreland basin with continuous marine facies (Dickinson et al., 1988). Crustal shortening during the Laramide orogeny between 75 and 50 Ma created the Bighorn Basin due shortening between the Beartooth basement cored uplift to the west, the Pryor mountains in the north, the Bighorn mountains in the east, and the Owl Creek mountains in the south (Fig. 1.1) (DeCelles, 2004). Syntectonic alluvial fan deposits preserved along the fringe of the Bighorn Basin suggests that Laramide crustal shortening created topographic relief in excess of 1-2 km between

~73 and 55 Ma (DeCelles et al., 1991). More than 5 km of sediment accumulated in the Bighorn Basin between the early Paleogene and Pliocene (Dickinson et al., 1988). Apatite fission track cooling ages from samples in the Beartooth Mountains range from 61 to 52 Ma document cooling associated with this thrust event (Peyton et al., 2012). Track length and thermal modeling indicates a second period of cooling started after 15 Ma and continues through present.

A period of arc magmatism in the Eocene associated with rapid shallow subduction and back arc extension followed the Laramide orogeny (Feeley, 2003). Volcanism began in British Columbia, and swept southeastward through Challis volcanic field in Idaho before reaching its easternmost extent in the Absaroka volcanic field (Figures 1.1 and 1.3) (Hiza, 1999). Long wavelength (>1000 km) tilting that has been ongoing the end of the Laramide orogeny is thought to be an additional driver of late Cenozoic landscape evolution (Mitrovica et al., 1989; Riihimaki et al., 2007). The tilting resulted from lithospheric rebound following dynamic subsidence caused by the passage of the subducting Farallon plate (Mitrovica et al., 1989).

The presence of north-south trending ranges and basins to the north and south of the Snake River Plain reflects the period of Basin and Range extension (Figure 1.3) (Sears et al., 2009; Sears, 2013). Extension in the vicinity of Yellowstone began in the middle Miocene (McQuarrie and Rodgers, 1998). Estimates for extension in this region range from 50-80 km and the structures are half-grabens bounded by normal faults and tilted horst blocks (Sears et al., 2009). The Teton and Madison Ranges are the easternmost extensional features in the Yellowstone area. Exhumation of the Teton range began at 9 Ma (Roberts and Burbank, 1993). Faults bounding the Madison Range are thought to have been active over the same time period (Stickney and Bartholomew, 1987). Strain continues to be partitioned on both the Madison and Teton faults.

The voluminous eruptions of the Columbia River and Steens Mountain flood basalts are considered to be the earliest record of Yellowstone hotspot activity (Camp, 1995; Camp, 2013). A northeastward-younging progression of volcanic centers from eastern Oregon to the Yellowstone caldera constrain the direction and rate of motion of the North American plate with respect to the plume (Figure 1.1) (Pierce and Morgan, 2009). The first volcanic center that formed at 15 Ma is the McDermitt caldera complex, then the Owyhee-Humboldt complex developed between 13.8 and 12 Ma (Pierce and Morgan, 2009). Calderas from southwest to northeast distributed along the Snake River Plain include the Bruneau-Jarbridge, which was an active rhyolitic eruptive center from 12.5-11.2 Ma, the Picabo Volcanic Field was active between 10.3 and 8 Ma, the Heise volcanic complex was active from 6-4 Ma, and finally the Yellowstone Volcanic Field formed after 2 Ma (Pierce and Morgan, 2009). The eruptive period at each individual volcanic center lasted approximately 2 Ma. Roughly 150-200 km separates each center (Figure 1). Spacing between the eastern margins of calderas suggests that rate of plate motion with respect to the hotspot slowed from 7 cm/yr to 2.9 cm/yr after 10 Ma.

The series of sub-aerial volcanic centers in the Snake River Plain represent the primary evidence of the track of the Yellowstone hotspot through the North American plate (Figure 1.3) (Pierce and Morgan, 1992; 2009; Smith et al, 2009; Christiansen, 2001). Hotspot volcanism in the YVF began at 2.1 Ma with activity that led to the eruption of the Huckleberry Ridge Tuff at 2.1 Ma and the formation of the 75-90 km long caldera (Christiansen, 2001). Two more caldera forming eruption cycles have taken place at 1.3 Ma (Mesa Falls) and 0.66 Ma (Lava Creek), with each cycle consisting of multiple bi-modal volcanic eruptions (Christiansen, 2001).

The Snake River Plain (SRP), is an arcuate West-East trending topographic and structural depression that is the combined result of Yellowstone hotspot volcanism and Basin and Range

extension, which is generally divided into Western and Eastern segments (Figure 1.3) (McQuarrie and Rodgers, 1998; Beranek et al., 2006). The Western SRP is a Northwest trending extensional basin that is roughly 70 km wide and 300 km long that was active between 11 and 9 Ma (Wood and Clemens, 2002; Beranek et al., 2006). The top 1-2 km of the western SRP consists of sedimentary cover and basin fill. Seismic surveys reveal a strongly mafic composition of the crust to a depth of 42 km beneath the basin fill (Wood et al., 2002). The Eastern SRP (ESRP) trends northeast that reflects the combined thermal contraction, volcanic and sediment loading, and the injection of dense mafic magma into the middle crust as North America passes over the Yellowstone hot spot (McQuarrie and Rodgers, 1998; Rodgers et al., 2002). The SRP creates a topographic and lithospheric dichotomy (Anders and Sleep, 1992). Subsidence at the northeast edge of the SRP creates a parabolic form in the high terrain (Anders et al., 1989; Wegmann et al., 2007; Pierce and Morgan, 2009). Seismicity and active faulting in the parabola occurs in the regionally extensive inter-mountain seismic belt and rheological differences accounts for the lack of active faulting within the subsiding volcanic basin (Smith and Sbar, 1974). This topographic form is a central piece of evidence that the parabolic distribution of seismicity in the region is an expression of plume-lithosphere interactions (Anders and Sleep, 1992).

The dramatic relief that dominates the Rocky Mountain landscape (Figure 1.6) reflects the result of intermittent and cyclical Pleistocene glaciation associated with Late Cenozoic cooling climate conditions (Small and Anderson, 1998). The record of glaciation in the Yellowstone region extends to roughly 170 ka. Well-constrained moraine cosmogenic chronologies indicate that alpine glaciation in the Rocky Mountains and western US are complex and glacier behavior (Moss and Bonini, 1961; Licciardi and Pierce, 2008; Thackray, 2008). Glacial events in the Cordillera are still generally recognized by their regional terms and are roughly correlated with

marine oxygen-isotope stages (MIS): Pre-Bull Lake, which is pre- MIS 6 or older than 160 ka; Bull Lake, thought to be MIS 6 and possibly 5d; early Wisconsin, which would be MIS 4, and Pinedale, which would be part of the Last glacial Maximum at 20ka (Pierce, 2003). Recessional moraines indicate that a major ice cap occupied the Yellowstone plateau during Pinedale until approximately 14 ka ago (Licciardi and Pierce, 2008).

Transient Topography in the Yellowstone Region

Geoid models are based on gravity measured at the Earth's surface and variations are the result of the opposing effects of density contrasts in the mantle and mass anomalies driven by mantle flow (Hager et al., 1985). Long wavelength (>1000 km) variations of the Earth's geoid have been interpreted as the topographic expression of deeper mantle convective processes (Hager and Richards, 1989). The highest geoid values observed in the continental United States is centered on the Yellowstone Volcanic Field (Figures 1.5 and 1.8). The geoid combines the effects of uncompensated high topography as well as zones that are underlain by lower density/hotter material (Hager et al., 1985; Smith et al, 2009). The geoid values centered on Yellowstone are over +12 m higher than the surrounding area, which translates to a positive gravity anomaly of 35 mGals (Smith et al., 2009).

Pierce and Morgan (1992; 2009) propose that Yellowstone hotspot is expressed topographically. They described the Yellowstone Crescent of High Terrain (YCHT) as being similar to the bow-wave of a ship, a topographic wave where incipient uplift is defined by an area of waxing topography, the apex of uplift in the region of highest topography, and a region of waning topography with subsidence in the wake (Figure 1). The YCHT corresponds with a parabolic region of seismicity, the so called tectonic parabola (Pierce and Morgan, 1992).

Comparison with oceanic hotspots and on the correspondence between the geoid high and the caldera, Pierce and Morgan maintain that the YCHT resulted from deformation of the North American plate above the mantle plume. Lowry et al (2000) synthesized elevation data, gravity, crustal-scale seismic refraction, and surface heat flow data in an attempt to isolate the dynamic topography in the Yellowstone region. Recognizing that the topography reflects the integrated effects of tectonism, volcanism, plate properties, and mantle buoyancy, their model sequentially subtracted the inferred contribution of each variable to arrive at the dynamically supported topography. Model results reveal dynamic topography that is asymmetric in the direction of plate motion, with a gentle SW slope and steep NE slope. The scale of the dynamic topography swell varies depending on the resolution of the data used in the analysis, an amplitude of 1.5 km and a 400 km wavelength or 2 km, and a ~1000 km wavelength (Figure 1.2) (Lowry et al., 2000; Becker et al., 2013).

METHODS

Geoid Analysis

The geoid is the equipotential surface of the gravity field that coincides with the ocean surface. It is more sensitive to than gravity to deeper and large scale density variations in the mantle, therefore it helps make observations of deeper mantle processes (Humphreys et al., 2000). Deviations from the predicted geoid are a result of mass differences within the Earth. The relationship between the geoid and gravity comes from the realization that gravitational attraction is proportional to $1/r^2$, where r is the distance from the subsurface mass; and gravitational potential is proportional to $1/r$. Thus, the geoid is representative of processes in the mantle and is a first order identifier of regions of the lithosphere where transient topography may be expected to occur (Davies, 2001; Turcotte and Schubert, 2002).

We present a simple analysis of the 2012B Geoid model (NOAA, Appendix 1.4) centered on the greater Yellowstone area (Figure 1.5). A significant body of work has demonstrated that the total geoid is positively correlated with seismically inferred density anomalies in the mantle (Hager et al. 1985), and particularly that geoid highs correlate with active hotspots (Richards et al., 1988). Geoid highs measured in oceanic lithospheric settings are correlated with active hotspots and the associated bathymetric swells that are interpreted to be the result of plume-lithosphere interactions (Richards et al., 1988; Kiefer and Hager, 1992; Saunders et al., 1992; Cazenave, 1995).

Topographic Analysis

Multiple wavelength low pass filters were used to analyze void-filled Shuttle Radar Topography Mission (SRTM) data in ArcGIS 10.21. We characterize the wavelength of different features preserved in the topography based on the greater Yellowstone area's maximum, mean, and minimum elevation profiles from 30m DEM SRTM dataset. We created a mosaic using the individual DEMs. Progressive smoothing removes high frequency and short wavelength topographic signals (Wegmann et al. 2007). A 100 km filter removes all topographic features that have a wavelength <100 km and preserves topography for features >100 km (Wegmann et al., 2007). The regional DEM was first resampled to a 500 m resolution in ArcMap. A moving window was passed through the DEM. Mean elevation of pixels in the moving window and the resulting mean values was re-plotted in each individual pixel (Brozovic et al., 1997). The neighborhood statistics tool allowed low- pass filtering of the DEM at 100 km, 150 km, and 200 km wavelengths. We compared the topography at these wavelengths with the locations and areal extent of the regional geologic provinces.

Topography results from crustal processes that have taken place over geologic time in a particular place (Pazzaglia and Brandon, 2001). Major geologic events contribute to the thickness of the crust, and influence mean regional elevation. Figure 1.2 is a kinked swath that begins at 44°N, 116°W and follows the hotspot track all the way to 46°N, 109°W. Figure 1.1 illustrates the location of the three additional profiles presented in Figure 5: A-A', B-B', and C-C'. We selected the location of the swaths to correspond with northern, central, and southern portions of the greater Yellowstone region. Swath profile extraction is useful for assessing longer wavelength topographic features because it removes noise associated with shorter wavelength topography and high relief (Wegmann et al. 2007). Mean elevation permits first order observations of tectonic processes that support crustal elevation (Coblentz and Karlstrom, 2011; Cassel et al., 2012).

The northernmost swath is taken from the westernmost Snake River Plain across the Idaho Batholith, Idaho-Montana Basin and Range, Sevier fold and thrust belt, and the Laramide foreland province. The central swath is taken along the Snake Rive Plain, crossing Snake River Plain, Yellowstone volcanic center, and the Beartooth mountains, which are a basement cored uplift in the Laramide foreland province. The southernmost swath extends from the Utah Basin and Range to the Bighorn Mountains, crossing the Wasatch front, Green River Basin, Wind River Mountains and the southern Bighorn Basin. We extracted a 4^{th} order polynomial regression for each mean elevation profile, which represents the long-wavelength structure of the lithosphere (Wegmann et al. 2007).

RESULTS

Analyses reveal the macrogeomorphic character of the Greater Yellowstone region that permits deconvolution of crustal from lithospheric controls on topography. Mean elevation maps sequentially remove crustal scale imprints on topography and reveal the long wavelength

topography. Swath profiles (Figures 1.2 and 1.6) identify physiographic features and topographic wavelengths associated with specific geologic events that contribute to the topographic nature of the region. Filtering Digital Elevation Models at multiple wavelengths (Figure 6) strips progressively longer wavelength crustal contributions to the region's topography to reveal long wavelength structure of the lithosphere in this region. We compare the long wavelength topography to a degree 1 filtered version of the GEOID12B model (Hager et al., 1985; Hager and Clayton, 1989, Appendix).

Topographic Analysis

We used the topographic wavelengths identified from Figure 1.6 to determine the appropriate filter wavelength that removes identified contributing geologic mechanisms to the region's elevation. The northern swath was taken between 46.6° to 47.1° N and is 900 km long, the polynomial regression applied to the mean elevation curve maintains an elevation between 1800m and 1500m from Km 0 at the western end of the swath until km 500 (Figure 1.6 A). This mean elevation is maintained by the northern Rocky Mountains, and does not include other physiographic provinces, the swath crosses the Idaho Batholith (IB), Centennial Tectonic Belt (CTB), and the Laramide Foreland Province (LFP). This swath includes mean elevation decreases east of the Crazy Mountains as the topography transitions away from the Rockies. The central swath passes over the Yellowstone volcanic field (YVF) and is identified by a star. The topography for the first 600 km of the swath maintains an elevation between 1800m and 2600m, with the peak in elevation occurring west of the YVF (Figure 1.6B). The shape of the mean elevation profile is nearly identical to Figure 1.6A, but has overall higher mean elevation values. The southern swath begins in the Basin and Range with high relief, low mean elevation (6A). The maximum mean elevation is centered on the Wind River Mountains (WRM) at just over 2500m, however the mean

elevation profiles is 300m lower at its apex than the mean elevation in the central swath. From the swath profiles, it is possible to determine the wavelength of the various processes preserved in the topography: Glacial and fluvial erosional processes have a wavelength which is <5 km, Volcanic wavelengths (<100 km), Basin and Range extension (<150 km), Laramide structures (<200 km) (Figure 1.6). Progressive filtering of SRTM datasets strips crustal and smaller-scale topographic features and reveals lithospheric scale features.

The 150 km filter smoothes Basin and Range fault controlled topography associated with crustal thinning. The wavelength of Laramide thickened crustal contributions to elevation is between 150 km and 200 km. This filtering smoothes the Bighorn and Beartooth mountains which occur in the LFP, and are basement cored uplifts separated by the intervening Bighorn Basin and are the result of Laramide shortening (DeCelles, 2004). These structures are visible with the 100 km filter, yet they smoothed at the 150 km wavelength. The 200 km wavelength filters all known geologic forcing mechanisms that contribute to the region's compounded topography.

The mean elevation along the southern profile is higher than 2000 m between ~km 150 and 500 and coincides with thickened Laramide crust and extended Sevier Belt topography. The position of the 2000 m contour to the northwest of Yellowstone outlines the Beaverhead Mountains, which are Laramide in age, and these also contribute to the mean elevation distribution of the region. The Beaverhead Range contribution is visible in 1.6C, since it creates a noticeable bump in the 2000 m contour. The Laramide structures, particularly the mountain ranges east and south of Yellowstone dominate the 100 km filtered topography. The wavelength of the Laramide basins is generally close to 100 km, because the imprint of the Bighorn basin on elevation begins to disappear when filtered at this wavelength. When the dataset is filtered at a 200 km wavelength (7D), we see the Laramide range and Snake River Plain structures dominate the long wavelength

topography. The tectonic parabola/ crescent of high terrain is an artifact of the SRP and B&R superimposed upon a region characterized by high mean elevation is well well represented to the North and East of the SRP.

Figure 1.8 compares the 200 km- filtered topography and the geoid along A-A', B'-B", and C-C' (Figure 1.8) that illustrate the correlation between geoid analysis results and the 200 km-filtered topography. All three profiles illustrate that the filtered geoid coincides with the shape of long wavelength topography across the the northern, central, and southern regions surrounding Yellowstone. In all three cases, the 200km filtered topography is what remains once all known topographic wavelengths have been stripped. This comparison suggests that the long wavelength topography represents transient topography associated with the hotspot. This inference is particularly well supported where there is good correlation between the long wavelength and filtered geoid along profile B'-B". Additionally, the 4^{th} order polynomial curve calculated from the mean elevation from figure 1.2 and Becker et al's (2013) analysis of dynamically supported topography in the Yellowstone region.

Model for Advection of Transient Topography

Having identified the transient topography and given the 29 mm yr^{-1} rate of motion of North America over the hotspot, it is possible to do a first order calculation for the rate of surface uplift that should accompany the advection of the transient topography. There is 1200 m difference in mean elevation between the apex and trough at the leading edge (north eastern) of the transient topography. This is confirmed because the same mean elevation relief is extracted from the 4^{th} order polynomial curve (Figure 1.2).

Figures 1.9 and 1.10 illustrates our preferred interpretation for advection of topography in space and time with conditions expected in the Yellowstone region. North American lithosphere

is passing over the Yellowstone hotspot at a rate of 29mm $yr^{-1}$and is moving towards the southwest relative to the hotspot. Abbreviations correspond to positions in space and time along the track of the hotspot for the Yellowstone-related transient topography. Spatial correlations were determined by the distance separating each of the major associated volcanic centers (Picabo, Heise, and Yellowstone) and one physiographic/tectonic boundary (western edge of the Bighorn Basin). Time was determined from youngest major erution associated with each one of the place-mark volcanic centers (Smith et al., 2009). The apex of the dynamic topography wave as it passes over the hotspot. The lower panel gives predicted uplift and subsidence rate associated with each time stamp. Results indicate that maximum uplift rate of 0.17 mm yr^{-1} aught to lead the apex of the dynamic topography swell by nearly 100 km. This means that presently, the western Bighorn basin is experiencing the effects of transient topography. Subsidence accompanying advection of the swell is the result of the combined effect of the surface being let down as the transient topography passes over the hotspot in addition to geomorphic agents acting on the uplifted surface, and the addition of dense mafic crust injected into the crust once it has been positively deformed as it passes over the plume (McQuarrie et al., 1998) .

DISCUSSION

The two-step analysis of topography presented in this study allows the identification of upper plate or crustal contributions to topography. First, swath profiles isolates and characterizes the relationship between geologic provinces and their associated wavelength. Once the wavelength for the features is determined, filtering a DEM at progressively longer wavelengths reveals long wavelength topographic features masked by shorter wavelength signals. For example, the wavelength of the Bighorn basin is 100km (Figure 6C), when a 150km filter is applied to the DEM

the contribution of Laramide shortening to topography is removed and reveals the long-wavelength topography.

Long wavelength topography reveals the shape and extent of transient topography associated with the hotspot, which extends for ~600 km along the Snake River Plain and has a minimum amplitude of 400 m and a maximum amplitude of 1200 m. Amplitudes were determined by measuring the difference between the maximum and minimum mean elevations (Figure 1.9 and 1.10). The 400 m minimum amplitude is determined from the 200 km filtered mean elevation maps and the maximum swath size was identified from the 4^{th} order polynomial (Figure 1.9). The wavelength was measured from the northeastern termination of the swell in the Bighorn Basin to the southwestern edge of the Snake River Plain. This analysis reconciles surface long wavelength topography characteristics with geophysical interpretations. Becker et al., (2013) predict a dynamic topography swell with a maximum amplitude range between 1 and 2 km and a wavelength between 600 and 1000 km in the Yellowstone area, depending on the model used for mantle circulation patterns. There is a strong correspondence between the long-wavelength topography and the predicted spatial extent of Becker et al.'s dynamic topography from the Beartooth Mountain front, north-east of Yellowstone volcanic field to the Idaho, Oregon, Nevada border (Figures 1 and 3). The shape of the long wavelength topography coincides with the asymmetric shape of the Becker et al.'s (2013) dynamic topography results. Additionally, there is agreement between the long wavelength topography and the filtered geoid (Figures 1.8 and 1.9). This reinforces the interpretation that long wavelength topography is proxy for deformed lithosphere that is independent of upper plate or crustal contributions to topography. Lowry et al.'s 2000 analysis (Figure 1.2) predicts dynamically supported topography that does not include the Beartooth mountains or adjacent basins. Becker et al.'s approach follows the methods outlined by

Lowry et al., but relied on higher resolution datasets and improved global and regional mantle circulation models; and this explains the discrepancy between these two results. There is good correlation between the wavelength of dynamically supported topography and the transient topography results of this study when we compare the long wavelength topography extracted from the 4th order polynomial and Becker et al.'s (2013) results. The wavelength of the transient topography that is perpendicular to the track of the hotspot is difficult to determine with this analysis.

Anderson (1990, 1994) first described advection of topography as the result of displacement through a restraining bend in the San Andreas fault. Advection occurs as patterns of coseisimc rock and surface uplift as crust passes over the uplift source and is followed by interseisimic relaxation and geomorphic decay and the thermal subsidence and crustal densification driven by mafic magma eruptions (McQuarrie et al., 1998). This study provides the dimensions of dynamic topography in the Yellowstone area, and we know the velocity of advection. Application of the model allows us to make a first order prediction that changes in surface uplift rates associated with Yellowstone transient topography. According to this analysis, there is a surface uplift rate propagating through the western edge of between 0.166 and 0.302 mm yr^{-1} but there is the potential that between 400 and 800m of surface uplift has occurred at the western edge of the basin since 3 Ma. The slope of the transient topography as it enters the Bighorn Basin is between 0.3° and 0.5°(Figure 1.10).

CONCLUSION

Interaction of the Yellowstone hotspot and the North American lithosphere has influenced the landscape evolution the Yellowstone region, namely through volcanism, deformation by advection of transient topography deflects the lithosphere by up to 1.2 km at its peak. Our results

illustrate a good correlation between analysis of surface data and geophysical proxies for the hotspot, which allows us to interpret long wavelength topography as the transient topography associated with the hotspot. There is maximum surface uplift rate between 0.166 and 0.302 mm yr^{-1} expected at the leading edge of the advecting topography and a maximum subsidence rate of 0.01 mm yr^{-1} at the trailing end of the transient topography (Figure 1.10). We consider it a tractable problem and future work on constraining landscape response to these styles of deformation, in particular drainage basins ahead of the advecting wave of topography will provide insight to the surface expression of hotspot-related transient topography in a continental setting.

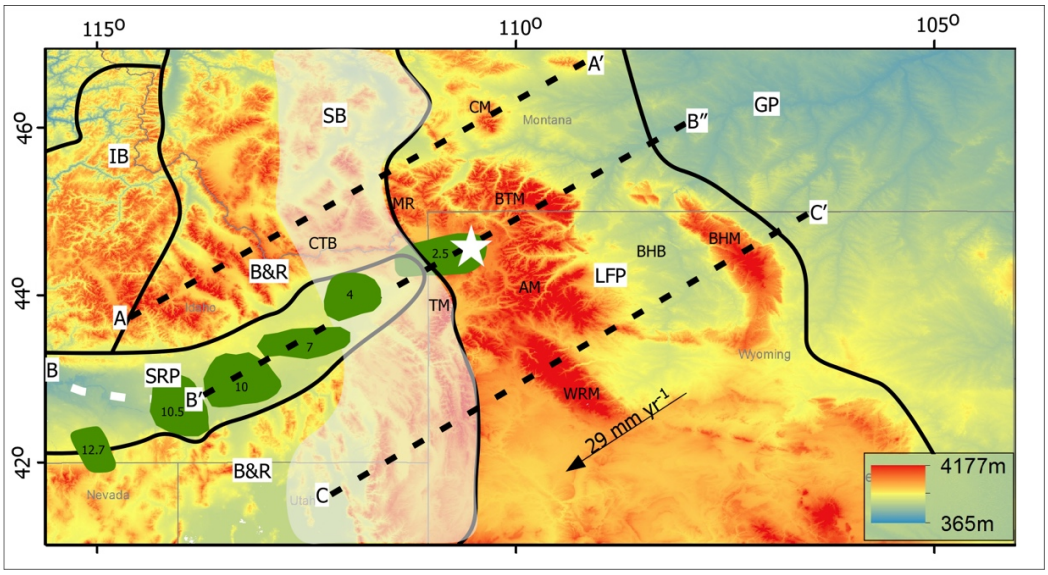

Figure 1.1 Regional topography and geologic provinces of the greater Yellowstone area. Star denotes the Yellowstone Caldera, a 2 Ma-old rhyolitic eruptive center (Christiansen, 2001). Thick lines enclose major tectonic provinces. The Snake River Plain (SRP) is the track of the Yellowstone hotspot and is an actively subsiding volcanic basin (McQuarrie et al. 1998). The Sevier fold-thrust belt (SB) is part of a thin-skinned thrust system which initiated in late Jurassic time (DeCelles, 2004). The Laramide foreland province (LFP) is characterized by basement-cored ranges and intervening sedimentary basins (Dickinson et al., 1988). The Idaho batholith (IB) is part of the Cordilleran magmatic belt (DeCelles, 2004) and is Late Cretaceous (Hyndman, 1983). The Great Plains province (GP) is a region that contains little to no evidence of Sevier or younger deformation and is considered part of the stable craton (McMillan et al., 2006). Subsequent extension began after 30 Ma (Smith et al., 2009). Basin and Range (B&R) extensional structures overprint the western SB and the Idaho Batholith. Dashed lines represent locations of profiles presented in figures 1.3 (B-B"), 1.6 , and 1.8 (A-A', B'-B", C-C'). BTM-Beartooth Mountains, AM- Absaroka Mountains, BHB-Bighorn Basin, BHM-Bighorn Mountains, MR- Madison Range, TM-Teton Mountains, CTB-Centennial Tectonic Belt, CM-Crazy Mountains. 29 mm yr-1 is the motion of North America with respect to the Yellowstone hostpot, based on geochronology of silicic eruptions along the Snake River Plain (Pierce and Morgan, 2009; Smith et al., 2009).

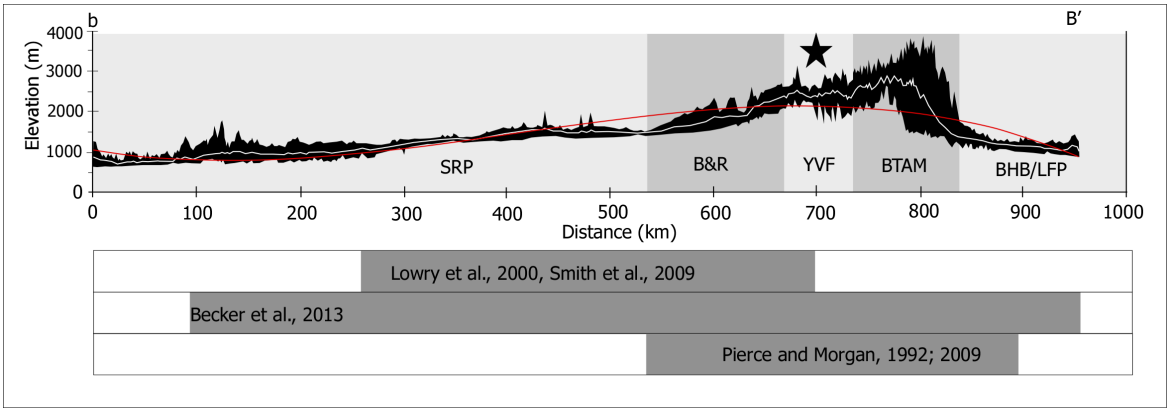

Figure 1.2 Hotspot track swath profile. Elevation profile extracted from a 100 km-wide swath along the Snake River Plain (B-B") (Figure 1). Top profile is maximum elevation, bottom profile is minimum elevation, and white profile is mean elevation. Red curve is 4th order polynomial of the mean elevation and represents an approximation to the long-wavelength topography of the SRP-GYA region. Gray boxes beneath profile are interpretations of extent of dynamically supported topography (Pierce and Morgan, 1992; Lowry et al., 2000; Becker et al., 2013). Geologic province abbreviations as in Figure 1.1. Pierce and Morgan's (1992) Yellowstone Crescent of High Terrain includes the Basin and Range (B&R), Yellowstone Volcanic Field (YVF), and the Beartooth/Absaroka Mountains (BTAM).

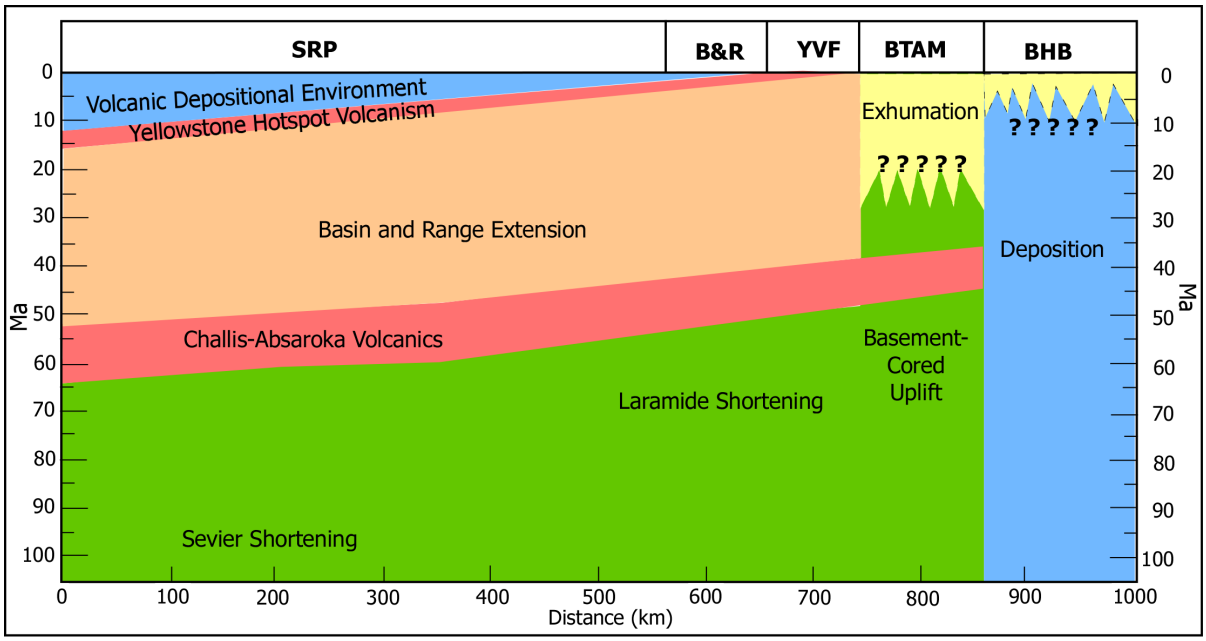

Figure 1.3 Geologic summary. Space-time diagram of the dominant geologic regimes that contribute to present topography preserved along the Yellowstone hotspot track. Spatial scale parallels that of Figure 1.2 and roughly follows the Snake River Plain. Labels above diagram indicate physiographic provinces that exist along the hotspot track. Abbreviations of geologic provinces are those of Fig. 1.1 Blue indicates deposition-dominated geologic regime, green indicates crustal shortening and thickening; peach indicates extensional regime; pink indicates volcanic activity, and yellow indicates erosion. Timing of the transition in the Bighorn basin from depositional to erosional regimes is also uncertain (Dickinson et al., 1988; Pierce and Morgan, 1992; McQuarrie and Rodgers, 1998; DeCelles, 2004; Sears et al., 2009).

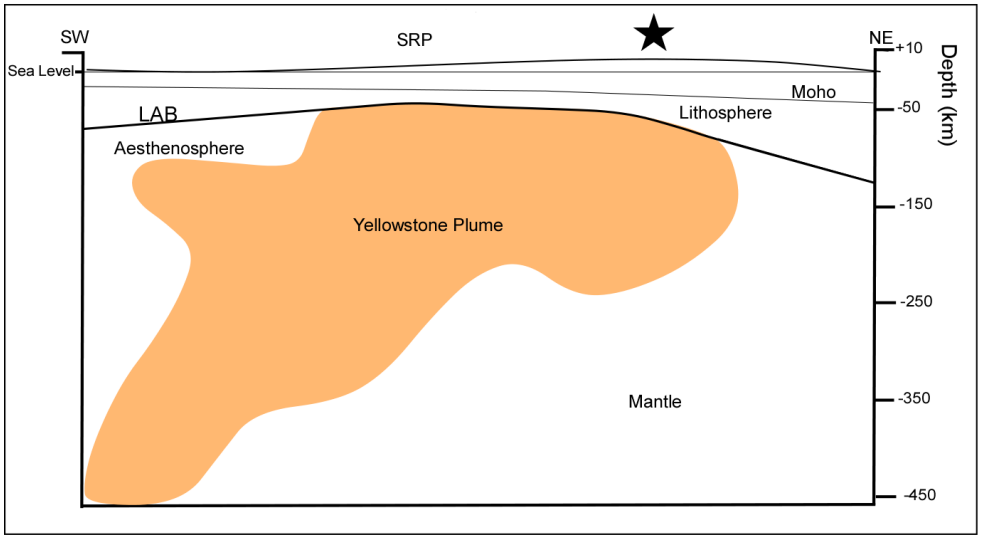

Figure 1.4 Lithosphere-scale cross section. Idealized cross section along the Snake River Plain (SRP) and Yellowstone(star) system including long wavelength topography as the transient topographic (1x VE) signal associated with the hotspot. Yellowstone plume is interpreted from Vp and Vs tomography maps as low velocity (hot) mantle (Schmandt et al., 2012). The Lithosphere-Asthenosphere boundary (LAB) and Moho depths are interpreted from Levander and Miller (2012). Surface is long wavelength topography from Figure 1.2, extracted along profile B-B".

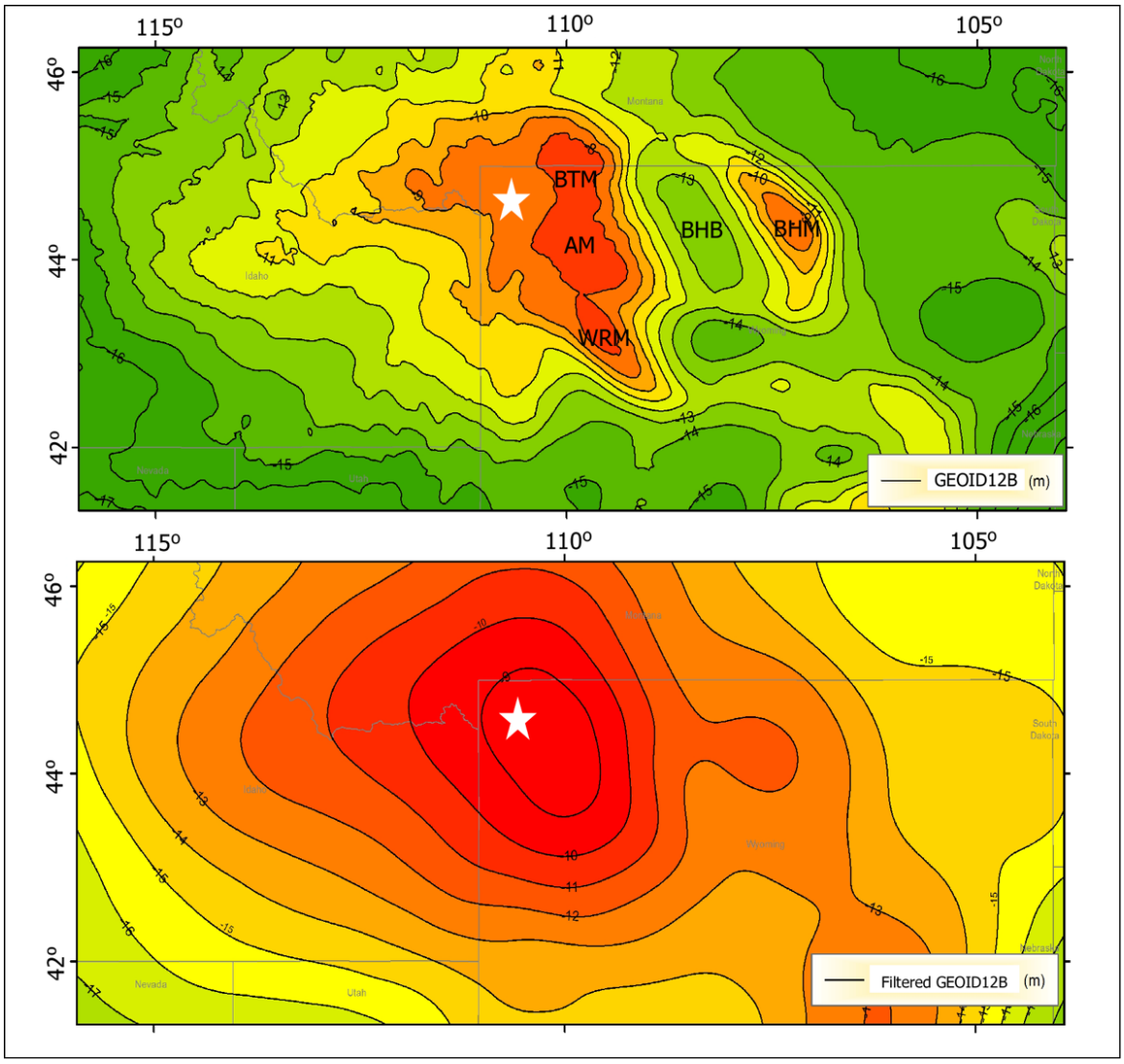

Figure 1.5 Greater Yellowston Area Geoid Values. A. Unfiltered GEOID12B model (NOAA, 2012) with 1m contour interval showing the highest geoid values in western North America are located in the GYA and are correlated with Laramide features (star). BTM, AM, BHB, and WRM included for reference. 0.5 Degree low-pass filter applied to GEOID12B model with 1m contour interval.

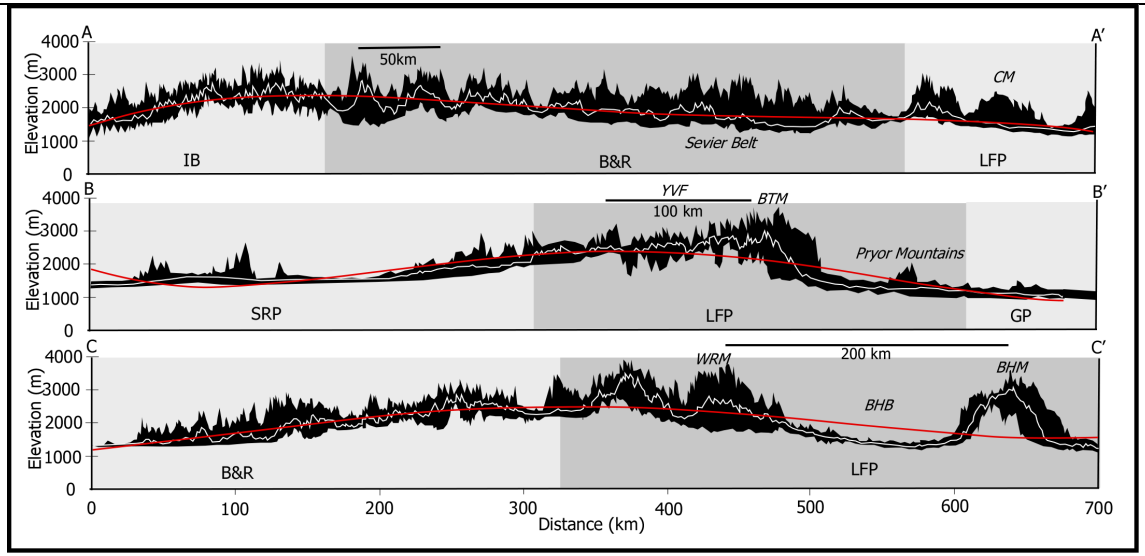

Figure 1.6 Swath Profiles. 100km-wide swath elevation profiles extracted from SRTM DEM datasets. Maximum, minimum, and mean elevation (white). Red curve is 4th order polynomial of mean elevation and reveals long wavelength topography along each profile. Profile A is northernmost profile and crosses Idaho Batholith (IB), Basin & Range(B&R), Sevier and Laramide Foreland Province (LFP). B crosses the central portion of the study area and includes the northern Snake River Plain, Yellowstone volcanic center, and Laramide foreland provinces. C crosses the southernmost portion of the study area an includes Basin & Range, Sevier, and Laramide foreland provinces. Grey boxes correspond to boundaries of the geologic provinces, labeled under profiles. Labels over profiles identify individual physiographic features. Measurements illustrate the wavelength of the individual contributors to the region's compounded topography: Laramide- 200 km, Basin and Range- 150 km, Volcanic- 75km, Glacial and Fluvial erosion- <20km. See Figure 1.1 for profile location.

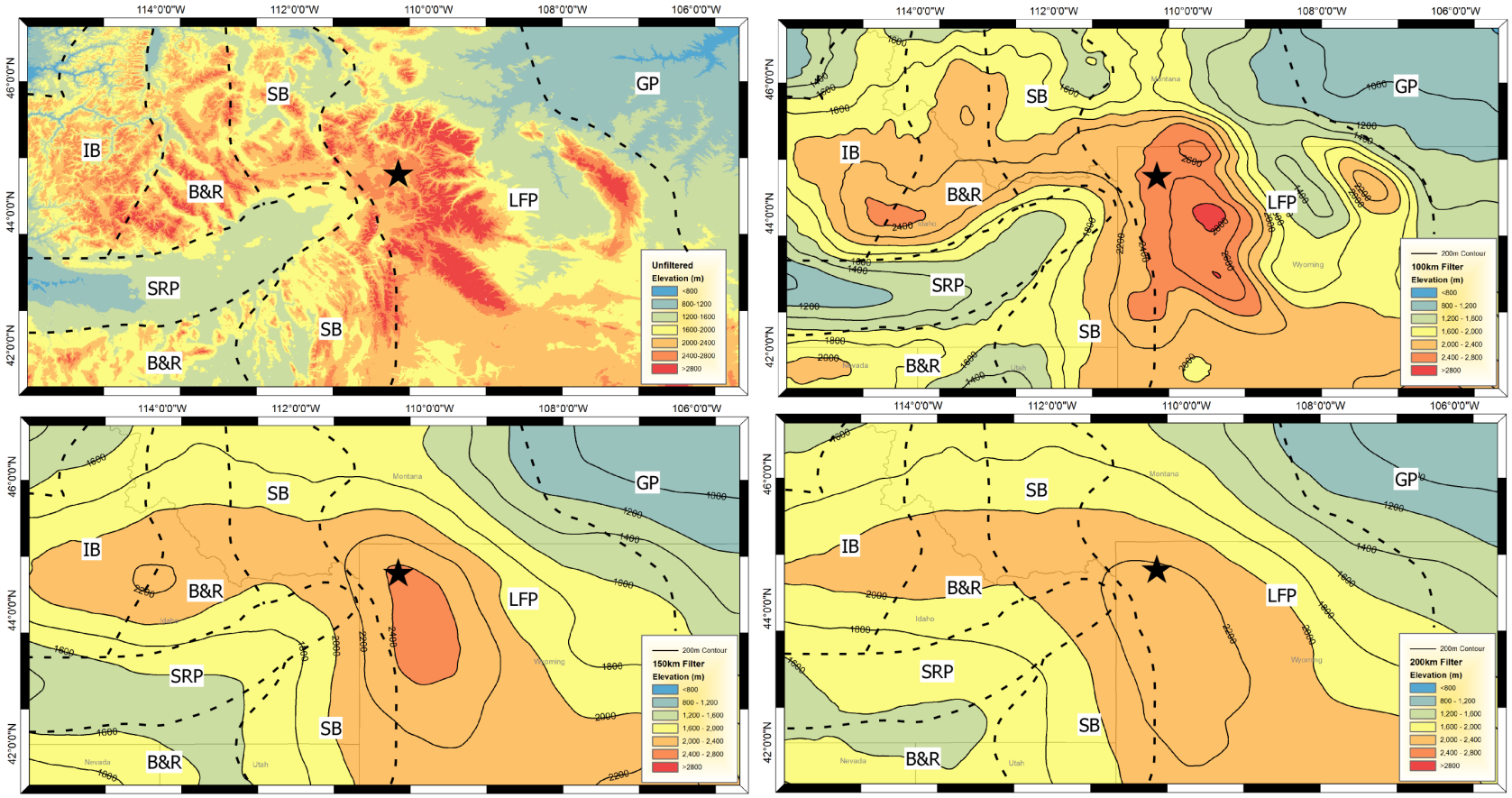

Figure 1.7 Mean elevation maps, produced by low-pass filtering SRTM 30m DEM at multiple wavelengths with 500m contour intervals. Start denotes location of Yellowstone volcanic center. A. Unfiltered B. 100 km filter C. 150 km filter. D. 200 km filter.

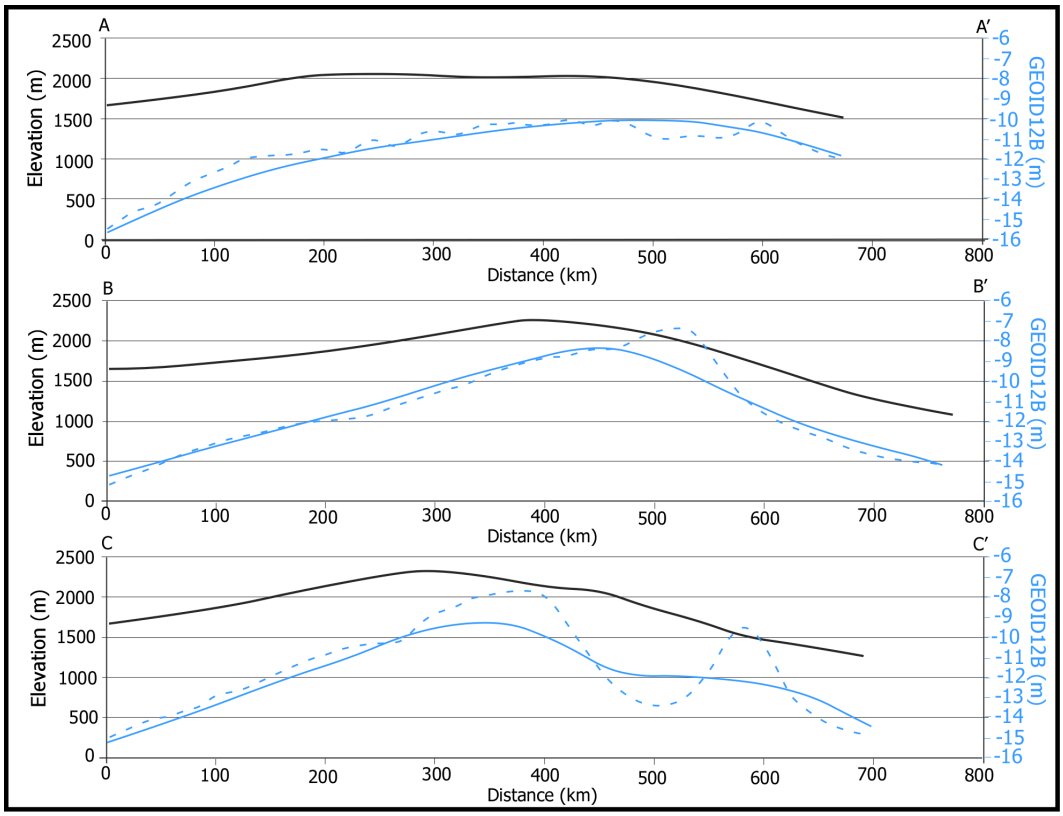

Figure 1.8 Filtered topography (black) comparison to unfiltered Geoid values(dashed blue) and filtered Geoid values (solid blue). Mean elevation data were extracted from 200 km filtered topography along the profiles from Figure 1.1 Geoid data, both filtered and unfiltered were extracted from GEOID12B (Figure 1.5 A, B). A-A' is the northernmost profile, B-B' is the central profile, and C-C' is the southernmost profile. All three profiles illustrate the close approximation of the 200 km topographic wavelength to the filtered geoid values.

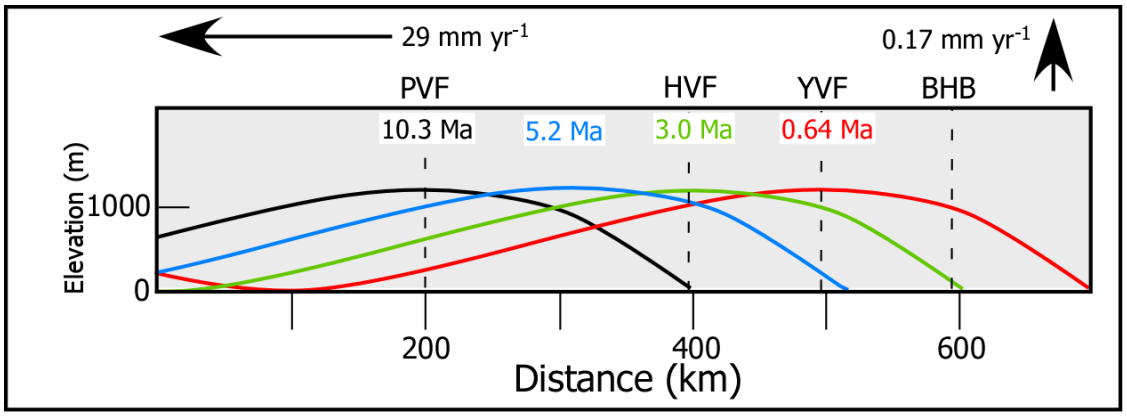

Figure 1.9 Model for advection of transient topography based on interpretation of long wavelength topography as the transient topography signal associated with hotspot. PVF is Picabo Volcanic Field, active at 10.3 Ma; HVF is Heise Volcanic Field, active at 3 Ma; YVF is Yellowstone Volcanic field, with it's last major eruption at 0.64 Ma; BHB corresponds to the western edge of the Bighorn Basin, along the front of the Beartooth-Absaroka ranges. Ages for position of the dynamic topography come from youngest caldera-forming eruption at each volcanic center. (A) Is the mean elevation, long wavelength topography that is interpreted to be dynamic topography. 0.17 mm yr^{-1} is expected surface uplift rate expected along deformation front to the northeast of the present position of North America with respect to the hotspot.

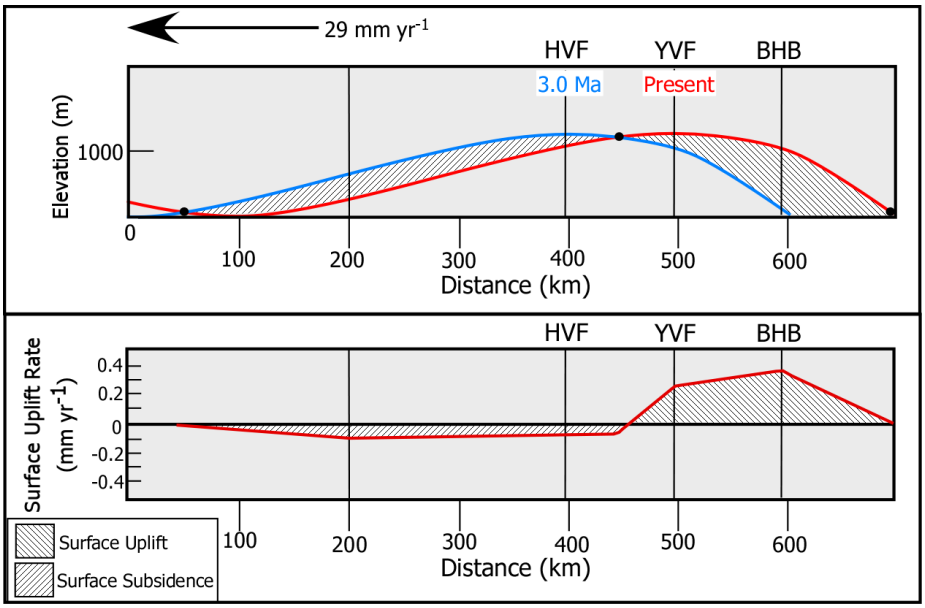

Figure 2.3 Model of surface uplift rate for past 3 Ma. Illustrates model results for shape of long wavelength topography along the track of the Yellowstone hotspot, which is interpreted to be the transient topography. Blue curve is position of transient topography at 3 Ma, red is present position of transient topography. Black dots are locations where uplift and subsidence rate is 0, where the blue curve is above represents active subsidence, where the red curve is above represents active uplift. Difference between two curves dictates rates of deformation. Maximum uplift rate of between 0.166 and 0.302 mm yr^{-1} 29 mm yr^{-1} is the rate of motion of North America with respect to the hotspot. Lower panel illustrates variations in uplift rate

REFERENCES

Anders, M.H., and Sleep, N.H., 1992, Magmatism and extension: The thermal and mechanical effects of the Yellowstone Hotspot: Journal of Geophysical Research: Solid Earth (1978–2012), v. 97, no. B11, p. 15379–15393.

Anders, M.H., Geissman, J.W., Piety, L.A., and Sullivan, J.T., 1989, Parabolic distribution of circumeastern Snake River Plain seismicity and latest Quaternary faulting: Migratory pattern and association with the Yellowstone hotspot: Journal of Geophysical Research: Solid Earth (1978–2012), v. 94, no. B2, p. 1589–1621.

Becker, T.W., Faccenna, C., Humphreys, E.D., Lowry, A.R., and Miller, M.S., 2013, Earth and Planetary Science Letters: Earth and Planetary Science Letters,, p. 1–13.

Beranek, L.P., Link, P.K., and Fanning, C.M., 2006, Miocene to Holocene landscape evolution of the western Snake River Plain region, Idaho: Using the SHRIMP detrital zircon provenance record to track eastward migration of the Yellowstone hotspot: Geological Society of America Bulletin, v. 118, no. 9-10, p. 1027–1050.

Anderson, R.S. 1990, Evolution of the northern Santa Cruz Mountains by advection of crust past a San Andreas fault bend: Science, v. 249, p. 397–401.

Anderson, R. S. 1994, Evolution of the Santa-Cruz Mountains, California, through tectonic growth and geomorphic decay: J. Geophys. Res., 99, 20,161–20,179.

Braun, J., 2010, The many surface expressions of mantle dynamics: Nature Geoscience, v. 3, no. 12, p. 825–833.

Braun, J., Robert, X., and Simon-Labric, T., 2013, Eroding dynamic topography: Geophysical Research Letters, v. 40, no. 8, p. 1494–1499.

Brozovic, N., Burbank, D.W., and Meigs, A.J., 1997, Climatic limits on landscape development in the northwestern Himalaya: Science.

Camp, V.E., 1995, Mid-Miocene propagation of the Yellowstone mantle plume head beneath the Columbia River basalt source region: Geology, v. 23, no. 5, p. 435.

Camp, V.E., 2013, Origin of Columbia River Basalt: Passive rise of shallow mantle, or active upwelling of a deep-mantle plume?: Geological Society of America Special Paper 369.

Carminati, E., Cuffaro, M., and Doglioni, C., 2009, Cenozoic uplift of Europe: Tectonics, v. 28, no. 4.

Cassel, E.J., Graham, S.A., Chamberlain, C.P., and Henry, C.D., 2012, Early Cenozoic topography, morphology, and tectonics of the northern Sierra Nevada and western Basin and Range: Geosphere, v. 8, no. 2, p. 229–249.

Cazenave, A., 1995, Geoid, Topography and Distribution of Landforms: Global earth physics a

handbook of physical constants. Edited by Thomas J. Ahrens. AGU Reference Shelf Series, p. 32.

Christiansen, R.L., 2001, The Quaternary and pliocene Yellowstone plateau volcanic field of Wyoming, Idaho, and Montana, USGS Profesisonal Paper 729-G .

Christiansen, R.L., Foulger, G.R., and Evans, J.R., 2002, Upper-mantle origin of the Yellowstone hotspot: Geological Society of America Bulletin, v. 114, no. 10, p. 1245–1256.

Coblentz, D., and Karlstrom, K.E., 2011, Tectonic geomorphometrics of the western United States: Speculations on the surface expression of upper mantle processes: Geochemistry, Geophysics, Geosystems, v. 12, no. 11, p. n/a–n/a, doi: 10.1029/2011gc003579.

Crough, S.T., 1983, Hotspot swells: Annual Review of Earth and Planetary Sciences.

DeCelles, P.G., 2004, Late Jurassic to Eocene evolution of the Cordilleran thrust belt and foreland basin system, western USA: American Journal of Science.

DeCelles, P.G., Gray, M.B., Ridgeway, K.D., and Cole, R.B., 1991, Controls on synorogenic alluvial-fan architecture, Beartooth Conglomerate (Palaeocene), Wyoming and Montana: ….

Dickinson, W.R., Klute, M.A., Hayes, M.J., Janecke, S.U., Lundin, E.R., McKittrick, M.A., and Olivares, M.D., 1988, Paleogeographic and paleotectonic setting of Laramide sedimentary basins in the central Rocky Mountain region: Geological Society of America Bulletin, v. 100, no. 7, p. 1023–1039.

Feeley, T.C., 2003, Origin and tectonic implications of across-strike geochemical variations in the Eocene Absaroka volcanic province, United States: The Journal of Geology, v. 111, no. 3, p. 329–346.

Flament, N., Gurnis, M., and Müller, R.D., 2013, A review of observations and models of dynamic topography: Lithosphere, v. 5, no. 2, p. 189–210.

Gurnis, M., 1990, Bounds on global dynamic topography from Phanerozoic flooding of continental platforms: Nature. p. 754-756.

Gurnis, M., Mitrovica, J.X., and Ritsema, J., 2000, Constraining mantle density structure using geological evidence of surface uplift rates: The case of the African superplume: Geochemistry Geophysics Geosystems. p. 1-35.

Hager, B.H., and Clayton, R.W., 1989, Constraints on the Structure of Mantle Convection Using Seismic Observations, Flow Models, and the Geoid.

Hager, B.H., and Richards, M.A., 1989, Long-Wavelength Variations in Earth's Geoid: Physical Models and Dynamical Implications: Philosophical Transactions of the Royal Society A: Mathematical, Physical and Engineering Sciences, v. 328, no. 1599, p. 309–327.

Hager, B.H., Clayton, R.W., Richards, M.A., Comer, R.P., and Dziewonski, A.M., 1985, Lower

mantle heterogeneity, dynamic topography and the geoid: Nature (ISSN 0028-0836), v. 313, no. 6003, p. 541–545.

Heller, P.L., and Liu, L., 2016, Dynamic topography and vertical motion of the U.S. Rocky Mountain region prior to and during the Laramide orogeny: Geological Society of America Bulletin,, p. 1–17.

Hiza, M.M., 1999, The geochemistry and geochronology of the Eocene Absaroka volcanic province northern Wyoming and southwest Montana, USA. PhD Dissertation, Oregon State University. p. 1-261.

Humphreys, E.D., Dueker, K.G., Schutt, D.L., and Smith, R.B., 2000, Beneath Yellowstone: Evaluating plume and nonplume models using teleseismic images of the upper mantle: GSA Today, v. 10, no. 12.

Hyndman, D.W., 1983, The Idaho batholith and associated plutons, Idaho and Western Montana: Geological Society of America Memoirs, v. 159, p. 213–240.

Karlstrom, K.E., Coblentz, D., Dueker, K., Ouimet, W., Kirby, E., Van Wijk, J., Schmandt, B., Kelley, S., Lazear, G., Crossey, L.J. and Crow, R., 2012. Mantle-driven dynamic uplift of the Rocky Mountains and Colorado Plateau and its surface response: Toward a unified hypothesis. *Lithosphere*, *4*(1), pp.3-22.

Kiefer, W.S., and Hager, B.H., 1992, Geoid anomalies and dynamic topography from convection in cylindrical geometry: Applications to mantle plumes on Earth and Venus: Geophysical Journal International, v. 108, no. 1, p. 198–214.

Licciardi, J.M., and Pierce, K.L., 2008, Cosmogenic exposure-age chronologies of Pinedale and Bull Lake glaciations in greater Yellowstone and the Teton Range, USA: Quaternary Science Reviews, v. 27, no. 7-8, p. 814–831.

Lowry, A.R., Ribe, N.M., and Smith, R.B., 2000, Dynamic elevation of the Cordillera, western United States: Journal of Geophysical Research: Solid Earth (1978–2012), v. 105, no. B10, p. 23371–23390.

McMillan, M.E., Heller, P.L., and Wing, S.L., 2006, History and causes of post-Laramide relief in the Rocky Mountain orogenic plateau: Geological Society of America Bulletin, v. 118, no. 3-4, p. 393–405.

McQuarrie, N., and Rodgers, D.W., 1998, Subsidence of a volcanic basin by flexure and lower crustal flow: The eastern Snake River Plain, Idaho: Tectonics, v. 17, no. 2, p. 203–220.

Mitrovica, J.X., Beaumont, C., and Jarvis, G.T., 1989, Tilting of continental interiors by the dynamical effects of subduction: Tectonics, v. 8, no. 5, p. 1079–1094.

Molnar, P., 1988. Continental tectonics in the aftermath of plate tectonics. Nature, *335*(6186), pp.131-137.

Molnar, P., England, P.C., and Jones, C.H., 2015, Mantle dynamics, isostasy, and the support of high terrain: Journal of Geophysical Research: Solid Earth. p. 1-26

Morgan, W.J., 1971, Convection Plumes in the Lower Mantle: Nature, v. 230, no. 5, p. 42–43.

Moss, J.H., and Bonini, W.E., 1961, Seismic Evidence Supporting a New Interpretation of the Cody Terrace Near Cody, Wyoming: Geological Society of America Bulletin, v. 72, no. 4, p. 547.

Nereson, A., Stroud, J., Karlstrom, K., and Heizler, M., 2013, Dynamic topography of the western Great Plains: Geomorphic and 40Ar/39Ar evidence for mantle-driven uplift associated with the Jemez lineament of NE New Mexico.

Olson, P., and Nam, I.S., 1986, Formation of seafloor swells by mantle plumes: … of Geophysical Research: Solid Earth.

Pazzaglia, F.J., and Brandon, M.T., 2001, A fluvial record of long-term steady-state uplift and erosion across the Cascadia forearc high, western Washington State: American Journal of Science.

Peyton, S.L., Reiners, P.W., Carrapa, B., and DeCelles, P.G., 2012, Low-temperature thermochronology of the northern Rocky Mountains, western U.S.A.: American Journal of Science, v. 312, no. 2, p. 145–212.

Pierce, K.L., 2003, Pleistocene glaciations of the Rocky Mountains, in Developments in Quaternary Sciences, Developments in Quaternary Sciences, Elsevier, p. 63–76.

Pierce, K.L., and Morgan, L.A., 1992, Chapter 1: The track of the Yellowstone hot spot: Volcanism, faulting, and uplift: Geological Society of America Memoirs, v. 179, p. 1–54.

Pierce, K.L., and Morgan, L.A., 2009, Is the track of the Yellowstone hotspot driven by a deep mantle plume? — Review of volcanism, faulting, and uplift in light of new data: Journal of Volcanology and Geothermal Research, v. 188, no. 1-3, p. 1–25.

Puskas, C.M., and Smith, R.B., 2009, Intraplate deformation and microplate tectonics of the Yellowstone hot spot and surrounding western U.S. interior: Journal of Geophysical Research, v. 114, no. B4, p. B04410.

Richards, M.A., Hager, B.H., and Sleep, N.H., 1988, Dynamically supported geoid highs over hotspots - Observation and theory: Journal of Geophysical Research (ISSN 0148-0227), v. 93, no. B7, p. 7690–7708.

Riihimaki, C.A., Anderson, R.S., and Safran, E.B., 2007, Impact of rock uplift on rates of late Cenozoic Rocky Mountain river incision: Journal of Geophysical Research, v. 112, no. F3, p. F03S02.

Roberts, S.V., and Burbank, D.W., 1993, Uplift and thermal history of the Teton Range (northwestern Wyoming) defined by apatite fission-track dating: Earth and Planetary Science Letters, v. 118, no. 1-4, p. 295–309.

Saleeby, J., Le Pourhiet, L., Saleeby, Z., and Gurnis, M., 2012, Epeirogenic transients related to mantle lithosphere removal in the southern Sierra Nevada region, California, part I: Implications of thermomechanical modeling: Geosphere, v. 8, no. 6, p. 1286–1309.

Saunders, A.D., Storey, M., Kent, R.W., and Norry, M.J., 1992, Consequences of plume-lithosphere interactions: Geological Society, v. 68, no. 1, p. 41–60.

Schmandt, B., and Humphreys, E.D., 2010, Earth and Planetary Science Letters: Earth and Planetary Science Letters, v. 297, no. 3-4, p. 435–445.

Schmandt, B., Dueker, K., Humphreys, E.D., and Hansen, S., 2012, Hot mantle upwelling across the 660 beneath Yellowstone: Earth and Planetary Science Letters, v. 331-332, p. 224–236.

Sears, J.W., 2013, Late Oligocene–early Miocene Grand Canyon: A Canadian connection?: GSA Today, p. 4–10.

Sears, J.W., Hendrix, M.S., Thomas, R.C., and Fritz, W.J., 2009, Journal of Volcanology and Geothermal Research: Journal of Volcanology and Geothermal Research, v. 188, no. 1-3, p. 250–259.

Shephard, G.E., Liu, L., Müller, R.D., and Gurnis, M., 2012, Gondwana Research: Gondwana Research,, p. 1–6.

Small, E.E., and Anderson, R.S., 1998, Pleistocene relief production in Laramide mountain ranges, western United States: Geology, v. 26, no. 2, p. 123.

Smith, R.B., and Sbar, M.L., 1974, Contemporary tectonics and seismicity of the western United States with emphasis on the Intermountain Seismic Belt: Geological Society of America Bulletin, v. 85, no. 8, p. 1205.

Smith, R.B., Jordan, M., Steinberger, B., Puskas, C.M., Farrell, J., Waite, G.P., Husen, S., Chang, W.-L., and O'Connell, R., 2009, Journal of Volcanology and Geothermal Research: Journal of Volcanology and Geothermal Research, v. 188, no. 1-3, p. 26–56.

Stickney, M.C. and Bartholomew, M.J., 1987. Seismicity and late Quaternary faulting of the northern Basin and Range province, Montana and Idaho. Bulletin of the Seismological Society of America, 77(5), pp.1602-1625.

Thackray, G.D., 2008, Varied climatic and topographic influences on Late Pleistocene mountain glaciation in the western United States. Journal of Quaternary Science, v. 23, no. 6-7, p. 671–681.

Wegmann, K.W., Zurek, B.D., Regalla, C.A., Bilardello, D., Wollenberg, J.L., Kopczynski, S.E., Ziemann, J.M., Haight, S.L., Apgar, J.D., Zhao, C., and Pazzaglia, F.J., 2007, Position of the Snake River watershed divide as an indicator of geodynamic processes in the greater Yellowstone region, western North America: Geosphere, v. 3, no. 4, p. 272.

Wood, Spencer H., and Drew M. Clemens. "Geologic and tectonic history of the western Snake River Plain, Idaho and Oregon." Tectonic and Magmatic Evolution of the Snake River Plain Volcanic Province: Idaho Geological Survey Bulletin 30 (2002): 69-103.

CHAPTER 2

Sensitivity of the Surface to Topographic Uplift: Channel Profile Analysis in the Yellowstone Area

Eduardo Guerrero and Andrew Meigs

Manuscript to be submitted to *Geomorphology*

INTRODUCTION

Advances in the representation of the Earth's surface via digital elevation models led to a significant body of work that demonstrates that spatial patterns of rock deformation can be identified from topography (Kirby and Whipple, 2001; Kirby and Whipple, 2012). A key implication is that a change in uplift rate introduces a transient signal that can be interpreted from the channel morphology (VanLaningham et al., 2006), and transients reflected by knickpoints in the channel profile provide clues to the possibility that uplift rate has changed and the interpretation of potential forcing mechanism (Harkins et al., 2007). Analysis of channel profiles is one key approach to deconvolving deformation acting on a landscape because of the central role that streams play in lowering landscapes and transferring mass out of the system (Snyder et al., 2000). In this study, we analyze channel profiles and steepness patterns of the 6 major drainage basins that head in the greater Yellowstone area to evaluate whether river, and thus, the landscapes respond to the effects of sub-lithospheric mantle forcing.

Horizontal motion and interaction between lithospheric plates dictates much of the geologic evolution of western North America (DeCelles, 2004). Recent advances in geophysical data acquisition and interpretation indicate that convective processes beneath North America must have strongly influenced Late Cenozoic through Holocene landscape evolution throughout the Cordillera (Mitrovica et al., 1989; Becker et al., 2013; Heller and Liu, 2016). Transient topography with a wavelength of 600 km and an amplitude of up to 1200m correlates with seismic velocity and geoid data that is associated with the Yellowstone hotspot (Chapter 1) Geophysical studies indicate that the Yellowstone hotspot is a source of a transient topography signal on the surface, yet geologic evidence is sparse and the signal obscured by multiple forcing mechanisms preserved

in the landscape (Lowry et al., 2000; Pierce and Morgan, 2009; Smith et al., 2009; Becker et al., 2013).

A series of subaerial silicic eruptive centers that increase in age away from Yellowstone indicate that North America passes over the hotspot that has remained fixed for the past 15-17 Ma (Morgan, 1971; Smith et al., 2009). A ~600 km-long and 1.2 km transient topography signal is interpreted to be the surface manifestation of the dynamic topography that results from viscous stresses associated with mantle flow impinging on the base of the North American lithosphere (Chapter 1) (Figure 2.2). We refer to the deformation signal as transient because deformation evolves over million year timescales as lithosphere passes over the hotspot (Chapter 1).

Analysis of the the channel morphology in the upper portions of the Yellowstone, Bighorn/Wind, Green, Snake, and Madison Rivers seeks to determine whether advection of transient topography effects measureable geomorphic change in continental landscapes. Motion of the continent over the hotspot advects transient topography towards the northeast deformation rates that are spatially variable in both sign (uplift or subsidence) and magnitude (Chapter 1). Given the rate of North American plate motion with respect to the hotspot, a surface uplift rate of between 0.166 and 0.302 mm yr^{-1} over 3 Ma is expected along the deformation front, which subsidence rates are between -0.0938 and -0.0454 mm yr^{-1} over 10.3 Ma once the lithosphere has passed over the hotspot in the Yellowstone region. The region within a 250 km to the north and east of the Beartooth-Absaroka mountains is experiencing the long term surface uplift rate of up to 0.302 mm yr^{-1} because it is the direction of the propagating wave front, and the western edge of the Bighorn Basin may have experienced between 400 and 800 m of surface uplift (Figure 3.3). The physical nature of advection means that dynamic topography-forced deformation should be expressed as a transient signal in both landscapes and stream profiles, (eg, Anderson, 1990).

Stream channel analysis is a powerful tool for identifying spatial and temporal patterns of deformation. Analysis of drainage networks in the Siwalik hills in the Nepalese Himalaya, as one example, demonstrates that channels adjust to tectonic forcing in a steady-state landscape at uplift rates greater than 6mm yr^{-1} (Lave and Avouac, 2000; Kirby and Whipple, 2012). Work in the northern California coastal King Range identified a transient deformation signal in channel profiles that experience uplift rates of 0.5 to 4mm yr^{-1} (Snyder et al., 2000). These two examples describe a situation where uplift rates can be high (> 1 mm yr^{-1}), however uplift rates associated with transient topography rarely exceed 1 mm yr^{-1}.

Analysis of channel morphology has also been used as one tool to identify surface expression of sub-lithospheric processes. (Rosenberg et al., 2014)examined the relationship between late Cenozoic incision, channel morphology, and variations in mantle velocity in the western slope of the Rocky Mountains. Results from this study, including between high channel steepness values and high to low mantle velocity transitions, support the hypothesis that the southern Rocky Mountains landscape evolution is influenced by dynamic topography (Karlstrom et al., 2012). Analysis of channel morphology and erosion rates in the Susquehanna river drainage system revealed ~100-150m of surface uplift in the last 3.5 Ma in the Appalachian mountains, which indicates an uplift rate of 0.042mm yr^{-1}(Miller et al., 2013).

Pritchard et al.(2009) developed a methodology for assessing dynamic topography and determining landscape-wide uplift rates from longitudinal profiles using a forward modeling technique that focused on central and southern Africa. This approach was then applied to quantify the level of dynamic support of the Colorado Plateau (Roberts et al., 2012b), Madagascar (Roberts et al., 2012a), Australia (Czarnota, 2014), Crete (Roberts et al., 2013), and Mexico (Stephenson et al., 2014). Results from analysis in Mexico indicate dynamic support that is ~1 km, and started

at ~30 Ma. In this study we use stream profile analysis to determine whether or not channel steepness patterns coincide with model predictions for transient deformation associated with Yellowstone hotspot.

Stream Profile Analysis Background

Field observations in the Bighorn Basin led J. Hoover Mackin to describe the concept of a grade, as a reflection of equilibrium in river systems (Mackin, 1948). Over a period of time, the channel slope is adjusted to provide the velocity required to transport load supplied from the upstream area given available discharge and channel characteristics (Mackin, 1948). The graded stream will respond to a change in conditions by adjusting the channel profile by aggradation or degradation and transmits this signal up or downstream from the disturbance (Mackin, 1948).

Flint's law (Flint, 1974) describes the tendency towards smooth concave-upward shape of equilibrium longitudinal profiles of stream channels and is described by a power-law relationship between local channel slope (S) and drainage area (A) (Howard and Kerby, 1983; Whipple and Tucker, 1999):

$$S = k_s A^{-\theta} \qquad (1)$$

Where the local channel gradient is S. A is the upstream drainage area, and is a proxy for water and sediment discharge, and k_s is the local channel steepness index, and θ is the concavity index, and is described as:

$$\theta = \frac{m}{n} \qquad (2)$$

which is the ratio of the area exponent m and the slope exponent n. The exponent θ reflects the profile concavity, which is typically between 0.4 and 0.6 (Whipple and Tucker, 1999; Kirby and Whipple, 2012). The channel steepness index k_s is described by:

$$k_s = (\frac{U}{K})^{1/n} \qquad (3)$$

Where U is the uplift rate relative to base level fall (Whipple and Tucker, 1999), K is the erosion coefficient, which is influenced by lithology, material covering the channel bed, channel width, frequency of debris flows, surface runoff, and tectonic forcing (Howard, 1998; Snyder et al., 2000). The relationships that (2) and (3) describe hold true if the drainage system is at an equilibrium with respect to current climate and uplift if both uplift rate (U) and erosion coefficient (K) are uniform throughout the channel reach. Both parameters in (2) and (3) can be estimated through a regression of channel gradient against drainage area for a basin.

A longitudinal profile that deviates from the expected equilibrium has knickpoints that are revealed in slope/area space as having unique steepness values (k_s) but similar concavity or when a channel has a smooth profile with a concavity where $\theta > 0.6$ (Wobus et al., 2006). Knickpoints can result from spatial and temporal changes in the lithology, rock uplift rate (Snyder et al., 2000; VanLaningham et al., 2006), and/or variations in sediment/water supply due to climate (Brocklehurst and Whipple, 2006).

Small variations or uncertainties in the concavity index (θ) lead to wide variations in the steepness index (k_s). In this study, we compare channel steepness patterns among channels with variable areas in order to determine if the deformation signal from transient topography is recorded by the major rivers in the Yellowstone area. In order to accomplish this goal, assume on that concavity indices (θ) of steady-state channels should be within a range of 0.4 and 0.6 (Wobus et al., 2006), the average concavity for the analyzed area is 0.45. Slope-area analysis with a reference concavity index (θ_{ref}) allows determination of a normalized steepness index (k_{sn}), that results in channel steepness indices that are comparable across drainage basins with different-sized areas (Kirby and Whipple, 2012) and is described by:

$$S = k_{sn} A^{-\theta_{ref}} \qquad (4)$$

High k_{sn} values (>200) in segmented channels are diagnostic of rapid incision rates, resistant lithology, or erosion regimes dominated by episodic large flooding (Kirby and Whipple, 2012; Darling and Whipple, 2015). Normalized channel steepness indices are expected to display linear scaling with rock uplift rates when channels develop within a specific climate regime and in similar lithology (Kirby and Whipple, 2012; Snyder et al; 2003). High k_{sn} values are thus representative of a change in a graded system, and understanding the channel's response to perturbations is necessary to gleam information about tectonics from river profiles (Kirby and Whipple, 2012). Changes in tectonic or climatic forcing of river profiles are expressed as a transient signal that is propagated throughout the system, and the response time depends on how efficiently a system is able to remove mass and return to its equilibrium state (VanLaningham et al., 2006).

Transient signals are expressed as knickpoints along a river's longitudinal profile, and represent the boundary between the downstream part of the profile that has adjusted to the forcing mechanism and the upstream portion of the profile that has yet to adjust (Howard et al., 1994; Crosby and Whipple, 2006). There are two general styles of knickpoints: (1) Vertical step knickpoints tend to correlate spatially with isolated heterogeneities such as lithology contacts in the substrate (Kirby, 2003), or other discrete events such as landslides or debris flows (Korup et al., 2010). Vertical step knickpoints are normally fixed in place and are generally not thought to contain much tectonic significance (Kirby and Whipple, 2012). (2) Break in slope-area scaling knickpoints typically evolve in response to a persistent change in spatial and/or temporal forcing, and are useful for interpretation of tectonics from channel profiles (Kirby and Whipple, 2012). Distribution of break in slope-area scaling knickpoints can form systematic steepness patterns

across channels of different sizes and orientations, and can identify spatial patterns of deformation when corroborated by additional data (Kirby, 2003; Wobus et al., 2006).

METHODS

Analysis is based on 30 m resolution Shuttle Radar Topography Mission (SRTM). Watersheds with areas that ranged from $10^7 m^2$ to $10^{11} m^2$ were extracted using the Spatial Analyst toolkit in ArcGIS 10.3. Resulting watersheds were then converted into American Standard Code for Information Interchange (ASCII) format and analyzed using Topotoolbox 2.0, which is a Matlab-based set of functionsto analyze DEM data (Schwanghart and Scherler, 2014). Resulting shapefiles containing k_{sn} values are then projected in ArcGIS and merged for display (see Appendix 2 for full routine and instructions).

The large, regional-scale basins that were extracted and analyzed at the regional scale head in the greater Yellowstone area, and are: Yellowstone, Madison, Snake, and Bighorn (includes the Wind River, which becomes the Bighorn after it crosses the Owl Creek Mountains). We only include k_{sn} analysis of the upper reaches of each one of the basins. The upper Clark Fork of the Columbia is included in regional analysis as a reference watershed because its distance from Yellowstone should make it insensitive to any associated transient topography. Four major streams are presented as longitudinal profiles and in log/log space: Madison, Yellowstone, Wind, and North Fork Shoshone. Catchment-scale analyses are presented for the major streams draining the Beartooth mountains, which are made up of uniform Precambrian crystalline basement rocks (Omar et al., 1994). These streams were chosen because of the uniform lithology in the catchments, and because they drain a region that is modeled to be experiencing the maximum uplift rate related to dynamic topography. These streams are: Clarks Fork Yellowstone, Rock Creek, East Fork Rosebud, West Fork Rosebud Creek, Stillwater, and Boulder Rivers is also included.

United States State Geologic map and fault location data for Montana, Idaho, and Wyoming were downloaded from the USGS mineral resources geospatial database (http://mrdata.usgs.gov/geology/state/) and projected in ArcGIS. Geologic units were simplified and merged into the following rock-type categories: igneous intrusive, igneous extrusive, metamorphic, marine sedimentary, terrigenous sedimentary, and (unconsolidated) sediment. These data are displayed together with k_{sn} results in Figures 2.5-2.9.

RESULTS

We report results from our analysis in three separate sections. The first section describes the regional extent and distribution steepness patterns throughout the entire Yellowstone area. The second section describes results from the analysis of major river basins that drain radially away from the Yellowstone high country. The third section describes results for the major streams that drain away from the Beartooth block.

Figure 2.4 is the full extent of k_{sn} analysis in the greater Yellowstone area that includes portions of Montana, Wyoming, and Idaho. Roughly 75% of channels analyzed in the greater Yellowstone region have of k_{sn} values in the range of 0-100. About 6% have k_{sn} values that are >150, which includes intermediate to highest (100 to >250). Based on these results, patterns of steepness emerge throughout the study area. At the regional scale, intermediate (yellow) k_{sn} values occur at the range-valley transitions. Regions of high relief are highlighted by these values. The Wind, Absaroka, Beartooth, and Bighorn Ranges are outlined by k_{sn} values of 150-200. k_{sn} values of 250 tend to cluster inside the Laramide ranges, typically within 20km from the range-fronts. There are a series of Snake River Basin channel segments with high k_{sn} values that occur along Basin and Range normal faults to the north of the Snake River plain, a region known as the Centennial tectonic belt that extends from the Madison range in the east to the Idaho

batholith in the west (Stickney and Bartholomew, 1987), This fault-coincident pattern is also evident along the eastern face of the Teton mountains, where k_{sn} values increase where streams cross the Teton fault (Byrd et al., 1994).

Regional-scale k_{sn} results

Yellowstone

The upper Yellowstone basin has an area of 10^{10}m (Figures 2.5, 2.6). The drainage extends from Billings, MT in the northeast to the western slope of the Absaroka Mountains. Approximately 600km of the reach are included in this analysis, in addition to all tributaries with a contributing area greater than 10^3m. There is a series of intermittently high k_{sn} values calculated for lower reaches of the channel, these elevated indices occur in unconsolidated sediment (Figure 2.5B). A Slope/Area plot in log space reveals that the linear relationship between slope and area becomes deconvolved in the lowest reaches of the analyzed channel when the contributing area increases beyond 10^8m^2 (Inset, Figure 2.6), which corresponds to the alluvial reach of the Yellowstone river.

There is another area of the Yellowstone drainage that contains a high concentration of elevated k_{sn} indices between km ~320 and ~430 (Figure 2.6), which coincides with a reach that experienced late Cenozoic extension and is known as the East Gallatin-Washburn zone (Christiansen, 2001). This segment of the drainage also contains glacial deposits that indicate climate forcing of the river profile (Licciardi and Pierce, 2008).

The most significant zone of elevated k_{sn} values occurs at km ~450 (Figure 2.6) and are coincident with the largest knickpoint in the profile. This knickpoint marks the edge of the Yellowstone volcanic plateau, and includes the spectacular waterfalls for which the National Park is known for: upper and lower Yellowstone Falls, Twin Falls, and Tower Fall. This zone of high steepness indices is a transition both in lithology and active faulting associated with the caldera's

eruptive history (Figure 2.5B) (Christiansen, 2001). The horizontal segment of the profile corresponds to the Yellowstone lake which now occupies a substantial fraction of the caldera.

Drainages within the Beartooth mountains contain the other high concentration of k_{sn} values. There is a clear transition in lithology at the range front from the Precambrian crystalline block that was thrust over Mesozoic sedimentary units during the Laramide orogeny (Omar et al., 1994). The zones of high k_{sn} indices are located away from the range front in drainages that cross the central region (Figure 6B).

Bighorn River Basin

The combined Wind-Bighorn basins presented in Figure 2.7 includes the full extent of the Bighorn river's contributing area. These are structural basins formed during the Laramide orogeny and are separated by the Owl Creek mountains (Dickinson et al., 1988). The two basins are connected across the Wind River Canyon; however, timing of basin integration is not known. Channel steepness patterns in the basin system are associated with variation in lithology.

Wind River Canyon, in the south-central portion of the basin, is one site where a cluster of high k_{sn} values are correlated with a persistent zone of steepness associated with a change in lithology in the core of the range. Composition is dominated by Precambrian metavolcanic and metasedimentary units (Mueller et al., 1985). Another cluster of high k_{sn} values exists in the northwestern portion of the Bighorn basin, where the Shoshone River (Figure 9) enters the Shoshone Canyon. This canyon bisects an uplifted Laramide crystalline block known as Rattlesnake Ridge to the northwest and Cedar Mountain to the southeast. Another cluster of high k_{sn} values occurs where the downstream reach of the Bighorn River enters Bighorn Canyon, a location where the lithology changes from volcanic-sedimentary units of the Eocene Willwood Formation (Kraus, 1997) to the Cretaceous Mesaverde Formation, to the Pennsylvanian Tensleep

Formation (Pierce, 1997). These persistent knickzones have been exploited as locations to build dams; Buffalo Bill dam on the Shoshone, Yellowtail dam at the lowest reach of the Bighorn, and Boysen dam at the entrance to Wind River Canyon.

There are consistently linear patterns of high k_{sn} values that occur in channels across drainage basins throughout the Bighorn system. These linear trends cross watershed boundaries and are associated with changes in lithology between the Laramide-associated uplifted crystalline Wind River and Bighorn blocks. The linear steepness patterns trend southeast-northwest and follow the contact between the Precambrian crystalline units and the Meozoic sedimentary units that make up the footwall blocks of the thrust systems.

Figures 2.8 and 2.9 are longitudinal profiles and slope area plots of the North Fork Shoshone and the uppermost Wind River respectively (See Figure 1 for location), which are tributaries to the Bighorn drainage system that head closest to Yellowstone. Both profiles have a knickpoint in the 2400-2500m elevation range, flattening of the profile is characteristic of catchments that experienced occupation by glaciers (Brocklehurst and Whipple, 2006). This observation agrees with conclusions by many workers who include moraines in these valleys in their chronologies of Rocky mountain glaciation (Holmes and Moss, 1955b; Moss, 1982; Licciardi et al., 2001). The only other knickpoint in the profile is the artificial one created by the Buffalo Bill dam at the mouth of the Shoshone Canyon. The distribution of k_{sn} values in the catchment suggest that a slope break knickpoint would be detectable from the DEM at the boundary between Eocene Absaroka volcanic rocks (Hiza, 1999) and Precambrian crystalline basement rocks of the Rattlesnake ridge (Pierce, 1997), however it is obscured by the presence of the Buffalo Bill Dam..

Snake River Basin

Channel steepness patterns in the Snake River drainage follow two general trends. First, k_{sn} spatial patterns vary with fault location. Second, high k_{sn} indices occur where streams cross rock type boundaries. There are a series of high k_{sn} values along the main stem of the Snake river as it enters the subsiding volcanic basin that shares names with the river (McQuarrie and Rodgers, 1998), these values occur in unconsolidated sediment and are attributable to dams along the river (Figure 2.10).

One example of co-location of high k_{sn} values and active faults is along the Lost River fault in the northwestern sector of the Snake River Basin (Figure 2.10B). The fault trends northwest-southeast and a series of $>250m^{0.9}$ occur in streams that cross the fault. The 1983 M_w 7.0 Mt. Borah earthquake ruptured along the Lost River fault, a west dipping high angle normal fault associated with Basin and Range stress regime, and a slip rate of 0.2-0.4 mm yr^{-1} (Stein and Barrientos, 1985). The Teton Fault is an east-dipping high angle normal fault and there are high k_{sn} values with streams that cross the fault, which has a 2 mm yr^{-1} slip rate, which results from both normal faulting and isostatic rebound caused by the disappearance of the Yellowstone Ice cap (Hampel et al., 2007) (Figure 2.10B).

Madison River Basin

The Madison River heads in the Yellowstone Caldera (Figures 2.11, 2.12), and flows into Hebgen Lake, which occupies the reach from km~260 to ~310 and formed after the construction of Hebgen Dam in 1914. The dam is at the upstream entrance to the Madison Gorge where the river crosses the range that shares its name. The river crosses the Madison fault as it exits the range and enters a half-graben (Alexander and Leeder, 1990). The Madison fault is a high angle westward-dipping normal fault that locally marks the eastern edge of the Centennial Tectonic belt

(Stickney and Bartholomew, 1987). A transient knickpoint is likely to exist at this location because 10-30 m high scarps are documented to be the cumulative offset over a few hundred years of movement along the range-front fault (Alexander and Leeder, 1990; Zreda and Noller, 1998). The knickpoint does not appear on the profile (Figure 12), but there are intermediate to high high k_{sn} indices that have a linear pattern that follows the trace of the the Madison range front fault across minor catchment divides in Figure 11.

Green River Basin

The upper Green River basin drains the western slope of the Wind River Range, and contains a high concentration of >250 k_{sn} indices in the northeastern part of the basin (Figure 13). The headwaters for the Green river itself originate from a glacier adjacent to Gannett Peak (Holmes and Moss, 1955a) in the northwestern sector of the Wind River Range. Pinedale, WY is on western slope of the Wind River range and is the type-location for the morphology of the most recent glacial advance in the Cordillera (Holmes and Moss, 1955a; Hall and Shroba, 1993). Pinedale terminal moraines in the northern Yellowstone region and in the Teton valley have been dated from 14.6ka to 18.8ka (Licciardi and Pierce, 2008). High k_{sn} values in the western slope of the Wind River Range are the result of glacier occupation in the valleys. Oversteepened reaches occur in cirques and in tributary junctions where the valley base level dropped, yet the main channel retains an overall lower gradient (Brocklehurst, 2002).

Beartooth Mountains Channel Analysis

The morphology of the channels that drain the Beartooth block is analyzed for two reasons: First, the range corresponds with the crest of the modeled advecting wave of dynamic topography and are should be experiencing approximately 0.23 mm yr^{-1}. Second, is to explore high k_{sn} values in detail, because the patterns observed in the Beartooth match other Laramide ranges with high ksn values that occur away from breaks in lithology. (Figure 4). Small and Anderson (1998)

attribute production of relief in Laramide ranges to increasing glacial erosive activity in valleys that accompanied global cooling during the Late Cenozoic. A 3km-thick ice cap at it's highest extent during the Last Glacial Maximum occupied the Yellowstone plateau during the Pinedale glacial time, which culminated during the last glacial maximum (Pierce, 2003) (Figure 15). The Yellowstone ice cap expanded westward from the high terrain that surrounds the caldera, and at its maximum extent, integrated drainages to include alpine glaciers that developed in north and eastward draining valleys (Licciardi et al., 2001).

Licciardi and Pierce (2008) describe an out of phase relationship between the ice cap and the valleys that drained away from the caldera. Cosmogenic dating of boulders in a terminal moraine indicate that glacial retreat did not begin until approximately 18.8 ka in the Clarks Fork Canyon (Figure 2.15) (Licciardi and Pierce, 2008). Figure 2.14A is the longitudinal profile of the Clarks Fork upstream of the canyon; the shape of the profile contains four flattened reaches at 1400 m, 1800 m, 2100 m, and 2600 m that are connected by over steepened reaches. The other longitudinal profiles presented in Figure 14 display the same characteristic stair-step shape that is typically interpreted to be the result of glacial erosion (Brozovic et al., 1997; Brocklehurst, 2002). These 6 profiles confirm previous mapping and interpretation of most recent alpine glacier distribution in the Beartooths, Rock Creek is the only channel that does not exhibit profile disturbances, which agrees with regional glacial mapping, Figure 15 (Licciardi and Pierce, 2008). The lowest elevation knickpoint for four of the northward draining catchments is between 1600 and 1700m, however it is >1400m for the Clarks Fork drainage.

DISCUSSION

Channel steepness patterns show strong variation at the range scale (~100 – 200 km) but do not clearly correlate with either long-wavelength topography or geoid anomalies, which are two proxies associated with transient topography (Figure 2.4) (Chapter 1). We are able to clearly identify channel steepness patterns associated with volcanic eruptions and caldera forming processes, regional basin and range extension, changes in lithology, and glacial erosion. When studied in detail, glaciated catchments in the Beartooth block only had a few knickpoints at similar elevations, and these reflect glacial imprints on the profiles. The only indication that the Beartooth mountains have experienced greater rock uplift than Laramide ranges in similar settings comes from (Small and Anderson, 1998) who identified 290m (without accounting for flexure) and 90m (when accounting for flexure) of total rock uplift, when compared to the Wind River (250m/70m) and Uinta (240m/55m). We speculate that this increased uplift rate could be associated with transient topography.

The foundation of J. Hoover Mackin's 1948 'Concept of the Graded River' resulted from his fifteen years of work in the Bighorn basin, and he presents the North Fork of the Shoshone as an ideal example as a stream in which, "*over a period of years, slope is delicately adjusted to provide with available discharge and the prevailing channel characteristics, just the velocity required for transportation of all the load supplied from above"*. Analysis of k_{sn} patterns requires the assumption that fluvial systems are in steady state and will thus display evidence for a disturbance to the channel (Kirby and Whipple, 2001; Kirby and Whipple, 2012). Many of the channels analyzed displayed profile disturbances as stated above. However, Rock Creek and the North Fork Shoshone, which were not glaciated at the LGM and drain roughly parallel to the direction of advection of topography (Figure 2.1), did not display convexities that may be

interpreted as profile disturbance. Thus, their equilibrium form indicates that either their response time is less than 3 Ma, a period when uplift rate increased by 0.3 mm yr^{-1} or that the rate of change in uplift rate in space is marker signal that climatically controlled change in discharge or sediment supply.

In this study we assess the geomorphic expression of transient topography related to the Yellowstone hotspot. We consider that the deformation style to be a lithospheric-scale version of the principle of advection of topography through topographic growth and geomorphic decay articulated by (Anderson, 1990). (Braun et al., 2013) articulate the same principle of advection and present modeling results that indicate that large scale and low amplitude topography can be efficiently eroded and results in sedimentary deposits that are easily identifiable in the geologic record. A maximum uplift rate of 0.302 mm yr^{-1} is predicted when we parameterize (Braun et al., 2013)'s model to the Yellowstone area, with a change in surface elevation between 400-1200 m accompanying advection of dynamic topography (Chapter 1). Uplift rate is likely the highest estimate for transient deformation in this part of the world, if the rates were higher, the signal associated with Yellowstone would have likely been detected in the channel steepness patterns. The predicted uplift rate is low enough that the cumulative effects of advection force the entire profile equally and does not leave an imprint on the longitudinal profile or on channel segments.

CONCLUSION

We analyzed stream channel morphology from the regional to the catchment scale in the Yellowstone area to investigate if advection of dynamic topography has a measureable deformation signal in channel steepness (k_{sn}). High k_{sn} values do not coincide with transient topography inferred from long wavelength topography or with geoid values. High k_{sn} values at

the drainage basin scale illustrate the coincidence with changes in lithology, active Basin and Range faulting, volcanic processes, glacio-fluvial transitions, tributary junctions, or landslides. Knickpoints at the catchment scales in uniform lithology coincide with tributary junctions and glacio-fluvial transitions. Deformation rates of >0.302 mm yr^{-1} are below the detection limit of k_{sn} analysis because the impact of other variables like discharge or sediment supply are larger and have a higher frequency than does surface suplift associated with advection of the transient topography. Either deformation signal does not reach the surface and dynamic topography does not have a geomorphic expression or lithosphere-scale response to deformation is more complex and requires additional metrics to be quantified. Surface uplift rates with transient topography are small and are spatially distributed relative to the drainage baisns of the greater Yellowstone region.

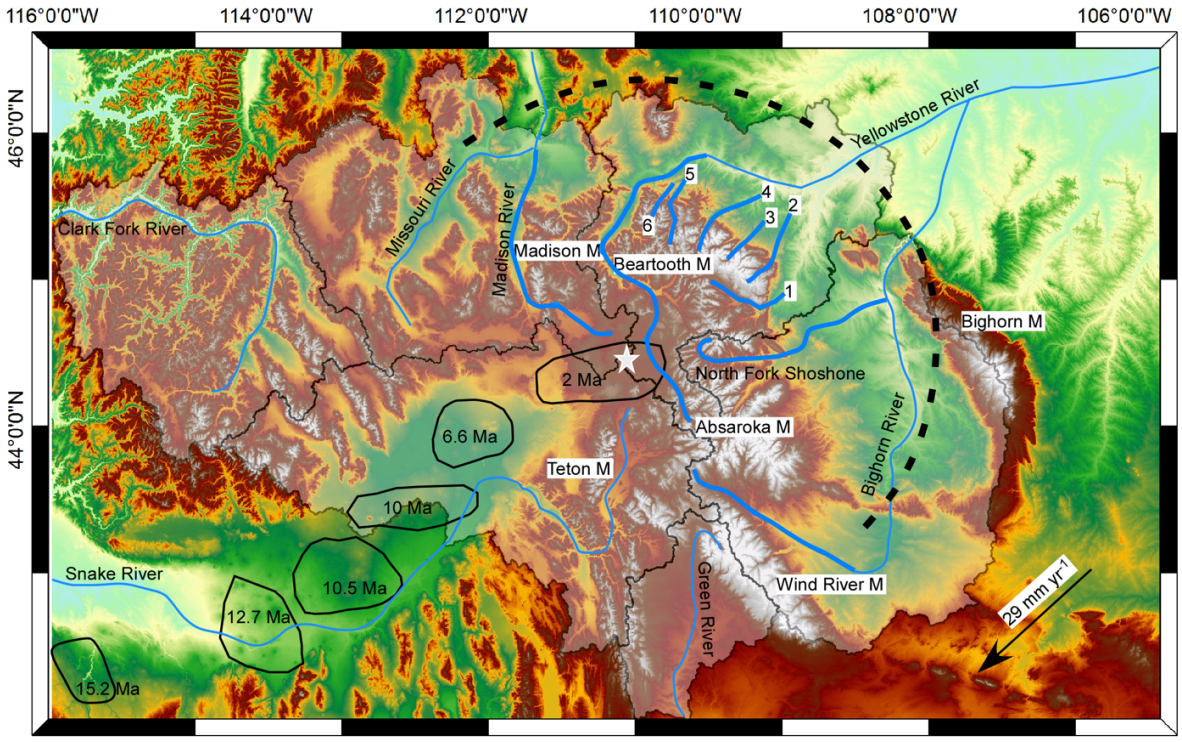

Figure 2.1 Location Map. Star identifies position of Yellowstone volcanic field. Lightly shaded polygons are the drainage area of the main rivers presented in this study. Rivers were selected because of proximity of head to Yellowstone volcanic field. Only upper portions of some drainage basins were selected to avoid influence of alluvial reaches in analysis. Black elipses with ages depict location of magmatic centers associated with Yellowstone hotspot. Vector of 29 mm yr^{-1} shows velocity and direction of the motion of North America with respect to the hotspot, as inferred from volcanic centers (Pierce and Morgan, 1992; 2009). Dashed line shows inferred deformation front of advecting transient topography.

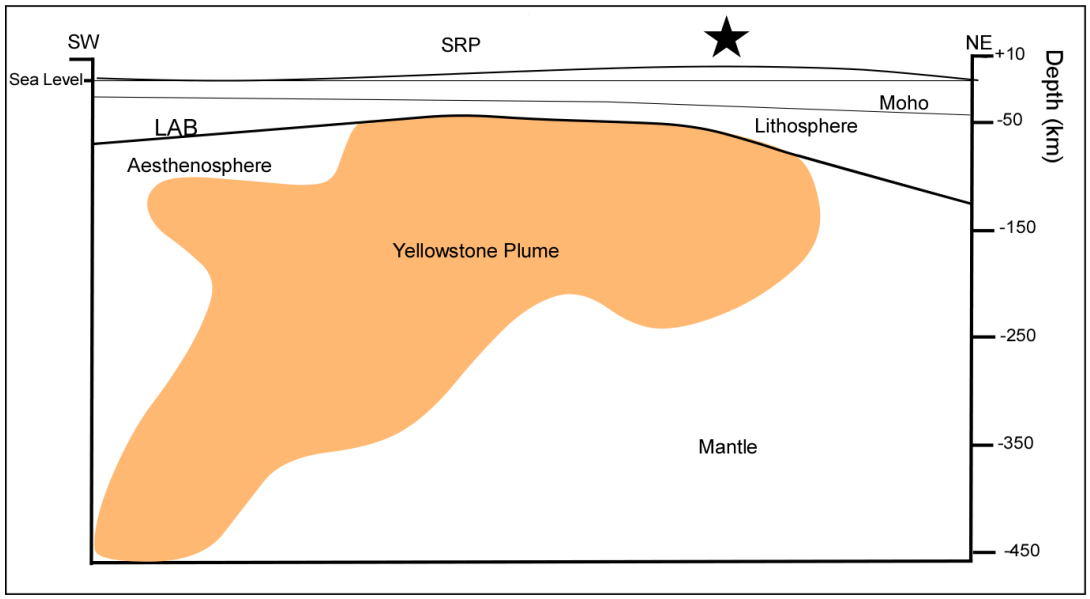

Figure 2.2 Lithosphere-scale cross section through the Snake River Plain illustrating long-wavelength topography (Chapter 1). Inferred mantle plume extent based on p-wave velocity perturbations (Schmandt et al., 2012). Lithosphere thickness is based on analysis by (Levander and Miller, 2012).

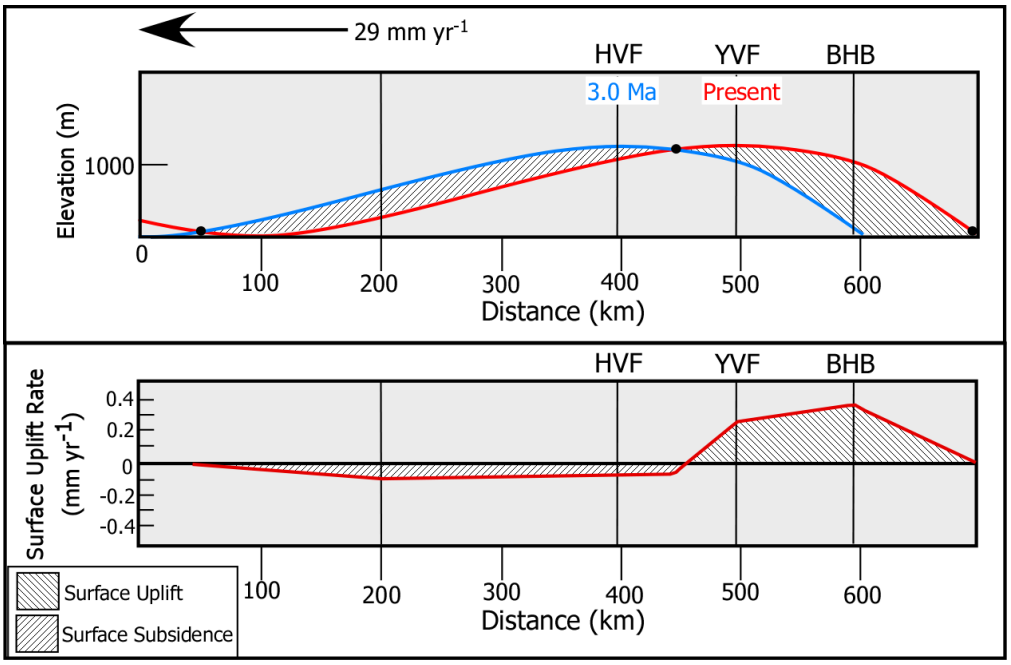

Figure 2.3 Model for advection of transient topography and surface uplift from Chapter 1. Illustrates model results for shape of long wavelength topography along the track of the Yellowstone hotspot, which is interpreted to be the transient topography. Blue curve is position of transient topography at 3 Ma, red is present position of transient topography. Black dots are locations where uplift and subsidence rate is 0, where the blue curve is above represents active subsidence, where the red curve is above represents active uplift. Difference between two curves dictates rates of deformation. Maximum uplift rate of between 0.166 and 0.302 mm yr^{-1} 29 mm yr^{-1} is the rate of motion of North America with respect to the hotspot. Lower panel illustrates variations in uplift rate

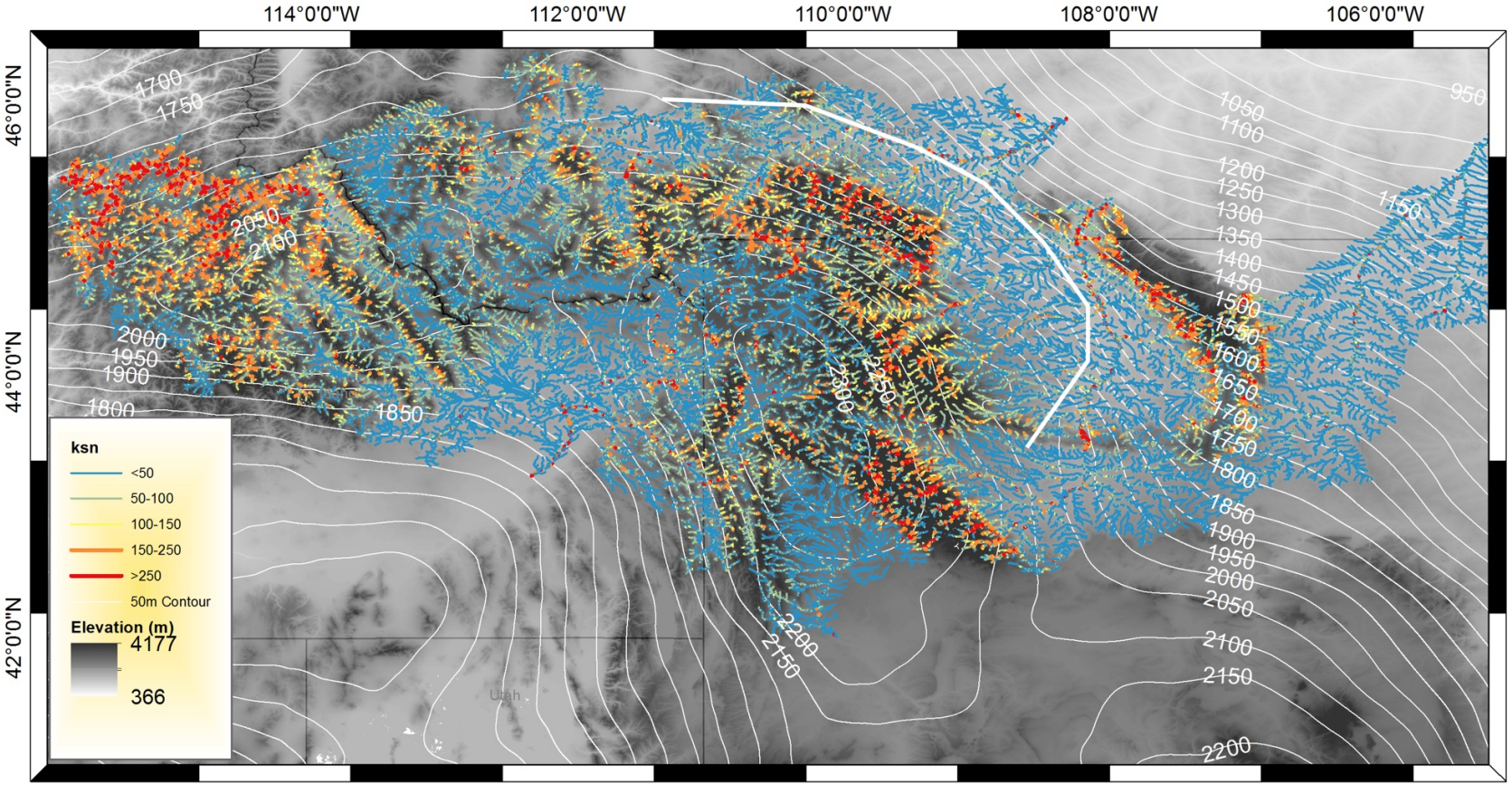

Figure 2.4 Regional extent of k_{sn} analysis throughout greater Yellowstone area. Stream segments with intermediate (150) to high (250+) k_{sn} values are graded from yellow to red. White 50m contours are from 200km mean elevation map, interpreted to be the present transient topography associated with the hotspot (Chapter 1). Elevation scale is the same for subsequent figures.

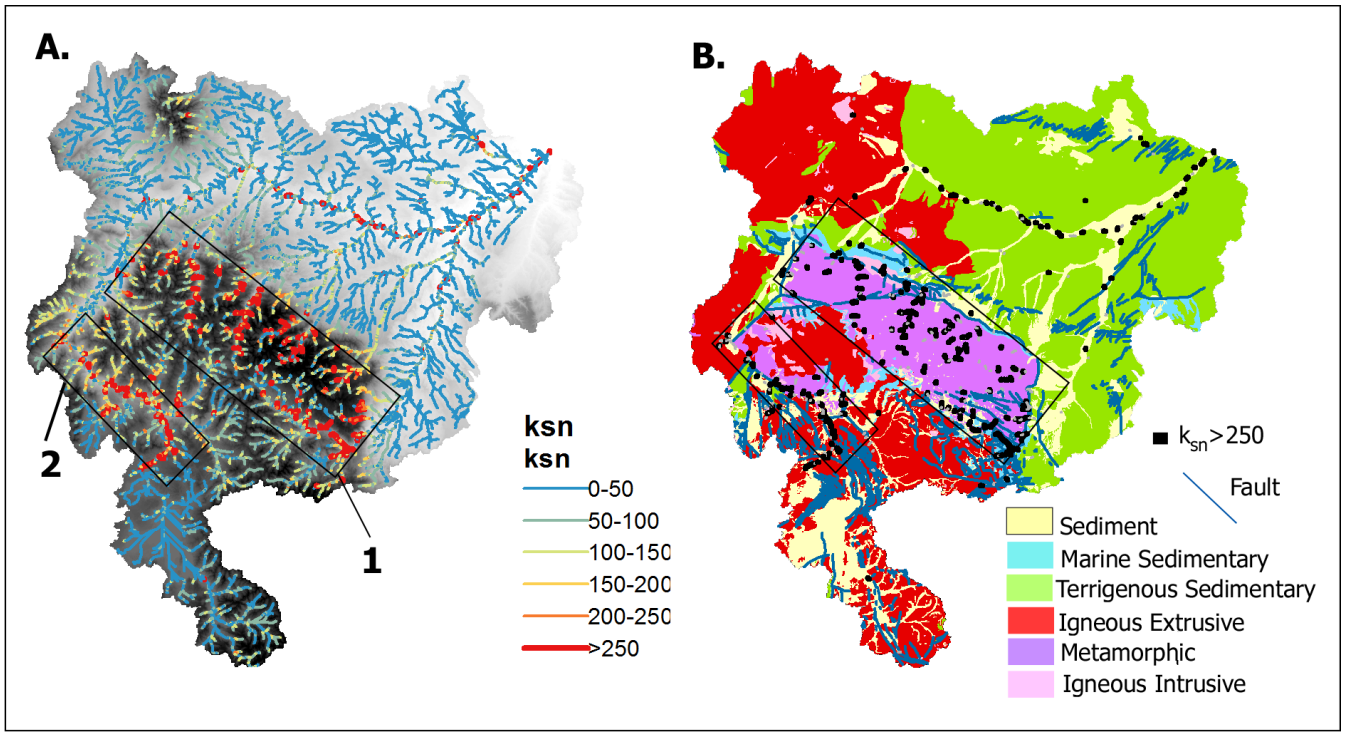

Figure 2.5 A. Yellowstone River basin k_{sn} results of the. **B**. Generalized geologic map of the analyzed reach, only k_{sn}values >250 are displayed. The Beartoth block is northwest trending block of metamorphic rocks that contains the highest concentration of k_{sn} values in the Yellowstone basin. Black boxes depict sites discussed in text 1- Beartooth Range 2 Canyon of the Yellowstone.

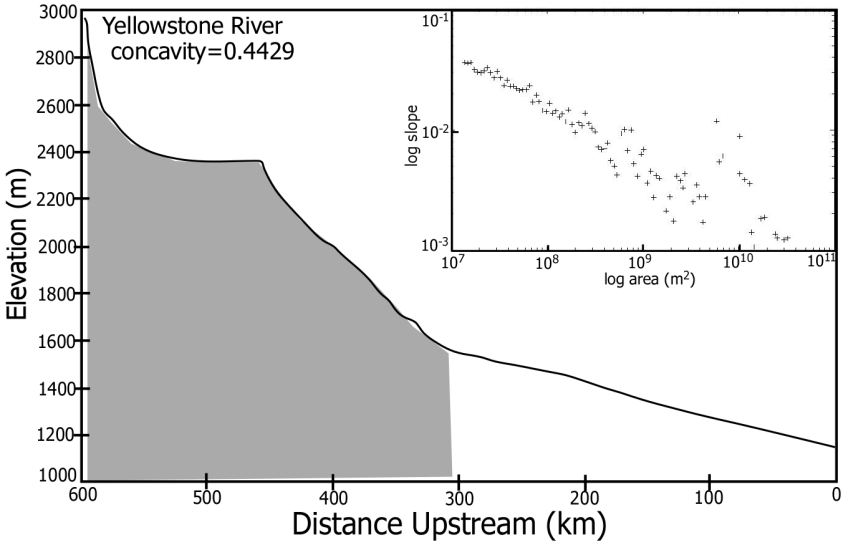

Figure 2.6 Yellowstone River longitudinal channel profile. Inset figure is the profile data in slope-area space. See results section for full description. Shaded area is portion of profile used to calculate concavity.

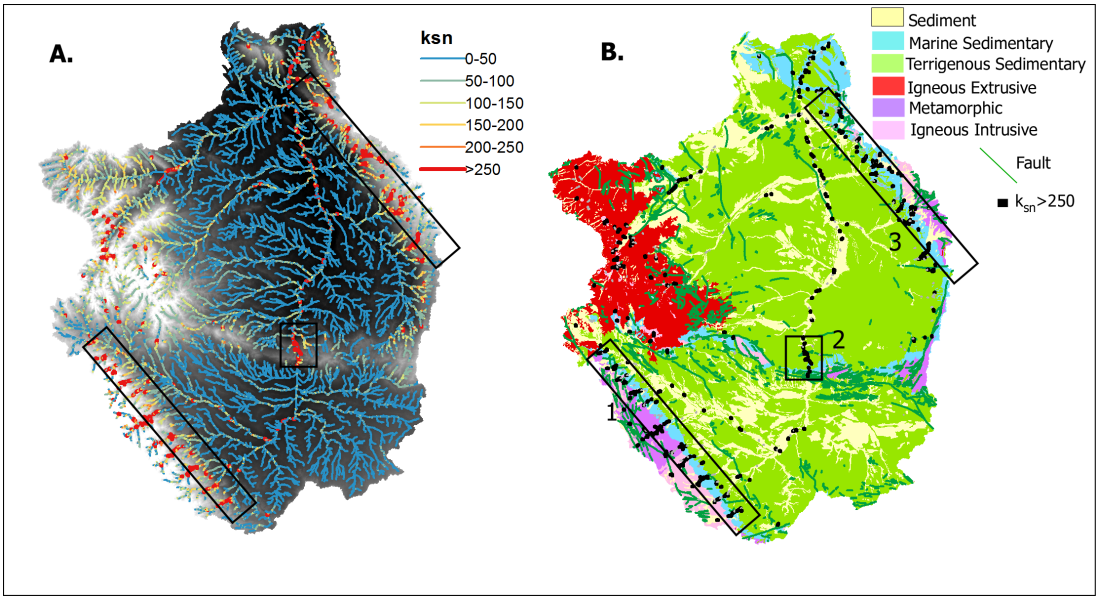

Figure 2.7 A. Bighorn River Basin k_{sn} analysis results. **B.** Generalized geologic map of, k_{sn} values are simplified to only display values greater than 250. Black boxes depict sites discussed in text. 1. Wind River Mountains 2. Wind River Canyon 3. Bighorn Mountains

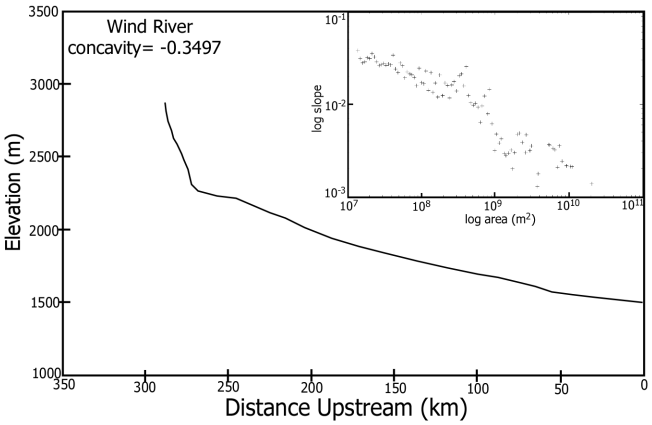

Figure 2.8 Longitudinal profile of the Wind River. Inset figure is the profile data in slope area space. Displays knickpoint that resulted from glacial erosion at km 250

Figure 2.9 Longitudinal channel profile of the North Fork Shoshone River. Inset figure is the profile data in slope area space. See results section for full description. Shaded area was used to calculate longitudinal profile concavity.

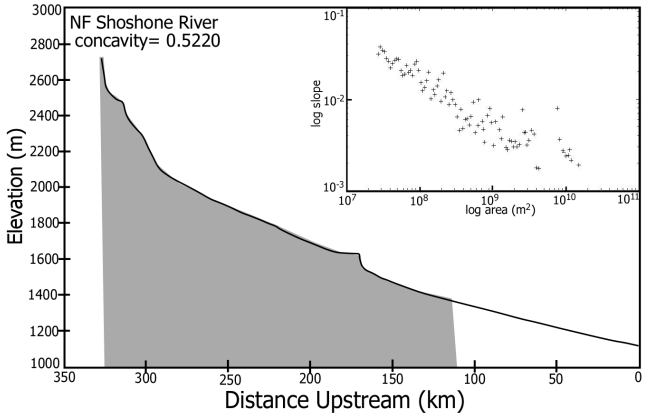

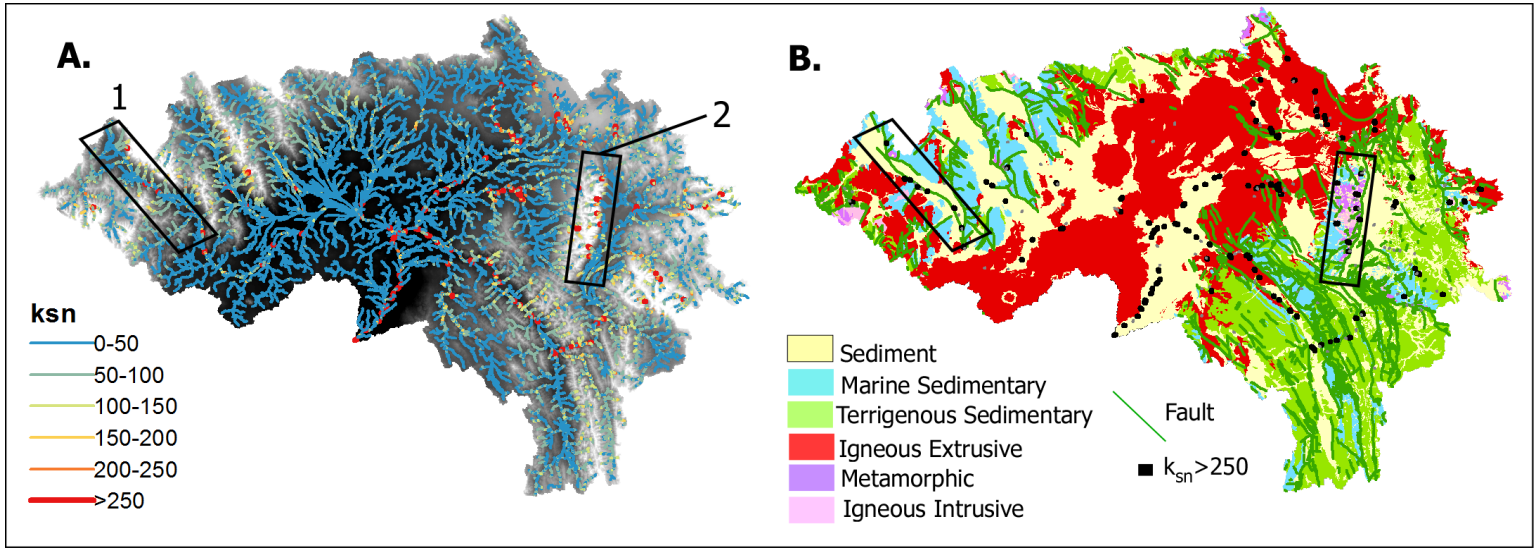

Figure 2.10 A. Snake River Basin k_{sn} analysis. **B.** Generalized geologic map of the analyzed reach, k_{sn} values are simplified to only display values greater than 250. Black boxes outline regions discussed in text 1. Lost River Fault, 2. Teton Fault.

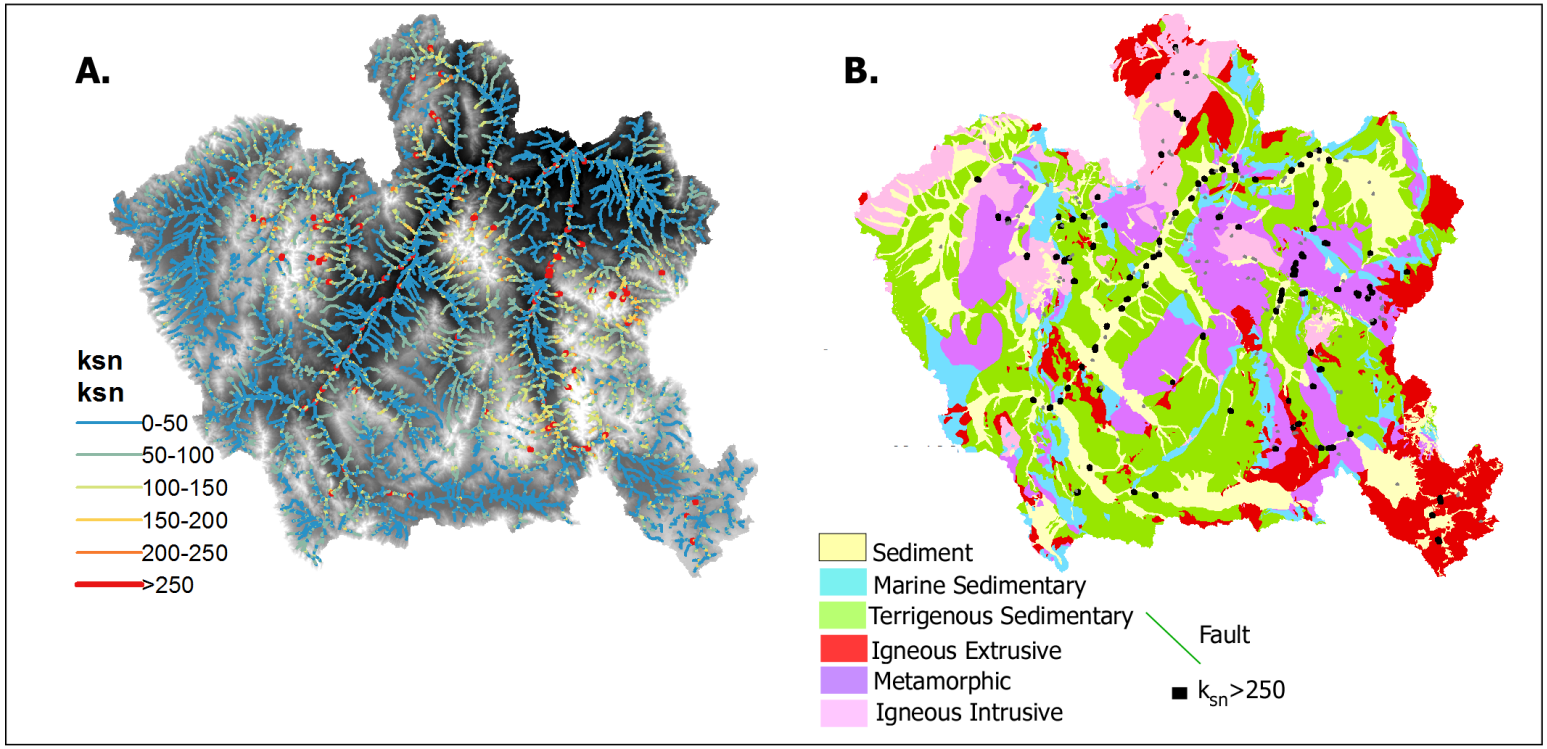

Figure 2.11 **A.** Madison River Basin k_{sn} analysis results. **B.** Generalized geologic map of the analyzed reach, k_{sn} values are simplified to only display values greater than 250.

Figure 2.12 Longitudinal channel profile of the Madison River. Inset figure is the profile data in slope-area space, shaded area is river reach that was used to calculate river concavity.

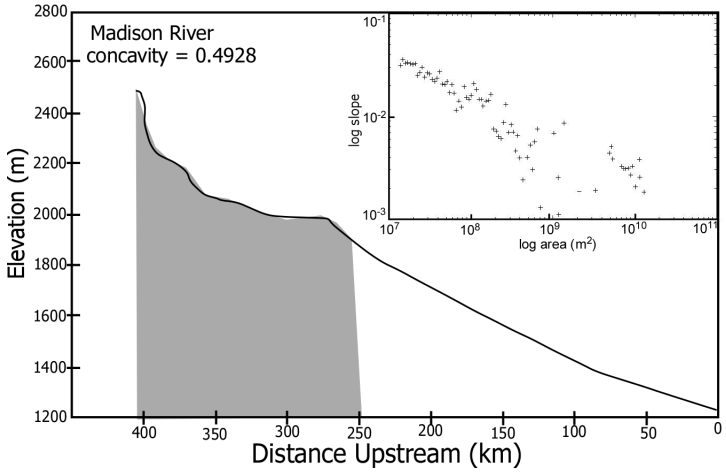

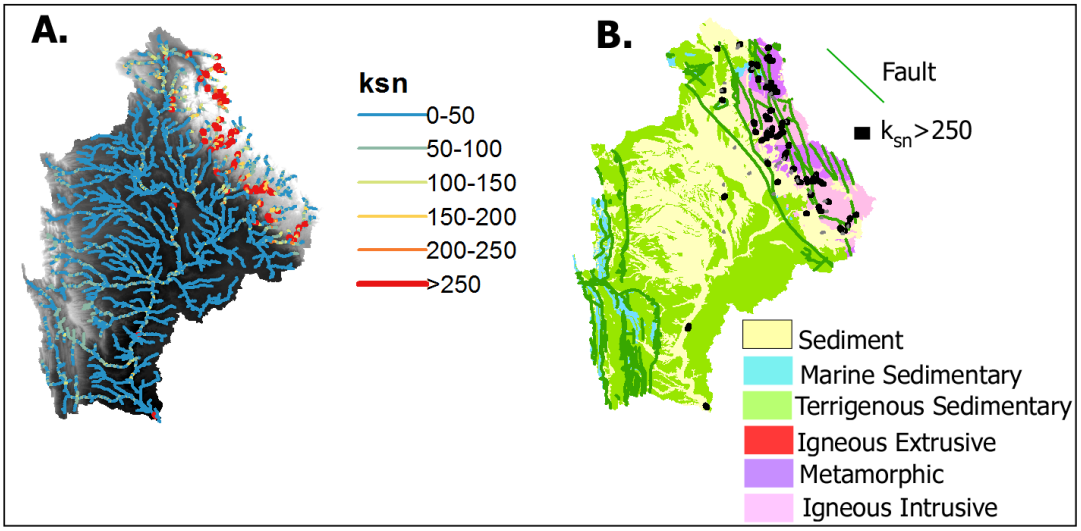

Figure 2.13. **A.** k_{sn} analysis results of the Green river basin. **B.** Generalized geologic map of the analyzed reach, k_{sn} are simplified to only display as black dots.

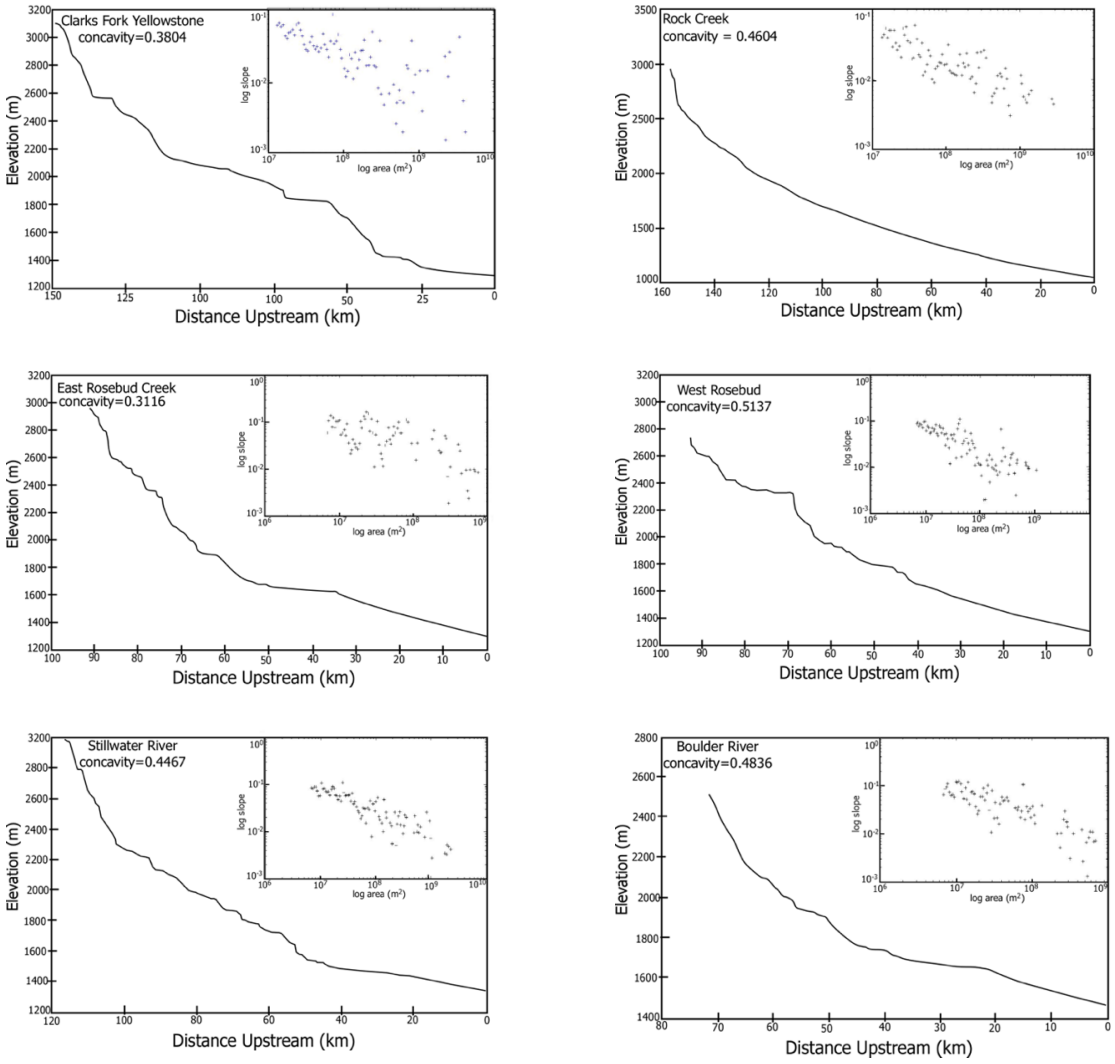

Figure 2.14 Beartooth Mountains longitudinal profiles (1-6 from Figure 1). Each figure contains slope and area data in. These are the major streams that drain away from the Beartooth mountains. All streams except for Rock Creek display characteristic convexities that indicate glacial erosive influence on the profiles. Concavity is calculated for entire longitudinal profile.

REFERENCES

Alexander, J., and Leeder, M.R., 1990, Geomorphology and surface tilting in an active extensional basin, SW Montana, USA: Journal of the Geological Society, v. 147, no. 3, p. 461–467.

Anderson, R.S., 1990, Evolution of the Northern Santa Cruz Mountains by Advection of Crust Past a San Andreas Fault Bend: Science, v. 249, no. 4967, p. 397–401.

Becker, T.W., Faccenna, C., Humphreys, E.D., Lowry, A.R., and Miller, M.S., 2013, Earth and Planetary Science Letters: Earth and Planetary Science Letters,, p. 1–13.

Braun, J., 2010, The many surface expressions of mantle dynamics: Nature Geoscience, v. 3, no. 12, p. 825–833.

Braun, J., Robert, X., and Simon-Labric, T., 2013, Eroding dynamic topography: Geophysical Research Letters, v. 40, no. 8, p. 1494–1499.

Brocklehurst, S.H., 2002, Evolution of topography in glaciated mountain ranges: PhD Dissertation. MIT. 236 p.

Brocklehurst, S.H., and Whipple, K.X., 2006, Assessing the relative efficiency of fluvial and glacial erosion through simulation of fluvial landscapes: Geomorphology, v. 75, no. 3-4, p. 283–299.

Brozovic, N., Burbank, D.W., and Meigs, A.J., 1997, Climatic limits on landscape development in the northwestern Himalaya: Science. p. 571-576.

Byrd, J., Smith, R.B., and Geissman, J.W., 1994, The Teton fault, Wyoming: Topographic signature, neotectonics, and mechanisms of deformation: Journal of Geophysical Research. p. 20,095-20,122.

Christiansen, R.L., 2001. The Quaternary and pliocene Yellowstone plateau volcanic field of Wyoming, Idaho, and Montana (No. 729-G).

Crosby, B.T., and Whipple, K.X., 2006, Knickpoint initiation and distribution within fluvial networks: 236 waterfalls in the Waipaoa River, North Island, New Zealand: Geomorphology, v. 82, no. 1-2, p. 16–38.

Czarnota, Roberts, G.G., White N.J., Fishwick, S. 2014, Spatial and temporal patterns of Australian dynamic topography from river profile modeling. p. 1384-1424.

Darling, A., and Whipple, K.X., 2015, Geomorphic constraints on the age of the western Grand Canyon: Geosphere, v. 11, no. 4, p. 958–976.

DeCelles, P.G., 2004. Late Jurassic to Eocene evolution of the Cordilleran thrust belt and foreland basin system, western USA. American Journal of Science, 304(2), pp.105-168.

Dickinson, W.R., Klute, M.A., Hayes, M.J., Janecke, S.U., Lundin, E.R., McKittrick, M.A., and

Olivares, M.D., 1988, Paleogeographic and paleotectonic setting of Laramide sedimentary basins in the central Rocky Mountain region: Geological Society of America Bulletin, v. 100, no. 7, p. 1023–1039.

Flament, N., Gurnis, M., and Müller, R.D., 2013, A review of observations and models of dynamic topography: Lithosphere, v. 5, no. 2, p. 189–210.

Flint, J.J., 1974, Stream gradient as a function of order, magnitude, and discharge: Water Resources Research, v. 10, no. 5, p. 969–973.

Hall, R.D., and Shroba, R.R., 1993, Soils developed in the glacial deposits of the type areas of the Pinedale and Bull Lake glaciations, Wind River Range, Wyoming, USA: Arctic and Alpine Research, v. 25, no. 4, p. 368.

Hampel, A., Hetzel, R., and Densmore, A.L., 2007, Slip-rate increase on the Teton normal fault, northern Basin and Range Province, caused by melting of the Yellowstone ice cap and deglaciation of the Teton Range? Geology.

Harkins, N., Kirby, E., Heimsath, A., Robinson, R., and Reiser, U., 2007, Transient fluvial incision in the headwaters of the Yellow River, northeastern Tibet, China: Journal of Geophysical Research, v. 112, no. F3, p 1-21.

Heller, P.L., and Liu, L., 2016, Dynamic topography and vertical motion of the U.S. Rocky Mountain region prior to and during the Laramide orogeny: Geological Society of America Bulletin,, p. 1–17.

Hiza, M.M., 1999, The geochemistry and geochronology of the Eocene Absaroka volcanic province northern Wyoming and southwest Montana, USA. PhD Dissertation, Oregon State University. 261 p.

Holmes, G.W., and Moss, J.H., 1955, Pleistocene Geology of the Southwestern Wind River Mountains, Wyoming.: Geological Society of America Bulletin, v. 66, no. 6, p. 629-654.

Howard, A.D., 1998, Long profile development of bedrock channels: Interaction of weathering, mass wasting, bed erosion, and sediment transport: Rivers Over Rock: Fluvial Processes in Bedrock Channels. v. 107, p. 297–319.

Howard, A.D., and Kerby, G., 1983, Channel changes in badlands: Geological Society of America Bulletin, v. 94, no. 6, p. 739–752.

Howard, A.D., Dietrich, W.E., and Seidl, M.A., 1994, Modeling fluvial erosion on regional to continental scales: Journal of Geophysical Research: Solid Earth (1978–2012), v. 99, no. B7, p. 13971–13986.

Karlstrom, K.E., Coblentz, D., Dueker, K., Ouimet, W., Kirby, E., Van Wijk, J., Schmandt, B., Kelley, S., Lazear, G., Crossey, L.J. and Crow, R., 2012. Mantle-driven dynamic uplift of the Rocky Mountains and Colorado Plateau and its surface response: Toward a unified hypothesis. Lithosphere, *4*(1), pp.3-22.

Kirby, E., 2003, Distribution of active rock uplift along the eastern margin of the Tibetan Plateau: Inferences from bedrock channel longitudinal profiles: Journal of Geophysical Research, v. 108, no. B4, p.16-1 - 16-24.

Kirby, E. and Whipple, K.X., 2012. Expression of active tectonics in erosional landscapes. Journal of Structural Geology, 44, pp.54-75.

Kirby, E., and Whipple, K.X., 2001, Quantifying differential rock-uplift rates via stream profile analysis: Geology, v. 29, no. 5, p. 415–418.

Korup, O., Densmore, A.L., and Schlunegger, F., 2010, Geomorphology, v. 120, no. 1-2, p. 77–90.

Kraus, M.J., 1997, Lower Eocene alluvial paleosols: pedogenic development, stratigraphic relationships, and paleosol/landscape associations: Palaeogeography, v. 129, no. 3-4, p. 387–406.

Lave, J., and Avouac, J.P., 2000, Active folding of fluvial terraces across the Siwaliks Hills, Himalayas of central Nepal: Journal of Geophysical Research: Solid Earth, v. 105, no. B, p. 5735–5770.

Levander, A., and Miller, M.S., 2012, Evolutionary aspects of lithosphere discontinuity structure in the western U.S.: Geochemistry, Geophysics, Geosystems, v. 13, no. 7. p. 1-22.

Licciardi, J.M., and Pierce, K.L., 2008, Cosmogenic exposure-age chronologies of Pinedale and Bull Lake glaciations in greater Yellowstone and the Teton Range, USA: Quaternary Science Reviews, v. 27, no. 7-8, p. 814–831.

Licciardi, J.M., Clark, P.U., Brook, E.J., Pierce, K.L., Kurz, M.D., Elmore, D., and Sharma, P., 2001, Cosmogenic 3He and 10Be chronologies of the late Pinedale northern Yellowstone ice cap, Montana, USA: Geology.

Lowry, A.R., Ribe, N.M. and Smith, R.B., 2000. Dynamic elevation of the Cordillera, western United States. Journal of Geophysical Research: Solid Earth, 105(B10), pp.23371-23390.

Mackin, J.H., 1948, Concept of the Graded River: Geological Society of America Bulletin, v. 59, no. 5, p. 463-511.

McQuarrie, N., and Rodgers, D.W., 1998, Subsidence of a volcanic basin by flexure and lower crustal flow: The eastern Snake River Plain, Idaho: Tectonics, v. 17, no. 2, p. 203–220.

Miller, S.R., Sak, P.B., Kirby, E., and Bierman, P.R., 2013, Neogene rejuvenation of central Appalachian topography_ Evidence for differential rock uplift from stream profiles and erosion rates: Earth and Planetary Science Letters, v. 369-370, no. C, p. 1–12.

Morgan, W.J., 1971, Convection plumes in the lower mantle: Science. p. 42-43.

Moss, J.H., 1982, The Relation of River Terrace Formation to Glaciation in the Shoshone River

Basin, Western Wyoming, *in* Glacial Geomorphology, Springer Netherlands, Dordrecht, p. 293–314.

Mueller, P.A., Peterman, Z.E., and Granath, J.W., 1985, A Bimodal Archean Volcanic Series, Owl Creek Mountains, Wyoming: The Journal of geology, v. 93, no. 6, p. 701–712.

Omar, G.I., Lutz, T.M., and Giegengack, R., 1994, Apatite fission-track evidence for Laramide and post-Laramide uplift and anomalous thermal regime at the Beartooth overthrust, Montana-Wyoming: Geological Society of America Bulletin, v. 106, no. 1, p. 74–85.

Pierce, K.L., 2003, Pleistocene glaciations of the Rocky Mountains, *in* Developments in Quaternary Sciences, Developments in Quaternary Sciences, Elsevier, p. 63–76.

Pierce, K.L., and Morgan, L.A., 2009, Is the track of the Yellowstone hotspot driven by a deep mantle plume? — Review of volcanism, faulting, and uplift in light of new data: Journal of Volcanology and Geothermal Research, v. 188, no. 1-3, p. 1–25.

Pritchard, D., Roberts, G.G., White, N.J., and Richardson, C.N., 2009, Uplift histories from river profiles: Geophysical Research Letters, v. 36, no. 24, p. L24301–5.

Roberts, G.G., Paul, J.D., White, N., and Winterbourne, J., 2012a, Temporal and spatial evolution of dynamic support from river profiles: A framework for Madagascar: Geochemistry, Geophysics, Geosystems, v. 13, no. 4. p. 1-23

Roberts, G.G., White, N.J., Martin-Brandis, G.L., and Crosby, A.G., 2012b, An uplift history of the Colorado Plateau and its surroundings from inverse modeling of longitudinal river profiles: Tectonics, v. 31, no. 4. p. 1-25.

Rosenberg, R., Kirby, E., Aslan, A., Karlstrom, K., Heizler, M., and Ouimet, W., 2014, Late Miocene erosion and evolution of topography along the western slope of the Colorado Rockies: Geosphere, v. 10, no. 4, p. 641–663.

Schmandt, B., Dueker, K., Humphreys, E.D., and Hansen, S., 2012, Hot mantle upwelling across the 660 beneath Yellowstone: Earth and Planetary Science Letters, v. 331-332, p. 224–236.

Schwanghart, W., and Scherler, D., 2014, Short Communication: TopoToolbox 2 – MATLAB-based software for topographic analysis and modeling in Earth surface sciences: Earth Surface Dynamics, v. 2, no. 1, p. 1–7.

Small, E.E., and Anderson, R.S., 1998, Pleistocene relief production in Laramide mountain ranges, western United States: Geology, v. 26, no. 2, p. 123.

Smith, R.B., Jordan, M., Steinberger, B., Puskas, C.M., Farrell, J., Waite, G.P., Husen, S., Chang, W.-L., and O'Connell, R., 2009, Journal of Volcanology and Geothermal Research: Journal of Volcanology and Geothermal Research, v. 188, no. 1-3, p. 26–56.

Snyder, N.P., Whipple, K.X., Tucker, G.E., and Merritts, D.J., 2000, Landscape response to tectonic forcing: Digital elevation model analysis of stream profiles in the Mendocino triple

junction region, northern California: Geological Society of America Bulletin, v. 112, no. 8, p. 1250–1263.

Stein, R.S., and Barrientos, S.E., 1985, Planar high-angle faulting in the basin and range: Geodetic analysis of the 1983 Borah Peak, Idaho, earthquake: Journal of Geophysical Research: Solid Earth (1978–2012), v. 90, no. B13, p. 11355–11366.

Stephenson, S.N., Roberts, G.G., Hoggard, M.J., and Whittaker, A.C., 2014, A Cenozoic uplift history of Mexico and its surroundings from longitudinal river profiles: Geochemistry, Geophysics, Geosystems, v. 15, no. 12, p. 4734–4758.

Stickney, M.C. and Bartholomew, M.J., 1987. Seismicity and late Quaternary faulting of the northern Basin and Range province, Montana and Idaho. Bulletin of the Seismological Society of America, 77(5), pp.1602-1625.

VanLaningham, S., Meigs, A.J., and Goldfinger, C., 2006, The effects of rock uplift and rock resistance on river morphology in a subduction zone forearc, Oregon, USA: Earth Surface Processes and Landforms, v. 31, no. 10, p. 1257–1279.

Whipple, K.X., and Tucker, G.E., 1999, Dynamics of the stream-power river incision model: Implications for height limits of mountain ranges, landscape response timescales, and research needs: Journal of Geophysical Research. p. 17,661-17,674.

Wobus, C., Whipple, K.X., and Kirby, E., 2006, Tectonics from topography: procedures, promise and pitfalls: Geological Society of America Special Paper, v. 398, p. 55–74.

Zreda, M., and Noller, J.S., 1998, Ages of Prehistoric Earthquakes Revealed by Cosmogenic Chlorine-36 in a Bedrock Fault Scarp at Hebgen Lake: Science, v. 282, no. 5391, p. 1097–1099.

CHAPTER 3

Pliocene-Pleistocene Landscape and Drainage Evolution of the Bighorn Basin, WY

Eduardo Guerrero and Andrew Meigs

To be submitted to the Geological Society of America Bulletin

INTRODUCTION

The Bighorn Basin of Wyoming and Montana (Figure 3.1) preserves the record of drainage and landscape evolution in the form of widely distributed fluvial terraces. Studies of the Quaternary deposits in the basin have served as the foundation for advances of key concepts in Geomorphology and the study of landscape evolution. The modern hydrological Bighorn Basin's drainage area includes structures resulting from the Laramide orogeny (Dickinson et al., 1988) and Eocene volcanism (Hiza, 1999). The diversity in rock types exposed around the basin (Figure 3.2) allows for correlation of terrace deposits and interpretations of internal drainage evolution. This study presents a new model of erosion of the Bighorn Basin that considers the degree of landscape forcing by advection of dynamic topography (Chapter 1). Lateral migration rate of the Bighorn River is within an order of magnitude of the rate of motion of North America with respect to the Yellowstone hotspot. Eastward shunting of the Bighorn River is due to basin tilting between 0.5° and 0.25°in response to advection of transient topography impinging on the basin.

Motivation

We reinterpret the Bighorn Basin's Pliocene-Pleistocene erosional history in light of the hypothesis that the deformation front associated with hotspot-related transient topography is propagating northwestward through North American lithosphere as it passes over the Yellowstone plume (Figure 3.2) (Pierce and Morgan, 1992; Pierce and Morgan, 2009). Evidence for transient topography associated with the mantle comes from sedimentary rock deposits, which suggests that fluvial systems record dynamic topographic response to mantle thermal anomalies (Braun et al., 2013). The maximum inferred surface uplift rate for the Yellowstone dynamic topography is 0.302 mm yr^{-1}, and is below the detection limit of vertical surface deformation via analysis of channel

steepness patterns in the greater Yellowstone area (Chapter 2), however the Bighorn Basin is an ideal location to study how transient topography forces erosion and influences landscape evolution.

Background

Hotspots are the surface manifestation of sub-lithospheric processes and chains of volcanic centers are the most obvious expression of hotspots in the crust, however progressive deformation of the crust that evolves over million year timescales and is known as transient topography. It is characterized by topographic wavelengths between 250 - 1,000km and can deflect of the Earth's surface by up to 1km (Braun, 2010; Flament et al., 2013). Studies confirm the presence of a mantle thermal anomaly signal below Yellowstone, which suggests the Greater Yellowstone area crustal processes affecting the region since the late Mesozoic account for the geologic features with a wavelength of <200km that masks the transient topography deformation signal (Chapter 1).

A series of subaerial silicic eruptive centers provide evidence for the motion of North America relative to the hotspot since 17 Ma (Smith et al., 2009) (Figure 3.1). A ~600 km-long and ~1.2 km high asymmetric topographic swell is interpreted to be the surface manifestation of the transient topography (Figure 3.2) Topographic analysis indicates that the apex of the transient topography could presently be located approximately under the Beartooth Mountains and the inferred deformation front is already east of the Bighorn River (Figure 3.1) (Chapter 1).

In this chapter, we attribute the internal drainage network reorganization from a primarily northward to eastward direction due to basin tilting accompanying the advecting transient topographic wave. We present a new model for the basin's evolution using an updated geochronology, field observations, and paleoflow data collected from fluvial terraces.

Structural Evolution of the Bighorn Basin

The modern hydrologic Bighorn Basin includes the Wind River Basin in its contributing area, however, the two basins as separate structural basins and timing of their integration is not known. From this point forward, Bighorn Basin refers specifically to the structural basin that evolved during the Laramide Orogeny (61-55 Ma in this region) (DeCelles, 2004), and is bounded by the Pryor and Bighorn Mountains in the North and East, Owl Creek and Absaroka Mountains to the south and west respectively (Love, 1960; Dickinson et al., 1988).

Subduction along the western margin of North America drove the region's crustal evolution (DeCelles, 2004). Prior to the onset of the Laramide orogeny, the thin-skinned Sevier overthrust of Wyoming and Idaho was the deformation front of the backarc deformation (Dickinson et al., 1988). The region east of the Sevier belt was below sea level because it was occupied by a broad foreland basin, which included the Cretaceous Western Interior Seaway (Dickinson et al., 1988; Heller and Liu, 2016). The extent of the basin reflects the combined effects of flexural subsidence enhanced by negative dynamic topography associated with foundering of the subducting Farallon plate (Mitrovica et al., 1989; Heller and Liu, 2016).

Initiation of the Laramide orogeny is not well constrained throughout the entire Cordillera, but the deformation front is thought to have migrated eastward and been active by 70 Ma (Dickinson et al., 1988). Laramide deformation led to the segmentation of the foreland province into smaller basins that were separated by basement cored uplifts (Dickinson et al., 1988), which is the explanation for the existence of crystalline basement rocks in the Laramide ranges surrounding the Bighorn Basin (Figure 3.3). Syntectonic alluvial fan deposits preserved along the fringe of the Beartooth Mountains suggests that Laramide crustal shortening created topographic relief in excess of 1-2 km between ~73 and 55 Ma (DeCelles et al., 1991b). Rock uplift in the

Wind River Range began around 85 Ma (Cerveny and Steidtmann, 1993), but accelerated between 62 and 57 Ma (Peyton et al., 2012). Apatite fission track data from the Beartooth range indicate exhumation from 61 to 52 Ma document cooling associated with rock uplift (Omar et al., 1994; Peyton et al., 2012). Uplift of the surrounding ranges led to the development of the Bighorn basin as a discrete depositional center by the early Paleocene (Figure 3.3) (Dickinson et al., 1988).

Volcanic activity swept southeastward towards the Bighorn Basin in concert with a decrease in angle of the Farallon plate's subduction (Dickinson et al., 1988). This magmatic event is known as the Challis-Absaroka volcanic trend and extended from ~70-43 Ma between the Challis volcanic field in Idaho and the Absaroka mountains in the southeast (Armstrong and Ward, 1993). The Absaroka volcanic center consists of 25,000 km^2 of lava flows, shallow intrusions, ash-flow tuffs and volcaniclasitc deposits marks the eastern limit of this volcanic flare-up and was active between 53 and 43 Ma (Hiza, 1999).

Each of the three major geologic events that led to the formation of the Bighorn Basin has a distinct associated lithologic signature (Figure 3.3). The core of the Laramide Ranges consists of crystalline metamorphic igneous intrusive and metasedimentary units. The margins of the basin include deformed sedimentary rocks that indicate a regressive sequence, grading from marine to terrigenous environments of deposition. The Absaroka volcanics have a mafic-intermediate character (Hiza, 1999).

Depositional Regime in the Bighorn Basin

The Bighorn Basin began to accumulate sediment with the onset of the Laramide orogeny and the development of the structural syncline (Dickinson et al., 1988). The oldest synorogenic deposits exposed in the basin are part of the Lance Formation, which is known as the Hell Creek Formation in Montana. These deposits consist mainly of interbedded sandstones, shale and

conglomerates that are earliest Paleocene in age (Finn, 2010). Formation thickness variations record the onset of Laramide orogeny and early basin segmentation of the foreland province (Finn, 2010).

The Fort Union Formation overlies the Lance Formation, and is also known locally as the Polecat Bench Formation (Bown and Kraus, 1981a). Coal, carbonaceous shale, conglomerates, sandstones, and siltstones comprise the Fort Union Formation (Yuretich and Hickey, 1984). The conglomerate clasts are composed of crystalline basement and metasedimentary units and are interpreted to be alluvial fan deposits sourced from the Beartooth block (DeCelles et al., 1991a), relief between the basin floor and the range is thought to have exceeded 1.5 km during deposition (DeCelles et al., 1991b). Thickness varies by ~300 m around the basin's margins, and is estimated to be ~2,200 m at its thickest (Finn, 2010).

An angular unconformity locally separates the Fort Union from the overlying Willwood Formation, which is ~700 m thick and was deposited beginning in the lower Eocene (Bown and Kraus, 1981b). The unconformity reflects the spatiotemporal variations in rock uplift and volcanic activity throughout the basin (Bown, 1980). The Willwood consists of variegated shales, sandstones, and conglomerates that point to rapid sediment accumulation punctuated by numerous pauses in deposition and soil development (Bown, 1980; Kraus, 1992; Finn, 2010). Paleoflow data from the Willwood formation indicate that the basin drained towards the South-South east during the Early Eocene towards the paleo-Wind River, however rock and surface uplift of the Owl Creek Mountains at this time forced a drainage reversal and transformed the Bighorn into a closed basin (Bown, 1980). Composition of the upper Willwood deposits point to increased volcanic activity in the Absaroka volcanic center, coarsening upward in the Willwood is

interpreted as the result of encroaching volcanic center reducing the transport distance for the deposited material (Bown, 1980).

The Tatman Formation conformably overlies the Willwood formation in the south central portion of the basin. It is ~200 m thick and composed mainly of fine grained clastic sedimentary units (Rohrer and Smith, 1969). The alternating shales, claystones, sandstones, and mudstones of the Tatman are interpreted to have been deposited in a lake that interfingers with the Willwood Formation (Bown, 1980). Tatman Mountain near Meteetsee, WY is the type locality for the Tatman Formation, however there is an unconformity between the top of the Tatman and the overlying Fenton Pass Formation, which is the oldest Quaternary deposit preserved in the Bighorn basin (Rohrer and Smith, 1969) (Figure 7). Interfingering deposits of Willwood and Tatman units are preserved in the vicinity of the Lysite Mountain at the southwestern margin of the Bighorn Basin, and are overlain conformably by the Pitchfork Formation (Bown, 1980).

The Pitchfork Formation is composed mainly of breccias and angular clasts that fine up towards the top of the formation are composed of basalt and basaltic andesite units (Hay, 1956). Correlation with units outside the Bighorn basin suggest that the volcanic detritus continued period of basin-fill. The highest volcanic sedimentary formation is the Wiggins Formation that covered the southern Bighorn Mountains and the Owl Creek Mountains (Love, 1960). Oligocene volcaniclastic deposits are found throughout high elevations in the Bighorn Mountains. Volcaniclastic sedimentation overtopped the Bighorn basin at Lysite Mountain, and were deposited in the wind River and Powder River Basins. This means that the basin reached its maximum fill by early Oligocene time (Bown, 1980), that reached maximum elevation of 2100 m (Heasler and Kharitonova, 1996), and some of these deposits are now at an elevation of 2700 m (Gingerich, 1979).

The gravel cap on top of Tatman Mountain which is interpreted as the oldest preserved terrace in the Bighorn Basin is made up by the Fenton Pass formation which unconformably lies over the the Tatman formation and is estimated to be 2.3 Ma (Rohrer and Smith, 1969)

Erosional Regime in the Bighorn Basin

A switch from deposition to incision occurred after the Pitchfork Formation overtopped the southern edge of the Bighorn basin (Hay, 1956). The period of time between the switch to erosion and the deposition of the Fenton Pass formation on Tatman mountain is unknown. J. Hoover Mackin's (1937) 'Erosional History of the Bighorn Basin, WY remains the authoritative interpretation of the post-basin fill landscape and drainage evolution. Subsequent work has confirmed Mackin's early interpretations and provided additional evidence to support his proposed sequence of events. Mackin's model for erosion of the Basin is constrained by the following observations: First, the existence of of high elevation gravel deposits in the Bighorn Mountains; second, the incision of the Wind and Shoshone river canyons through Laramide structural barriers; and third, the existence of high elevation erosional surfaces at elevations of ~2700m (Mackin, 1937; Love, 1960; Ritter, 1975; Heasler and Kharitonova, 1996). Incision of Wind River Canyon implies 800 m of erosion incision, because Bighorn river elevation at the mouth of the canyon is 1500 m and the Owl Creeks are at an elevation of 2300m. The difference in elevation between Shoshone River (1700 m) and the top of the Rattlesnake anticline (2500 m) in Shoshone Canyon is 900m (Heasler and Kharitonova, 1996). Details of the erosional story and updates to the Mackin's original interpretation are covered in the discussion section of this paper.

METHODS

This project relied on a combination of field work, published data compilation. Mapping was done using air photos and 10m resolution digital elevation model derived from the National Elevation Dataset., Google Earth, and fieldwork.

Fieldwork

Paleoflow data were collected from imbricated rounded cobbles and gravel contained within an individual terrace. Imbricated cobbles are commonly used to interpret fluvial transport direction. Inspection of an active channel will reveal that sediment that exceeds the river's capacity will deposit that sediment on one another with the plane that includes the long and intermediate axis dipping in the upstream direction (Krumbein, 1942; Kauffman and Ritter, 1981a). Terraces in the Bighorn Basin consist of sediment that ranges from 16 mm (medium gravel) to 200 mm (cobbles). Imbricated gravel and cobbles were measured only below a depth of 50 cm or where material did not display evidence of disturbance from frost heave (Kauffman and Ritter, 1981b). Dip direction was measured directly along elongated axis of imbricated cobbles following (Kauffman and Ritter, 1981b), paleoflow was then interpreted to be 180° from measured dip direction. Measurements were taken from soil pits, road cuts, or shallow excavations along terrace risers or gullies incising into terrace tread.

Geochronology Synthesis

Terrace chronologies have been published for many of the streams in the Bighorn Basin and Wind river basins, however authors identify terraces using local names and terraces chronologies are not easily related throughout the region (Mackin, 1937; Ritter, 1975; Moss, 1982a; Palmquist, 1983; Reheis et al., 1991b; Chadwick et al., 1997; Hancock et al., 1999; Sharp et al., 2003; Stock and Riihimaki, 2006). Age control is limited and primarily relies on inclusion

of tephras associated with Yellowstone eruptions (Izett, 1981; Christiansen, 2001; Lanphere et al., 2002). Terraces were correlated based on the local position of between bedrock strath and the modern channel, composition, and long-river terrace correlation. A number of terrace levels that were excluded from correlation because they were identified as cut and fill terraces, and these types of terraces are unreliable for incision rate or tectonic interpretations (Pazzaglia and Gardner, 1998; Lave and Avouac, 2000). Lateral migration of the Bighorn river was measured from the thalweg of the modern Bighorn to the terrace shoulder, where the riser and tread come together.

RESULTS

Geochronology

Figure 4 summarizes the correlation and available age control for terraces preserved along the major tributaries of the Bighorn River.

Bighorn River Terraces

A sequence of seven terrace levels occurs east of the Bighorn River near Worland, WY. Terraces are correlated upstream and downstream of Worland (Figure 3.6, after Palmquist, 1983). All terrace heights are measured between the average floodplain elevation of the modern Bighorn and the strath elevation: T1 strath is ~20 m, T2 is ~40 m, T3 is ~60 m, T4 is ~100 m, T5 is ~120 m, T6 is ~130 m, T7 is ~140m.

Average lateral migration rate of the Bighorn River between T7 and T5, which are terraces that contain Yellowstone tephras is 3.06 mm yr^{-1}, and 11.52 mm yr^{-1} between T5 and the thalweg of the modern Bighorn River (Figure 3.5). The tephras contained in T7 are dated to from the Mesa Falls eruption at 1.28 Ma, and are correlated to a T7 deposit in Pryor Creek (Reheis, 1992).

Greybull River Terraces

Figures 3.6 and 3.7 illustrates paleoflow results for terraces in the upper and lower Greybull river valley. Average flow direction for the Greybull river during T3 time was to the North-Northeast. Between T-3 and T2 (Figure 8A,8B, flow direction changed so that by T2 time flow was towards the East (Figure 8B). By T1 time, flow direction changed due to capture of the T2 Greybull by the T1-modern drainage. The abandoned drainage is now known as Dry Creek (Mackin, 1936; Palmquist, 1983). Palmquist (1983) attributes the capture of the Greybull River to the eastward lateral migration of the Bighorn River.

Shoshone River Terraces

Results for terrace correlation along the Shoshone River are presented in figures 3.8 and 3.9. Terrace T1 is the lowest terrace level throughout the entire Bighorn and is best preserved along the Shoshone River. T1 grades to a Pinedale (MIS 2) moraine in the South Fork Shoshone River valley, upstream of Buffalo Bill Reservoir (Moss, 1982b), surface exposure dating of boulders on a Pinedale moraine at the mouth of the Clarks Fork Yellowstone canyon gives an age of 18.8 ka +/- 0.9 ka (Licciardi and Pierce, 2008). T2 terrace is well developed throughout the entire valley, and is related to Bull Lake glaciation (MI6), ~140 ka (Moss, 1982a; Reheis et al., 1991b).

The Clarks Fork Yellowstone river now drains northward to the Yellowstone, Polecat Bench, which is correlated as T7 throughout the basin, contains crystalline clasts derived from the Beartooth block, which the Clarks Fork drains. Paleoflow measurements in Polecat Bench indicate a northward drainage direction during T7 time. An isolated T5 terrace located north of Heart Mountain contains crystalline clasts from the Clarks Fork as well, paleoflow measurement indicates a north-northeast flow during T5 time (Figure 10). Paleoflow measurements for T2

indicate that the Shoshone river flowed North-Northeast during T2 time, ~140 ka and then changed direction to have an east-directed flow by T1 time (~26 ka). T2 contains a much lower percentage of crystalline clasts compared to T5, which means that Clarks Fork and Shoshone were established as separate drainages between T5 and T2 times (600 ka and 140 ka).

Clarks Fork Yellowstone and Pryor Creek Terraces

The Clarks Fork Yellowstone (3.9) and Pryor Creek (Figure 3.10) are not presently within the Bighorn Basin drainage area, however terraces contained in both these drainage systems contain evidence that link them to the paleo-Bighorn Basin. Presence of Clarks Fork crystalline gravels in T5 terrace with a northeastward paleoflow towards the Shoshone river is interpreted to be the last period when these two drainages were combined. T3 terraces along the Clarks Fork indicate a northward flow direction by 300 ka, and a significant drainage contribution from a river south of the Clarks Fork Canyon. This interpretation is based on the observation that the modern streams in this area, Pat O'Hara and Paint Creek, are underfit compared to the T3 terraces.

Downstream of the Clarks Fork Yellowstone Canyon is the community of Silesia, and (Ritter, 1975) reported a high terrace deposit that was key terraces in the interpretation of the Bighorn Basin's drainage evolution North of the Clarks Fork Yellowstone Canyon. The Silesia gravel is ~300m above the Clarks Fork and contains basaltic andesite and basalt clasts and a reported a northeastward ward paleoflow direction (Reheis et al., 1991a). Mackin (1937) identified deposits in Pryor Creek (T7) as correlating to Polecat Bench, and identified a wind gap in the Pryor Mountains as being the valley through which a combined Clarks-Fork Shoshone flowed based on the terrace deposits containing similar percentages of Clarks Fork crystalline and Shoshone basaltic andesite clasts. This leads to the interpretation that a combined Greybull-Tatman, Clarks Fork-Shoshone river was the major outlet of the Bighorn Basin at T9 time. There

are a few T9 deposits to the North-East, in between present day Pryor Creek and the modern Bighorn River that suggest that the Clarks Fork Shoshone flowed to the North-East through T7 time.

DISCUSSION

Drainage and landscape evolution of the Bighorn Basin since the Pliocene-Pleistocene Transition

We propose that the timing of the drainage reorganization and lateral migration of rivers parallel to the deformation front in in the Bighorn Basin since the Pliocene is primarily driven by basin tilting due to surface uplift associated with the progressive incursion of transient topography into the basin. Figure 3.2 illustrates a model for advection of transient based on the long wavelength topography that is coincident with the Yellowstone hotspot (Chapter 1*)*. North American lithosphere is passing over the Yellowstone hotspot at a rate of 29 mm $yr^{-1}$and is moving towards the southwest relative to the hotspot (Chapter 1). Abbreviations correspond to positions in space and time along the track of the hotspot for the Yellowstone-related dynamic topography. Spatial correlations were determined by the distance separating each of the major associated volcanic centers (Picabo, Heise, and Yellowstone) and one physiographic/tectonic boundary (western edge of the Bighorn Basin). Time was determined from youngest major eruption associated with each one of the place-mark volcanic centers (Smith et al., 2009) , which is associated with each of the and coincides with the apex of the dynamic topography wave as it passes over the hotspot. The lower panel gives predicted uplift and subsidence rate associated with each time stamp. Results indicate that maximum uplift rate of 0.302 mm yr^{-1} aught to lead the apex of the transient topography swell by nearly 100 km. This means that presently, the

western Bighorn basin is experiencing the inferred effects of transient topography associated with Yellowstone.

During Plio-Pleistocene time, the central and northern western Bighorn Basin drained towards the Yellowstone river through Silesia, which is ~300 m above the modern Clarks Fork Yellowstone river (Ritter, 1975). Ritter (1975) interpreted the combined paleo Clarks Fork-Shoshone river to have been the dominant drainage at T9 time. We refer to this drainage as the Silesia River. Minimum ages for Silesia gravel are 2.2 Ma (Reheis et al., 1991b) and minimum ages for Tatman are 2.3 Ma. Agard and Reheis (1990) report a terrace west of the modern Bighorn and east of the modern Clarks Fork that is correlative in elevation to Tatman time. We interpret this terrace to represent the combined Clarks Fork-Shoshone-Greybull drainage through the dominant Silesia river.

By 1.28 Ma, the Silesia drainage was abandoned as the dynamic topography defrmation front forced slight tilting of the western Bighorn Basin (#1, Figure 12), the new dominant drainage became the combined Clarks-Fork Shoshone river, which we name the Polecat river and drained through Pryor Gap (Mackin, 1937; Ritter, 1975; Reheis, 1992). A paleo-Bighorn river began flowing through Bighorn Canyon, an interpretation based on terrace relations downstream of the Pryor Mountains (Reheis et al., 1991b), which are identified as T7 in plate 1. T7 near Worland is illustrates that the Bighorn River flowing northward through the center of the basin, east of Polecat River.

By 660 ka, the combined Clarks-Fork Shoshone was flowing into the Bighorn river as evidenced by the T5 deposit on the north flank of Heart Mountain that indicates east-northeast flow (#3, Figure 3.12), this capture coincides passage of modeled deformation front between

1.28Ma and 660 ka towards the northeast. Basin tilting also forced the Bighorn River to migrate ~4km eastward by 660 ka, position is recorded by T5 near Worland.

The a rough approximation of the modern Bighorn Basin drainage area was established by 140 ka, when the Clarks Fork drained northward and a drainage divide along Polecat Bench separated it from the Shoshone River. During this time, the Bighorn continued its eastward migration, continually being forced by slight tilting associated with dynamic topography signal. Bighorn terraces T3-T1 indicate an acceleration of lateral migration to ~11mm yr^{-1}. The modern Greybull river captured the T2 Greybull river and established the modern drainage, T2 Greybull river became Dry Creek between 140ka and 23ka.

The role of climate in driving vertical incision is well demonstrated in this region (Small and Anderson, 1998; Riihimaki and Reiners, 2012), without additional data, it is not possible to speak to vertical incision rates in the Basin and related them to potential forcing by dynamic topography, however the role of climate in the lateral motion of rivers is less well understood. This allows the interpretation that slight basin tilt that could result from an inferred ~0.5° slope (Chapter 1) is sufficient to force the migration of a river. The acceleration of the lateral migration rate is explained by the increasing tilt in the basin as it experiences higher surface uplift.

The last update to Makin's (1937) interpretation of the erosional history of the Bighorn Basin was by Reheis et al (1991). The interpretation that follows is based on work by Mackin (1937), Moss (1961), Ritter (1975), Palmquist (1983), and Reheis (1991). Interpretation includes age determination based on correlation with a cosmogenic terrace chronology for the Wind River (Hancock et al., 1999) and exposure ages for Pinedale moraines that T1 terraces grade into throughout the basin (Licciardi and Pierce, 2008). This relies on the assumption that terrace levels in the Wind River are correlated with terrace levels in the Bighorn.

CONCLUSIONS

Palmquist (1983) recognized the lateral migration of the Bighorn River as the controlling agent that forced the Plio-Pleistocene drainage reorganization from a primarily south to northward drainage direction to a west-east dominated system. He describes the lateral migration as 'unexplicable'. Incorporation of an advecting dynamic topography deformation signal could provide the mechanism for the lateral migration of the Bighorn River. This results from this work indicate that the key to quantifying the influence of dynamic topography on the erosion of the Bighorn basin requires detailed geochronology. Compilation of previous studies and an updated geochronology of the Plio-Pleistocene erosion of the Bighorn Basin suggests that dynamic topography associated with Yellowstone played a role in the basin's drainage reorganization and landscape evolution.

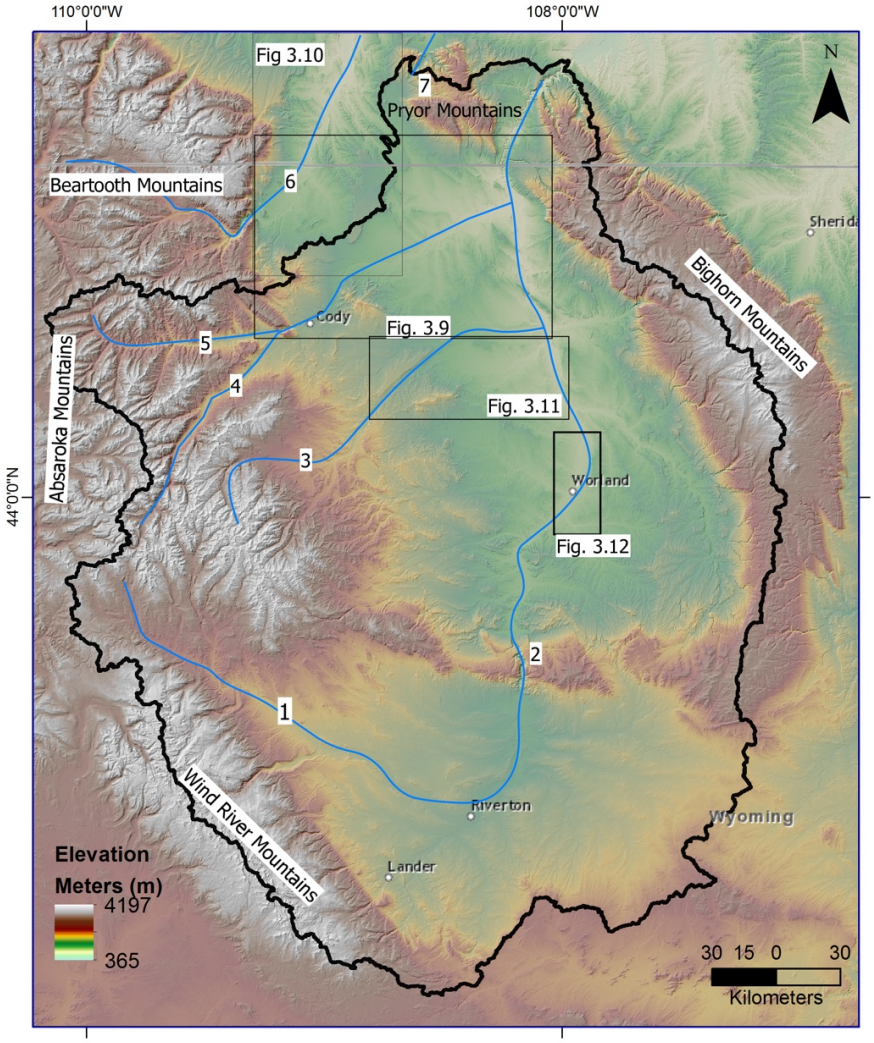

Figure 3.1 Bighorn Basin location map. Hydrologically integrated Bighorn Basin includes the Wind River. Structural Bighorn Basin is bounded by the Absaroka mountains to the west, the Pryor Mountains to the north, the Bighorn Mountains to the east, and the Owl Creek mountains to the south. Located in northwestern Wyoming. Dashed line represents deformation front inferred from observations (Chapter 1), see Figure 2. Vector is rate of motion with respect to the Yellowstone hotspot. Wind River (1) becomes the Bighorn River (2) when it crosses the Owl Creek Mountains (where "Wyoming" label is located). Greybull River (3), South Fork Shoshone (4), and North Fork Shoshone (5) are the major tributaries that drain the western side of the basin. Clarks Fork Yellowstone (6) and Pryor Creek (7) are now outside the Bighorn Basin's drainage basin. All of these rivers eventually drain to the Yellowstone River (not included in map).

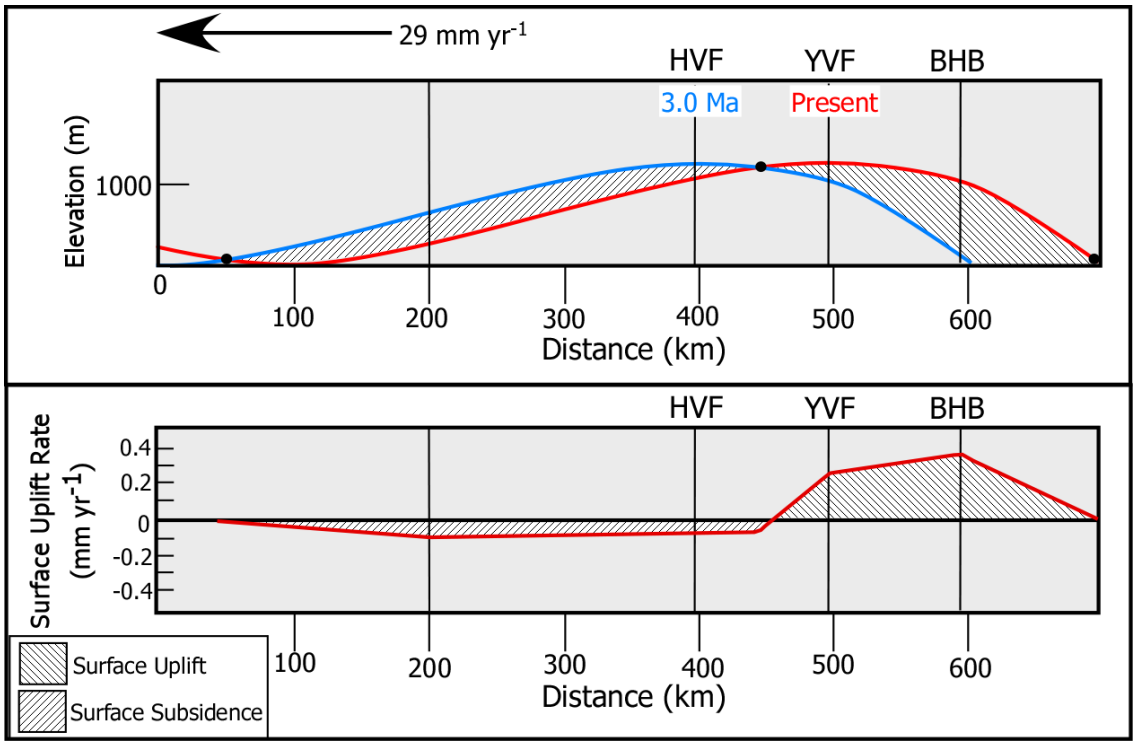

Figure 3.2 Model of advection of transient topography and surface uplift related to Yellowstone (Chapter 1). Upper panel illustrates observed and inferred position of transient topography in the Yellowstone area. Abbreviations identify locations of hotspot-related volcanic centers, which places constraints on the position of transient topography: Red- Present position of transient topography at the time of the Lava Creek eruption in the Yellowstone Caldera, Blue curve is position of transient topography at the time of Heise volcanic field eruption at 3 Ma. Diagonal hashes indicate either surface uplift or subsidence where. Lower panel illustrates rates of surface uplift and subsidence associated with advection of transient topography. The western margin of the Bighorn Basin (BHB) is currently experiencing maximum uplift rate of between 0.166 and 0.302 mm yr^{-1}.

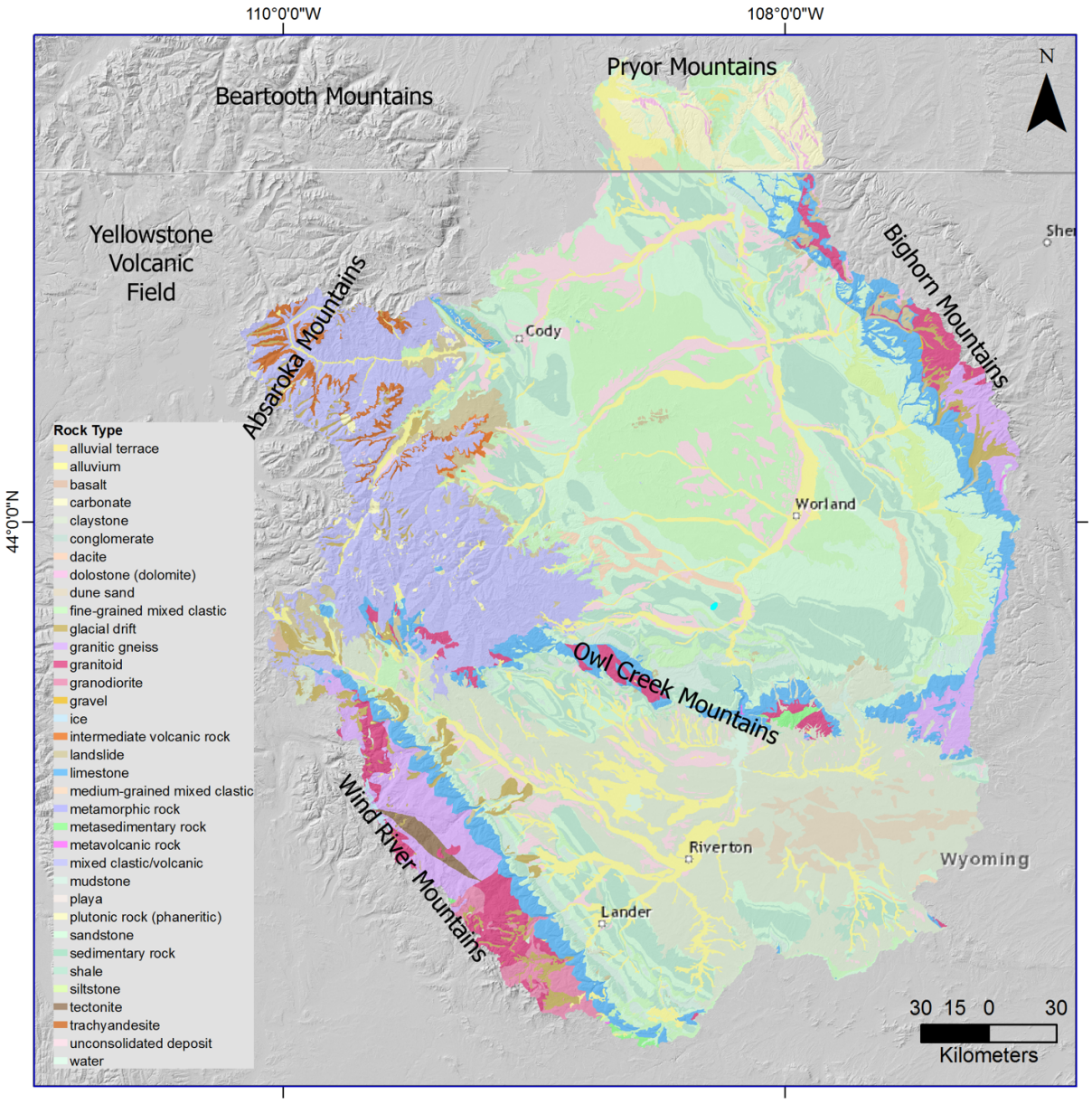

Figure 3.3 Rock type distribution in the Bighorn Basin (USGS State Geology geospatial data for Montana and Wyoming). Terrace mapping and interpretations based on fieldwork conducted north of Owl Creek Mountains, east of Absaroka and Beartooth Mountains, and south of Pryor Mountains. Mapping was restricted to alluvium terrace deposits and alluvium deposits (yellow units)

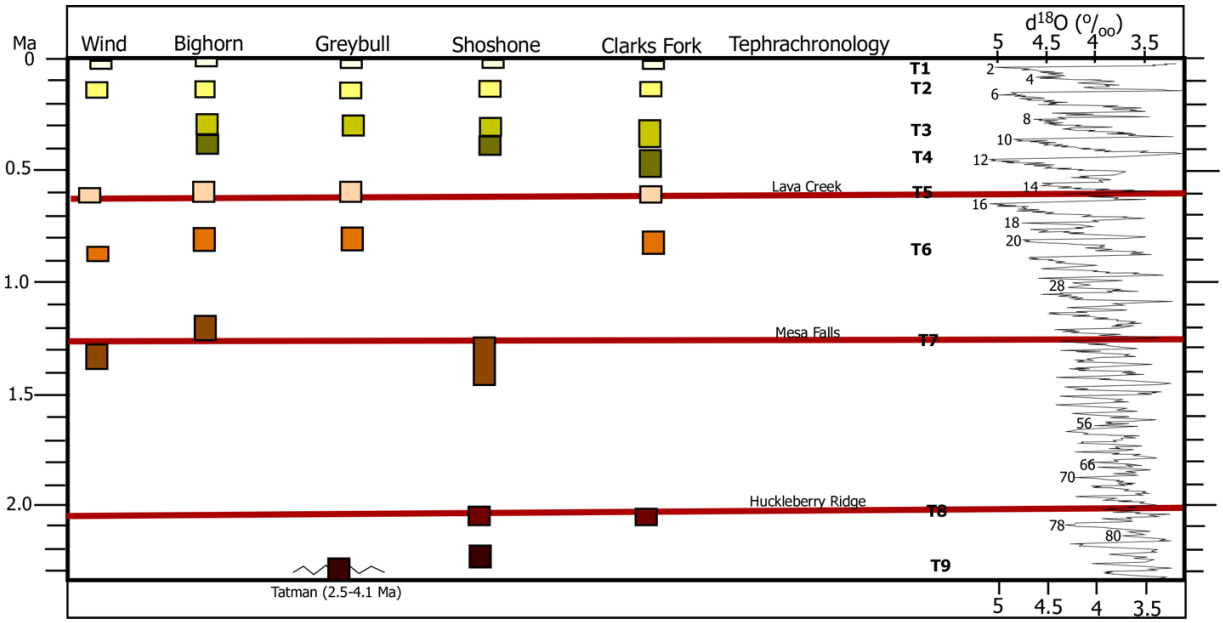

Figure 3.4 Terrace correlation for the Bighorn basin. Tephrachronology (Izett, 1981; Christiansen, 2001), $d^{18}O$ curve (Lisiecki and Raymo, 2005), Wind River ((Anderson et al., 1996; Chadwick et al., 1997; Hancock et al., 1999), Bighorn, Greybull, Shoshone, and Clarks Fork based on field relations and (Mackin, 1937; Palmquist, 1983; Reheis et al., 1991b; Stock and Riihimaki, 2006). Terrace nomenclature T1 to T-9 is used to aid in basin-wide correlation.

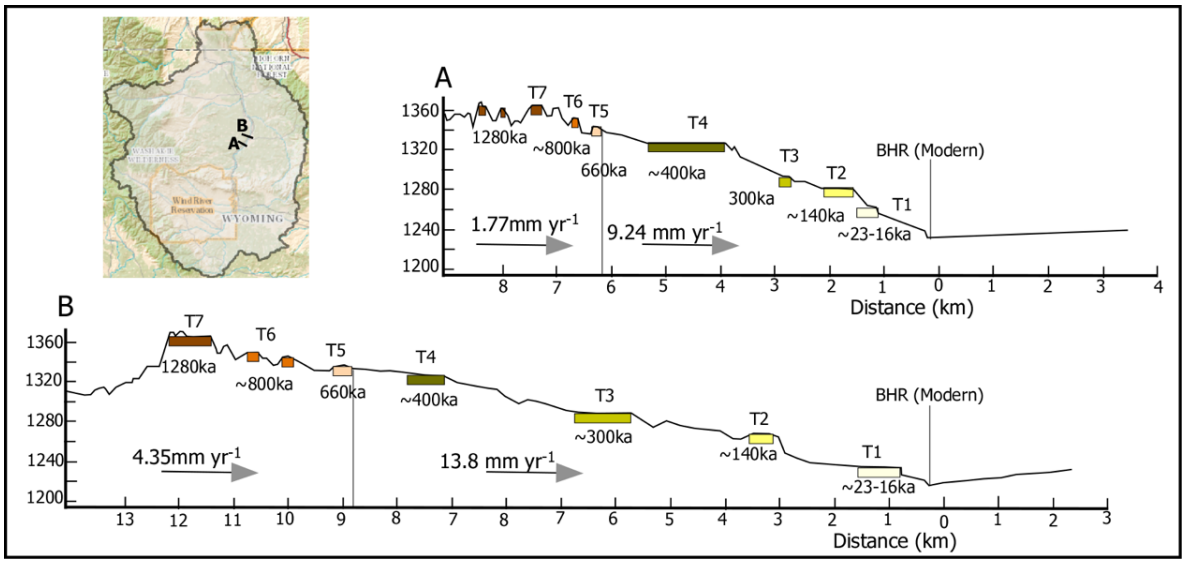

Figure 3.5 Terrace profiles across the Bighorn River illustrating the main channel's east-south east migration. Terraces were mapped originally by Andrews et al., (1947) and later by Palmquist (1983) and this study. Field relations were and contacts were confirmed and improved during fieldwork for this study. Terrace nomenclature as shown in Figure 3.4.

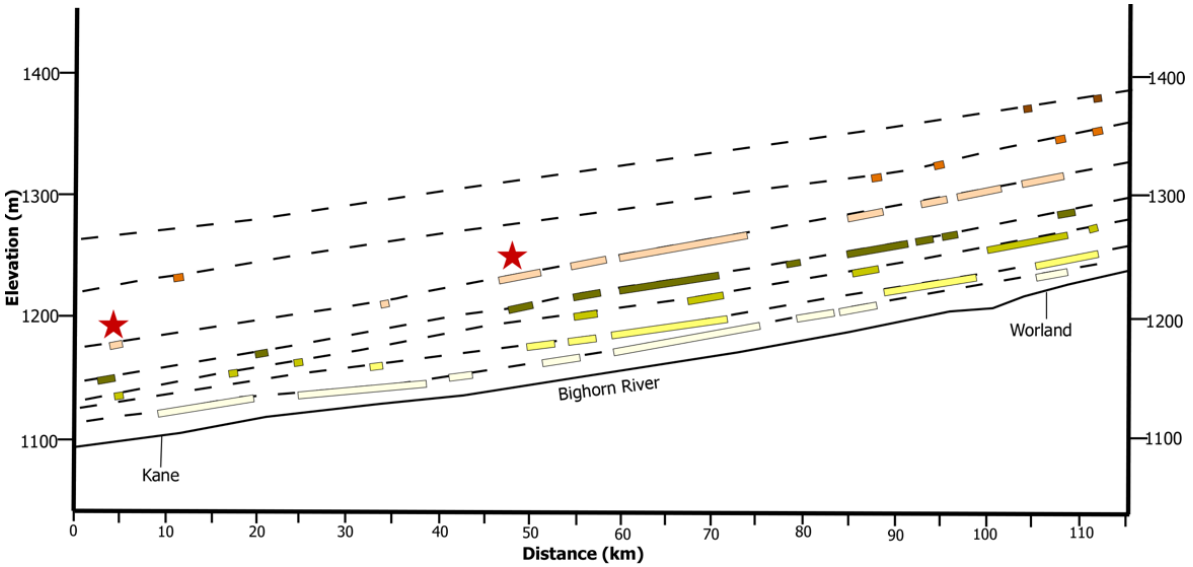

Figure 3.6 Bighorn River Long river and terrace profiles correlation (modified from Palmquist, 1983). Terrace locations and elevation based on field observations, measurements, and published sources. Stars denote the terraces that contain fluvially-reworked Mesa Falls tuff (1.28 Ma) deposits (Reheis, 1991). Terrace profiles record relatively uniform incision, since they mostly appear to be nearly parallel.

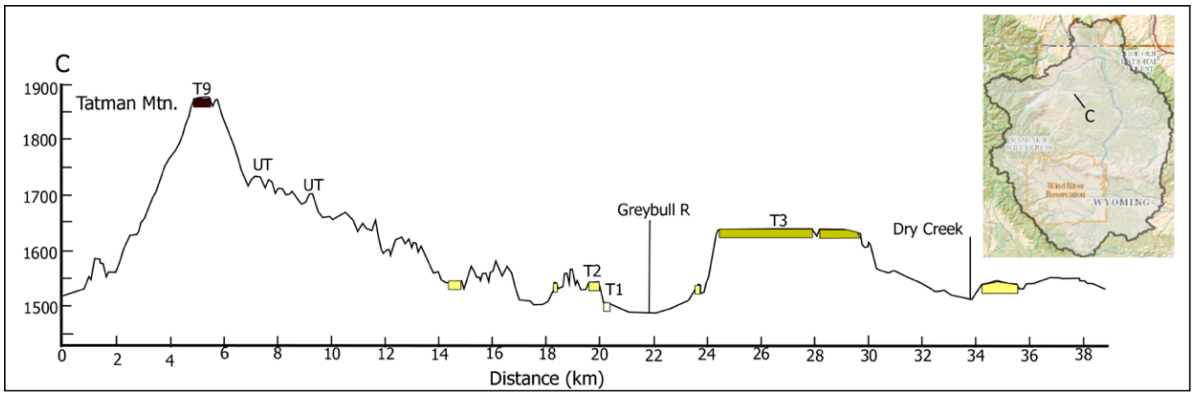

Figure 3.7 Terrace profile across Greybull River at Tatman Mountain. Numbered terraces are correlative throughout the Greybull river drainage. There are a number of unpaired terraces (UT) throughout the Greybull river valley, but only two are captured by this profile. Colors after Figure 3.4.

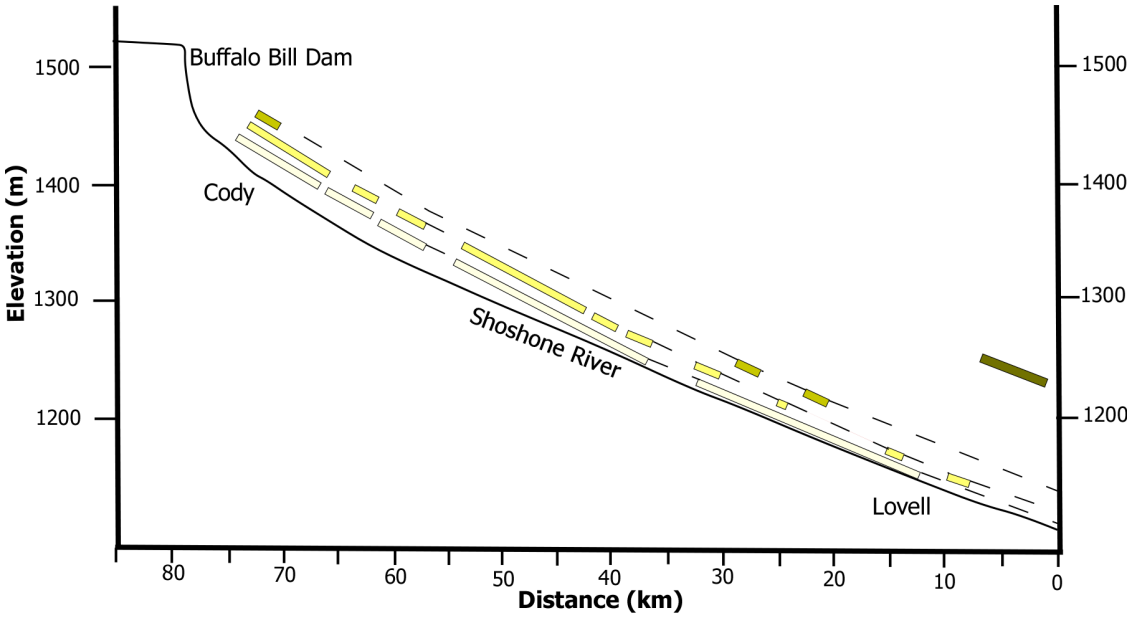

Figure 3.8 Long river profile of the Shoshone River between the Buffalo Bill Dam and Lovell (Kane), WY. Based on field observations and on previous work by by Andrews et al (1947), Palmquist, 1983, Pierce (1997). Colors after Figure 3.4. Terraces merge downstream, which suggests differential surface uplift between upstream (west) and downstream (east) portions of the Shoshone drainage. This coincides with model of advection of transient topography, where the western portion of the basin as undergone surface uplift longer than the eastern side, and may currently be experiencing a maximum uplift rate between 0.166 and 0.302 mm yr^{-1}.

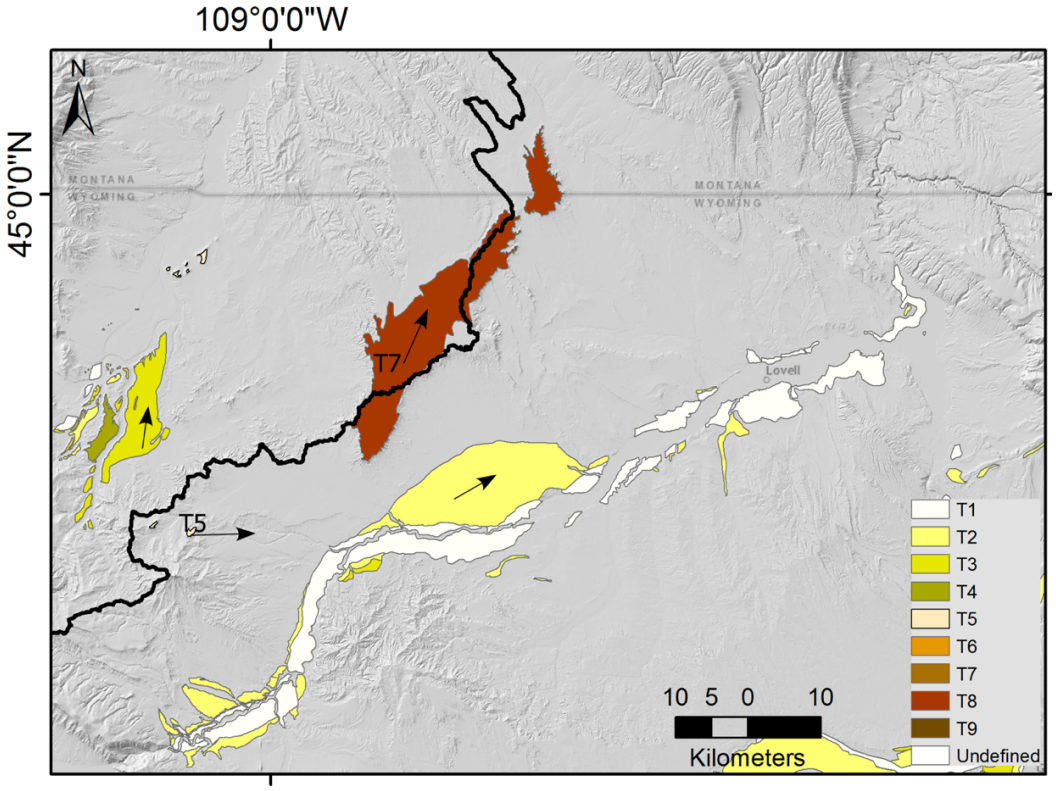

Figure 3.9 Terrace map for the Shoshone and Clarks Fork Yellowstone. Shoshone river is part of the Bighorn Basin, Clarks Fork is outside the basin and drains into the Yellowstone river upstream of the junction with the Bighorn. Vectors are average flow directions measured from individual terraces.

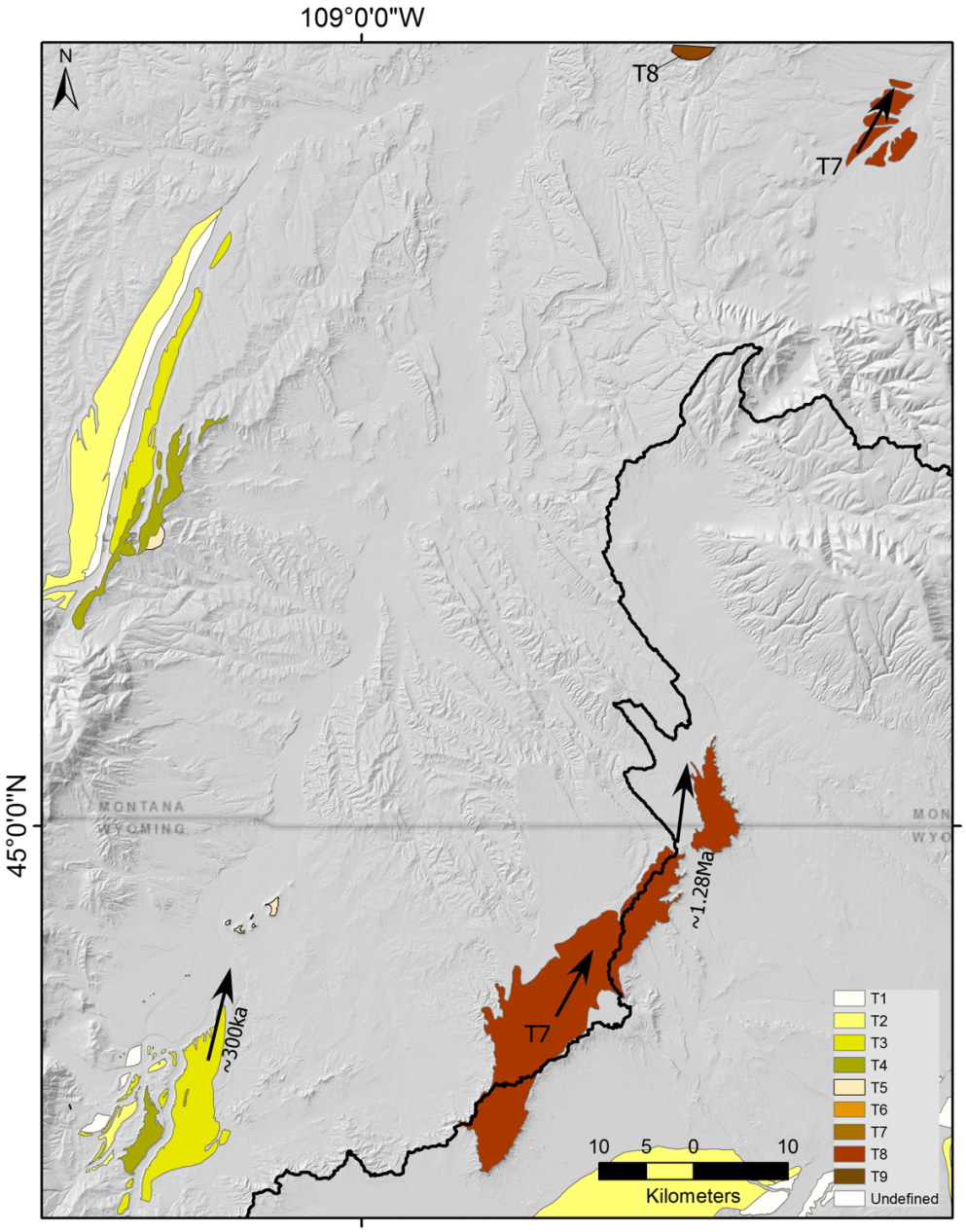

Figure 3.10 Detail of terrace distribution northwest of the modern Bighorn basin drainage divide. Terrace gravels near Silesia, MT contain clasts with lithology that correlates to Tatman Terrace (Ritter, 1975). Terrace deposits along Pryor Creek correlate to Polecat Bench (T7) (Figure 3.9). The combined Clarks Fork-Shoshone is interpreted to have occupied the present Clarks Fork river valley at 2.02 Ma, and the river migrated to the Pryor Creek drainage by 1.28 Ma, flowing through the Pryor Mountains wind gap (Reheis, 1992).

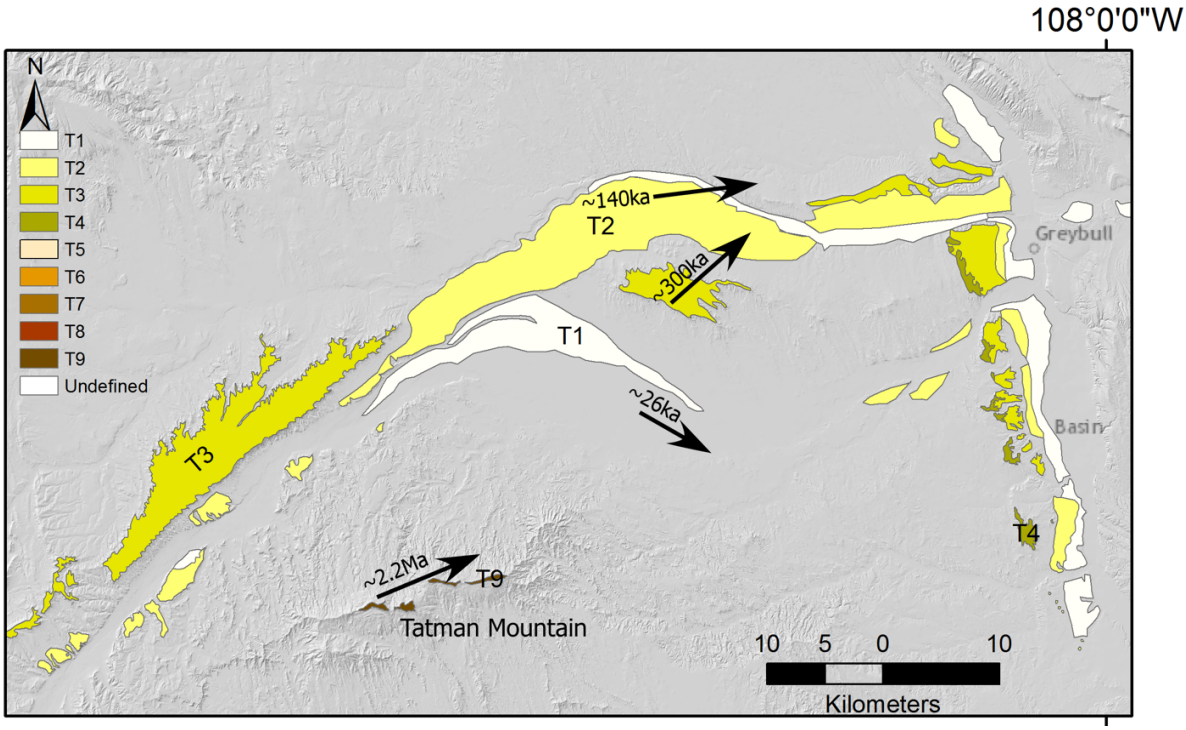

Figure 3.11 Detail map of terraces preserved in the vicinity of Greybull, Wyoming. Imbrication measurements are interpreted to mean changes in flow directions for the paleo-Greybull river. Map includes Tatman Mountain, which is the highest terrace level preserved in the Bighorn Basin.

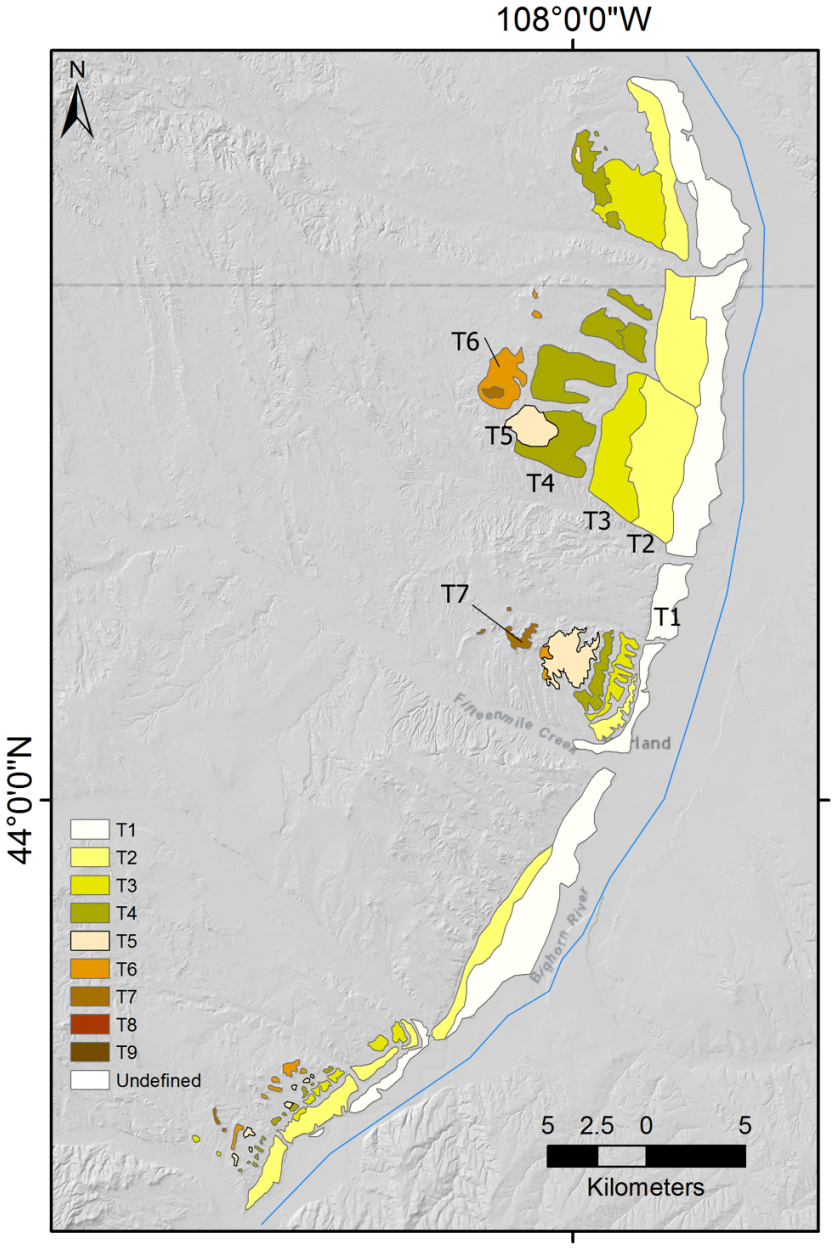

Figure 3.12 Sequence of terraces near Worland, Wyoming in the central-eastern Bighorn Basin. See Figure 3.1 for location. Terraces are only preserved on western bank of Bighorn River. Interpreted as recording the eastward migration of the Bighorn River.

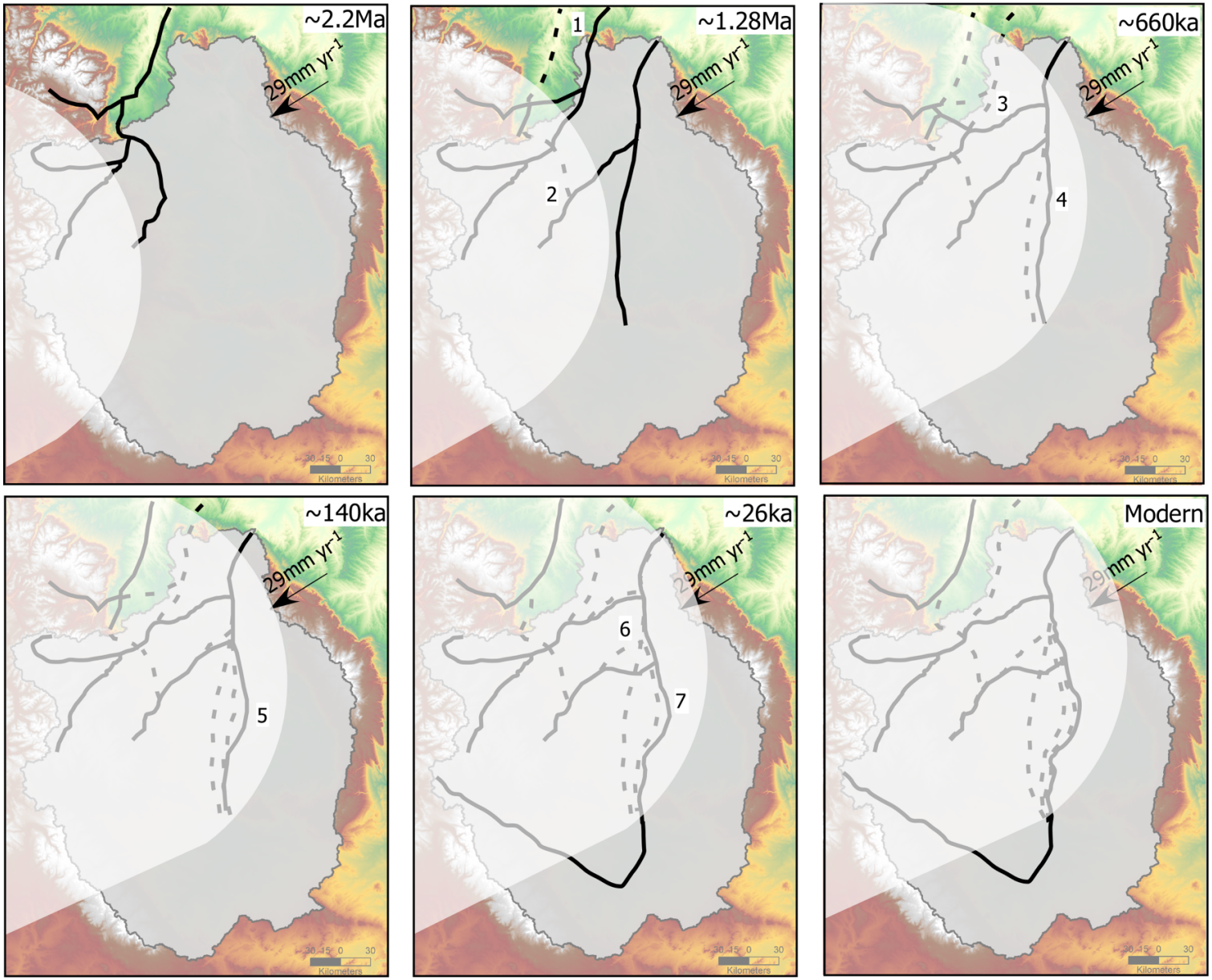
~2.2Ma
29mm yr-1
~1.28Ma
1
2
29mm yr-1
~660ka
3
4
29mm yr-1
~140ka
5
29mm yr-1
~26ka
6
7
29mm yr-1
Modern
29mm yr-1
30 15 0 30
Kilometers

Figure 3.13 Drainage evolution of the Bighorn Basin since Plio-Pleistocene time. Each panel represents the drainage configuration at the particular time. Black arc corresponds to modeled deformation front associated with the advection of dynamic topographic wave. Vector in 2.2 Ma panel is the motion of North America with respect to the Yellowstone hotspot. Ages indicate discrete stream capture or change in paleoflow direction events. **2.2 Ma:** Combined Clarks Fork-Shoshone (CFS) deposits Silesia gravel. Ritter (1975) proposes that this is major drainage outlet for BHB, assume that Tatman aged river drained through Silesia at this time **1.28 Ma:** Silesia river is abandoned, CFS flows north through Pryor Gap, depositing Polecant Bench gravels. **660 ka:** Bighorn River migrates eastward (4), At this time, the CFS is disrupted as Polecat Bench deposits indicate abandonment, Shoshone River flows eastward. **140 ka:** Bighorn Continues eastward migration, minor drainage captures by the Paleo-Greybull river (5). **26 ka:** Paleo-Greybull is captured by modern Greybull as Bighorn continues to migrate eastward (6,7). This drainage evolution records changes in flow regime from South to North dominated flow to West to East flow, we interpret this to be the result of the slight tilting (<0.3°) inferred to be the Yellowstone-related transient topography signal impinging on the Basin.

REFERENCES

Anderson, R.S., Repka, J.L., and Dick, G.S., 1996, Explicit treatment of inheritance in dating depositional surfaces using in situ 10Be and 26Al: Geology. p. 47-51.

Armstrong, R.L. and Ward, P.L., 1993. Late Triassic to earliest Eocene magmatism in the North American Cordillera: implications for the western interior basin. Evolution of the western interior basin: Geological Association of Canada Special Paper, 39, pp.49-72.

Bown, T.M., 1980, Summary of latest Cretaceous and Cenozoic sedimentary, tectonic, and erosional events, Bighorn Basin, Wyoming: Papers on Paleontology, v. 24, p. 25–32.

Bown, T.M., and Kraus, M.J., 1981a, Lower Eocene alluvial paleosols (Willwood Formation, Northwest Wyoming, U.S.A.) and their significance for paleoecology, paleoclimatology, and basin analysis: Palaeogeography, Palaeoclimatology, Palaeoecology, v. 34, p. 1–30.

Braun, J., 2010, The many surface expressions of mantle dynamics: Nature Geoscience, v. 3, no. 12, p. 825–833.

Braun, J., Robert, X., and Simon-Labric, T., 2013, Eroding dynamic topography: Geophysical Research Letters, v. 40, no. 8, p. 1494–1499.

Cerveny, P.F., and Steidtmann, J.R., 1993, Fission track thermochronology of the Wind River Range, Wyoming: Evidence for timing and magnitude of Laramide exhumation: Tectonics, v. 12, no. 1, p. 77–91.

Chadwick, O.A., Hall, R.D., and Phillips, F.M., 1997, Chronology of Pleistocene glacial advances in the central Rocky Mountains: Geological Society of America Bulletin, v. 109, no. 11, p. 1443–1452.

Christiansen, R.L., 2001. The Quaternary and pliocene Yellowstone plateau volcanic field of Wyoming, Idaho, and Montana (No. 729-G).

DeCelles, P.G., 2004, Late Jurassic to Eocene evolution of the Cordilleran thrust belt and foreland basin system, western USA: American Journal of Science. p. 105-168.

DeCelles, P.G., Gray, M.B., Ridgway, K.D., Cole, R.B., Pivnik, D.A., Pequera, N. and Srivastava, P., 1991. Controls on synorogenic alluvial-fan architecture, Beartooth Conglomerate (Palaeocene), Wyoming and Montana.Sedimentology, *38*(4), pp.567-590.

DeCelles, P.G., Gray, M.B., Ridgeway, K.D., Cole, R.B., Srivastava, P., Pequera, N., and Pivnik, D.A., 1991b, Kinematic history of a foreland uplift from Paleocene synorogenic conglomerate, Beartooth Range, Wyoming and Montana: Geological Society of America Bulletin, v. 103, no. 11, p. 1458.

Dickinson, W.R., Klute, M.A., Hayes, M.J., Janecke, S.U., Lundin, E.R., McKittrick, M.A., and Olivares, M.D., 1988, Paleogeographic and paleotectonic setting of Laramide sedimentary basins in the central Rocky Mountain region: Geological Society of America Bulletin, v. 100,

no. 7, p. 1023–1039.

Finn, T.M., 2010, Subsurface stratigraphic cross sections showing correlation of Cretaceous and lower Tertiary rocks in the Bighorn Basin, *in* Petroleum Systems and Geologic Assesment of Oil and Gas in the Bighorn Basin Province, Wyoming and Montana.p. 1-10.

Flament, N., Gurnis, M., and Müller, R.D., 2013, A review of observations and models of dynamic topography: Lithosphere, v. 5, no. 2, p. 189–210.

Gingerich, P.D., 1979, Early Cenozoic Paleontology and Stratigraphy of the Bighorn Basin, Wyoming. p. 1-143.

Hancock, G.S., Anderson, R.S., Chadwick, O.A., and Finkel, R.C., 1999, Dating fluvial terraces with 10Be and 26Al profiles: Application to the Wind River, Wyoming: Geomorphology. 41-60.

Hay, R.L., 1956, Pitchfork Formation, detrital facies of early basic breccia, Absaroka Range, Wyoming: AAPG Bulletin, v. 40. p. 1863-1898.

Heasler, H.P., and Kharitonova, N.A., 1996, Analysis of sonic well logs applied to erosion estimates in the Bighorn Basin, Wyoming: AAPG Bulletin, v. 80. p. 630-646.

Heller, P.L., and Liu, L., 2016, Dynamic topography and vertical motion of the U.S. Rocky Mountain region prior to and during the Laramide orogeny: Geological Society of America Bulletin, p. 1–17.

Hiza, M.M., 1999, The geochemistry and geochronology of the Eocene Absaroka volcanic province northern Wyoming and southwest Montana, USA. PhD Dissertation, Oregon State University. 220 p.

Izett, G.A., 1981, Volcanic ash beds: Recorders of Upper Cenozoic silicic pyroclastic volcanism in the western United States: Journal of Geophysical Research: Solid Earth (1978–2012), v. 86, no. B11, p. 10200–10222.

Kauffman, M.E., and Ritter, D.F., 1981a, Cobble imbrication as a sensitive indicator of subtle local changes in river flow direction: Geology, v. 9, no. 7, p. 299-301.

Kauffman, M.E., and Ritter, D.F., 1981b, Cobble imbrication as a sensitive indicator of subtle local changes in river flow direction: Geology, v. 9, no. 7, p. 299-302.

Kraus, M.J., 1992, Alluvial response to differential subsidence: sedimentological analysis aided by remote sensing, Willwood Formation (Eocene), Bighorn Basin, Wyoming, USA: …, v. 39, no. 3, p. 455–470.

Krumbein, W.C., 1942, Flood deposits of Arroyo Seco, Los Angeles County, California: Geological Society of America Bulletin, v. 53, no. 9, p. 1355–1402.

Lanphere, M.A., Champion, D.E., Christiansen, R.L., Izett, G.A., and Obradovich, J.D., 2002,

Revised ages for tuffs of the Yellowstone Plateau volcanic field: Assignment of the Huckleberry Ridge Tuff to a new geomagnetic polarity event: Geological Society of America Bulletin, v. 114, no. 5, p. 559–568.

Lave, J., and Avouac, J.P., 2000, Active folding of fluvial terraces across the Siwaliks Hills, Himalayas of central Nepal: Journal of Geophysical Research: Solid Earth, v. 105, no. B, p. 5735–5770.

Licciardi, J.M., and Pierce, K.L., 2008, Cosmogenic exposure-age chronologies of Pinedale and Bull Lake glaciations in greater Yellowstone and the Teton Range, USA: Quaternary Science Reviews, v. 27, no. 7-8, p. 814–831.

Lisiecki, L.E., and Raymo, M.E., 2005, A Pliocene-Pleistocene stack of 57 globally distributed benthic δ 18O records: Paleoceanography, v. 20, no. 1. p. 1-17.

Love, J.D., 1960, Cenozoic sedimentation and crustal movement in Wyoming: American Journal of Science. p. 204-216.

Mackin, J.H., 1937, Erosional history of the Big Horn basin, Wyoming: Geological Society of America Bulletin, v. 48, no. 6, p. 813–894.

Mackin, J.H., 1936, The capture of the Greybull River: American Journal of Science. p. 373-385.

Mitrovica, J.X., Beaumont, C., and Jarvis, G.T., 1989, Tilting of continental interiors by the dynamical effects of subduction: Tectonics, v. 8, no. 5, p. 1079–1094.

Moss, J.H., 1982, The Relation of River Terrace Formation to Glaciation in the Shoshone River Basin, Western Wyoming, *in* Glacial Geomorphology, Springer Netherlands, Dordrecht, p. 293–314.

Omar, G.I., Lutz, T.M., and Giegengack, R., 1994, Apatite fission-track evidence for Laramide and post-Laramide uplift and anomalous thermal regime at the Beartooth overthrust, Montana-Wyoming: Geological Society of America Bulletin.

Palmquist, R., 1983, Terrace Chronologies in the Bighorn Basin, Wyoming: Wyoming Geological Association Guidebook, v. 34, p. 217–231.

Pazzaglia, F.J., and Gardner, T.W., 1998, Bedrock fluvial incision and longitudinal profile development over geologic time scales determined by fluvial terraces: Rivers over rock: Fluvial Processes in Bedrock Channels. p. 207-235.

Peyton, S.L., Reiners, P.W., Carrapa, B., and DeCelles, P.G., 2012, Low-temperature thermochronology of the northern Rocky Mountains, western U.S.A.: American Journal of Science, v. 312, no. 2, p. 145–212.

Pierce, K.L., and Morgan, L.A., 2009, Is the track of the Yellowstone hotspot driven by a deep mantle plume? — Review of volcanism, faulting, and uplift in light of new data: Journal of Volcanology and Geothermal Research, v. 188, no. 1-3, p. 1–25.

Pierce, K.L., and Morgan, L.A., 1992, The track of the Yellowstone hot spot: Volcanism,faulting, and uplift: Geological Society of America Memoirs, vol 179, p. 1–52.

Reheis, M.C., 1992, Fluvial deposits of Yellowstone tephras: Implications for late Cenozoic history of the Bighorn basin area, Wyoming and Montana: Quaternary International, v. 13-14, p. 19–22.

Reheis, M.C., Palmquist, R.C., and Agard, S.S., 1991b, Quaternary history of some southern and central Rocky Mountain basins, *in* Quaternary Nonglacial Geology Conterminious U.S, Quaternary, GSA Special Publications, Vol. K-2 p. 407–440.

Riihimaki, C.A., and Reiners, P.W., 2012, Empirical evidence of climate's role in Rocky Mountain landscape evolution: Journal of Geophysical Research, v. 117, no. F2, p. F02007.

Ritter, D.F., 1975, New Information Concerning the Geomorphic Evolution of the Bighorn Basin: Wyoming Geological Association Guidebook,, p. 37–44.

Rohrer, W.L., and Smith, J.W., 1969, Tatman Formation: Wyoming Geological Association Guidebook, v. 21, p. 49–54.

Sharp, W.D., Ludwig, K.R., Chadwick, O.A., Amundson, R., and Glaser, L.L., 2003, Dating fluvial terraces by 230Th/U on pedogenic carbonate, Wind River Basin, Wyoming: Quaternary Research, v. 59, no. 2, p. 139–150.

Small, E.E., and Anderson, R.S., 1998, Pleistocene relief production in Laramide mountain ranges, western United States: Geology, v. 26, no. 2, p. 123.

Smith, R.B., Jordan, M., Steinberger, B., Puskas, C.M., Farrell, J., Waite, G.P., Husen, S., Chang, W.-L., and O'Connell, R., 2009, Journal of Volcanology and Geothermal Research: Journal of Volcanology and Geothermal Research, v. 188, no. 1-3, p. 26–56.

Stock, G.M., Riihimaki, C.A. and Anderson, R.S., 2006. Age constraints on cave development and landscape evolution in the Bighorn Basin of Wyoming, USA. Journal of Cave and Karst Studies, 68(2), pp.76-84.

Yuretich, R.F., and Hickey, L.J., 1984, Lacustrine deposits in the Paleocene Fort Union Formation, northern Bighorn Basin, Montana: Journal of Sedimentary Petrology, v. Vol. 54. p. 0836-0852.

CONCLUSIONS

There is a mantle hotspot that has influenced the landscape evolution the Yellowstone region, namely through volcanism, however deformation by transient topography is expected. Our results illustrate a good correlation between analysis of surface data and geophysical proxies for the hotspot, which allows us to interpret long wavelength topography as the transient topography associated with the hotspot. There is a 0.17 mm yr^{-1} surface uplift rate expected at the leading edge of the advecting topography. We consider it a tractable problem and future work on constraining the pace of landscape evolution, in particular drainage basins ahead of the advecting wave of topography will provide insight to the surface expression of hotspot-related transient topography in a continental setting.

We analyzed stream channel morphology from the regional to the catchment scale in the Yellowstone area to investigate if advection of dynamic topography has a measureable deformation signal. High k_{sn} values do coincide not with modeled dynamic topography deformation at the regional scale. High k_{sn} values at drainage scale illustrate the coincidence with changes in lithology, Basin and Range faulting, volcanic processes, glacio-fluvial transitions, tributary junctions, or landslides. Knickpoints at the catchment scales in uniform lithology coincide with tributary junctions and glacio-fluvial transitions. Deformation rates of >0.17 mm yr^{-1} are below the detection limit of k_{sn} analysis and not disturb longitudinal profiles enough to create transient deformation signal. Either deformation signal does not reach the surface and dynamic topography does not have a geomorphic expression or lithosphere-scale response to

deformation is more complex and requires additional metrics to be quantified. Surface uplift rates associated with dynamic topography are small and are spatially distributed.

Palmquist (1983) recognized the lateral migration of the Bighorn River as the controlling agent that forced the Plio-Pleistocene drainage reorganization from a primarily south to northward drainage direction to a west-east dominated system. He describes the lateral migration as 'unexplicable'. Incorporation of an advecting dynamic topography deformation signal could provide the mechanism for the lateral migration of the Bighorn River. This results from this work indicate that the key to quantifying the influence of dynamic topography on the erosion of the Bighorn basin requires detailed geochronology. Compilation of previous studies and an updated geochronology of the Plio-Pleistocene erosion of the Bighorn Basin suggests that dynamic topography associated with Yellowstone played a role in the basin's drainage reorganization and landscape evolution.

Conclusions regarding transient topography and erosion of the Bighorn Basin during Pliocene-Pleistocene time are that: Transient topography can affect drainage evolution because of potential to induce small, but important, change of river gradients through surface uplift. Transient topography has asymmetric long wavelength form, masked by crustal-controlled topographic wavelength and amplitude. Transient topography- associated surface uplift rates small and spatially distributed. Climate oscillations in sediment supply, processes (glacial; versus fluvial), and discharge larger, relatively faster, thus stronger driver of over elevation in space and time. Incision rates complicated because surface uplift steady and varying in space and time and river elevation up and down as a function of aggradation/degradation on shorter timescale.

GUIDE TO APPENDICES

The results of analysis presented in this research is publicly and freely available through the Oregon State University Scholar's archive (https://ir.library.oregonstate.edu/xmlui) (as of June, 2016). The data is presented in a variety of file formats, which depends on the program used to complete the analysis. Data that were analyzed using Microsoft Excel (.xlsx) and MatLab (.mat) should load automatically when the files are opened using either program. Opening .mat files requires owning a MatLab license, therefore, '.jpg' version of the files are included in the specific folders. Where applicable, folders include a .pdf or .docx file that contains step by step instructions on how analysis was completed. Results of analysis in ArcGIS (.shp, .txt) require processing in ArcGIS (or other GIS) in order to display correctly, please refer to read-me's or analysis instructions in order to display results correctly.

Unprocessed Data

Folder 1.1 contains elevation datasets which are organized into subfolders. Regional analysis datasets can reach sizes of up to 1.8 Gb. Subfolders included in this section are: Shuttle Radar Topography Mission (SRTM) data is in folder 1.1a, and is a 30m resolution elevation dataset that has been stitched from 1 degree quadrangles to create a regional digital elevation model. These elevation data were used in regional analysis presented in chapter 2 (Swath Profiles, Mean Elevation Maps) and chapter 3 (regional stream profile analysis). National Elevation Dataset (NED) is in folder 1.1b, and is a 10m resolution digital elevation model, and was used to create digital elevation model of the Bighorn Basin (chapter 4). Geoid model data (GEOID12) used in analysis for chapter 2 is located in folder 1.1c.

Swath Profiles

There are five spreadsheets (.xlsx) contained in folder 1.2. There is the master spreadsheet that contains the formulas used to calculate maximum, mean, and minimum elevation. The other four spreadsheets correspond to each of the swath profiles presented in chapter 2. There is additionally, a word document (.docx) which contains directions on how to extract swath profiles from the 30m SRTM datasets and create the swath profile charts.

Mean Elevation Maps

Raster versions of the mean elevation maps are included in folder 1.2. There are 4 rasters: each one is named after the wavelength at which the elevation data was filtered: 50km, 100km, 150km, 200km. The rasters will display in ArcGIS but must be projected (WGS 1984), display preferences must be adjusted in order to match user's preference. Directions for creating mean elevation map using the Spatial Analyst toolkit are included as a separate word document (.docx).

Geoid

There are two raster files contained in folder 1.4: Unfiltered GEOID12B and filtered GEOID12 rasters presented in chapter 2. The datasets were provided courtesy of National Oceanic and Atmospheric Administration (NOAA)'s gravity and geoid research group (http://www.ngs.noaa.gov/GEOID/).

Region al k_{sn} Analysis

This folder contains a word document (.docx) that gives step-by-step directions on performing the ksn analysis using the Topotoolbox 2.0 in MatLab. There is a folder containing MatLab scripts that was used in extracting and calculating ksn values for the greater Yellowstone area. There is an excel spreadsheet that contains regional ksn results summarized in table form ksn values, theta values, watershed area data and summary charts of ksn results. There are two

subfolders, each containing ksn analysis performed on drainages with a minimum contributing area of 30 km^2 and 15 km^2. The files contained in these subfolders are shapefiles (.shp) and are best viewed in ArcGIS 10.3 (or above). There is a bit of processing that must be done in order to display shapefiles, please refer to the instructions in the word document in the top-level folder in order to view results.

Detailed Stream Profiles, ksn analysis, and Slope Area Data

This folder contains a sub-folder structure, where each analyzed drainage basin is identified by either a number or by the basin name used in the text. Each folder contains figures in both .mat and .jpg versions of stream profiles and slope area. There is also a subfolder contained in each one that has the corresponding individual ksn analysis (same data contained in folder 1.5, but in individual form).

Terrace Correlation Spreadsheet

This folder contains the spreadsheet (.xlsx) with the terrace correlation compilation presented in chapter 4. This spreadsheet is an updated version of the terrace chronology published by {Reheis:1991wb}, and updated to include cosmogenic dating results along the Bighorn River Stock et al., (2006), Wind River (Anderson et al., 1996; Hancock and Anderson, 1996), and cosmogenic dating of LGM moraines that exist along the western margin of the Bighorn Basin (Chadwicket al., 1996; Licciardi et al, 2008)